REDUCING OPERATIONAL COSTS IN MEMBRANE BIOREACTORS USING SLUG BUBBLES

by

Christina Starke

B.Sc., Technische Universitaet Berlin, Germany 2013

A THESIS SUBMITTED IN PARTIAL FULFILLMENT
OF THE REQUIREMENTS FOR THE DEGREE OF

Master of Applied Science

in

THE FACULTY OF GRADUATE AND POSTDOCTORAL STUDIES
(Civil Engineering)

The University of British Columbia
(Vancouver)

January 2015

Abstract

Membrane bioreactors (MBRs) are commonly used in wastewater treatment processes. In fact, the demand is expected to increase with more than double digit growth annually over the next decade [5]. However, operational costs of MBRs are still higher compared to operational costs of conventional treatment plants due to the additional aeration and pumping required in MBRs. This study examines the feasibility of using excess air that was used to clean the membrane for water conveyance (known as airlift pump), for a minimized energy use in MBR processes.

In order to meet the objective, prototypes of airlift pumps were built with different dimensions. The experimental results of each prototype were comprehensively compared to existing models in the literature. The models were modified for a better fit of the experimental data.

It was determined whether a new apparatus, where many riser tubes were bundled together, would behave like many individual riser tubes. While the air was injected at the bottom of the individual riser tube previously, the bundled riser tubes of the new apparatus would be attached to a rubber sheet; this, was attached to a frame.

The rubber sheet was added to the apparatus in order to trap the air in the tank and lead it to the bundle of riser tubes. Different collector angles of the rubber as well as different water heights were investigated. The experimental results were compared to the previously modified models.

The last step was to design a system that redirects the pumped water so that it can be transported back to the head of the MBR plant.

The results suggest that air exiting to the atmosphere from an MBR can be used to transport the water. However, the models are only able to predict water flows for individual airlift pumps that consist of a single riser tube, where the air is injected at its bottom. Further research needs to be done in order to be able to predict water flows that can be achieved in systems, such as the one proposed in this present study, which uses a bundle of riser tubes.

Preface

This dissertation is original, unpublished, independent work by the author, Christina Starke.

Table of Contents

List of Tables

List of Figures

List of Acronyms

ADF	Average Daily Flow
CAS	Conventional Activated Sludge
EES	Engineering Equation Solver
HRT	Hydraulic Retention Time
lmh	Liter per m^2 per hour [L/m^2h]
MBR	Membrane Bioreactor
MF	Microfiltration
MGD	Million Gallons per Day
MLSS	Mixed Liquor Suspended Solids
PVC	Poly Vinyl Chloride
RAS	Return Activated Sludge
SCFM	Standard Cubic Feet per Minute
SRT	Sludge Retention Time
UF	Ultrafiltration

List of Symbols

Bo	Bond number
C_0	Liquid slug velocity coefficient
ρ_{tp}	Two-phase density
e	Average wall roughness
Eo	Eötvös number
ε	Gas void ratio
ε_h	Homogeneous void fraction (when S=1)
ε_r	Pipe roughness
η	Dynamic viscosity
f'_{tp}	Fanning friction factor
f_{tp}	Two-phase friction factor
Fr	Froude number
g	Gravity
h_l	head loss
K	Nominal head loss coefficient
k_s	Half-saturation concentration
L_c	Chexal-Lellouche fluid parameter

M	Morton number
μ	Dynamic viscosity
μ_g	Maximum specific growth rate
N_f	Archimedes Number
P	Pressure
R	Return Activated Sludge Rate
ϕ_{tank}	Membrane packing density
Re	Reynolds number
S	Substrate
σ	Surface tension
Σ	Surface tension number
θ	Hydraulic Retention Time (HRT)
θ_c	Sludge Retention Time (SRT)
V	Velocity
V_{gj}	Drift velocity
ν	Kinematic viscosity
X	Biomass
Y	Biomass yield

Acknowledgements

I would like to express my very great appreciation to my supervisor Dr. Pierre Bérubé. I am thankful for his guidance during this project as well as for support throughout my stay at UBC.

Thanks are extended to Paula Parkinson, Tim Ma and Bill Leung for all their help and advice on how to build my setups. Not only knowledge about work, but also life wisdoms were shared that embellished my daily routine.

I have also been lucky to have the support and input of many friends and labmates such as Shona Robinson, Patricia Oka, Jeff MacSween, Joerg Winter and Sepideh Jankhah. I would like to especially acknowledge the time and effort Syed Zaki Abdullah put into discussions about my work.

Finally, I would like to thank Greg Reynen and my family for their love and moral support.

Chapter 1

Introduction

About 2-3% of the world energy is consumed to treat and convey water and wastewater. For wastewater, pumping represents at least 30% of the energy demand. Therefore, reducing pumping costs is of importance [3]. Depending on the water source (freshwater, seawater or wastewater), the energy required to convey and treat water is in the range of 0.05 to 5 $^{kWh}/_{m^3}$. Typical energy footprint for conventional activated sludge (CAS) treatment ranges from 0.25 to 0.6 $^{kWh}/_{m^3}$. With an additional nitrification step, it may range from 0.3 to 1.4 $^{kWh}/_{m^3}$ [2] . The energy footprint for a membrane bioreactor (MBR) is higher and common values range between 0.5 and 2.5 $^{kWh}/_{m^3}$ [2]. Previous studies have demonstrated that MBRs can have lower capital costs than CAS plants [12], while producing a cleaner effluent. The demand for MBR systems is expected to further increase with more than double digit growth annually over the next decade [5], due to increasingly stringent regulations and the large demand in water reuse applications.

However, operational costs are still high in MBR systems due to the aeration (i.e.

air scouring) and pumping requirements. Over the past 15 years, the energy required for air scouring has decreased by a factor of 15 [12]. However, the costs for return activated sludge (RAS) pumping remain high. Figure 1.1 illustrates the energy cost distribution in MBRs, emphasizing the contribution of RAS pumping to the total operating costs. The present study examines the feasibility of using the energy associated with the air escaping from the tank after it has been used for air scouring, to convey RAS and minimize energy use in MBR processes.

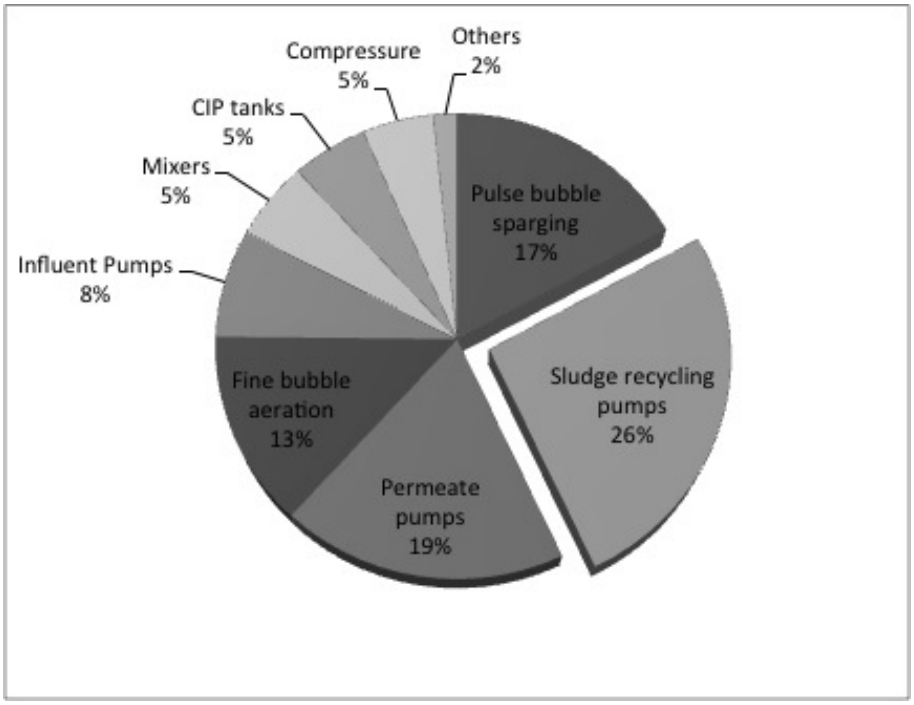

Figure 1.1: Power cost distribution for MBRs, modified from [21]. The exploded piece of the pie chart represents the energy required for RAS pumping.

The structure of this present document is as follows. Background information for MBRs and airlift pumps is provided in Chapter 2. The knowledge gap is iden-

tified, and the objectives are defined in detail in Chapter 3. Chapter 4 presents the materials and methods used to address the research objectives. Different airlift pump models were investigated and compared to the data from this study. Chapter 5 presents which model provided the best fit, including modifications that were made to the models. Assumptions for different scenarios (e.g. air is available at different locations in the MBR tank) that were considered, including their possible cost benefits, are outlined in Chapter 6. Results of the pilot scale air and water collection system tests are presented in Chapter 7, and Chapter 8 presents conclusions and discusses pertaining to the engineering significance of the present study.

Chapter 2

Literature review

2.1 Membrane bioreactor ((MBR)

A conventional activated sludge (CAS) plant typically consists of two systems, a suspended growth activated sludge biological reactor and a secondary clarifier. The bioreactor relies on microorganisms that metabolize nutrients and organic matter to remove contaminants from the wastewater. In the process, biomass (i.e. solids) is generated [40]. The biomass solids must settle easily for effective solid-liquid separation in the clarifier. The separated biomass is returned to the bioreactor. The return stream is generally called RAS, and the mixture of biosolids in the bioreactor is referred to as mixed liquor suspended solids (MLSS).

In a MBR the secondary clarifier is replaced by a membrane that performs the solid-liquid separation (Fig. 2.1). Typically, membranes are located external of the bioreactor in a separate tank. MBRs require higher RAS rates than CAS systems (300 to 500% compared to 50 to 100% of the average daily flow (ADF) [40]) in

order to avoid an accumulation of solids in the membrane tank.

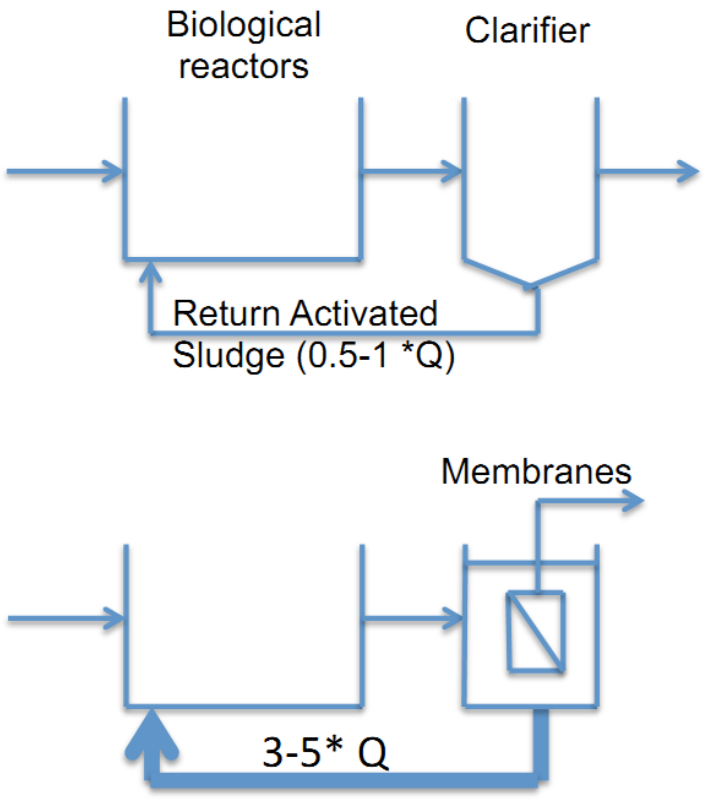

Figure 2.1: Process diagramm for CAS and MBR.

2.1.1 Membranes

A membrane is a semipermeable barrier that allows at least one component of a mixture to pass, while the other components are retained. Membranes generally separate mixtures based on molecular weight or particle size, driven either by a negative (vacuum) or positive pressure. The process consists of a feed flow that results in a permeate and a retentate. Membranes can be classified by their material (i.e. synthetic polymers or ceramic), pore size (i.e. microfiltration (MF), ultrafil-

tration (UF), nanofiltration (NF) and reverse osmosis (RO)), module configuration (i.e. flat sheet or hollow fiber) or pressure applied for operation (i.e. high or low pressure). In addition, membranes can be operated with a constant flux and variable pressure or variable flux and constant pressure. Material flowing to the membrane is generally referred to as feed, the material retained by the membrane as retentate, and material flowing through the membrane as permeate. The flux is defined as the permeate normalized by the membrane area, and will be further discussed in Section 2.1.2.

Both, flat sheet and hollow fibre polymeric MF and UF membranes are typically used in MBRs. The pore sizes of MF and UF membranes range between 0.1 to 0.4 μm and 0.01 to 0.05 μm, respectively, and are usually operated at low pressures (0.2 to 1 bar).

2.1.2 Flux

The flux is the permeate normalized by the membrane area. Lower flux operations are generally associated with longer membrane life, lower operational risk and less maintenance due to the reduced mass flow and fouling on the membrane surface. However, lower flux operations require a larger membrane surface area than high flux operations to treat a given feed flow, causing higher capital costs. Conversely, higher flux operations are often associated with a shorter membrane life, higher risk for breaches, more maintenance, but less capital costs. When selecting the flux, the composition of the wastewater, mixed liquor and temperature ranges should be considered. Plants are usually designed for peak flow conditions [40]. A permeate flux of 25 liter per m^2 per hour [L/m^2h] (lmh) is typical for commercial

MBR systems.

2.1.3 Fouling

Over time, material (microorganisms, colloids, solutes, and cell debris) retained by the membrane can accumulate on its surface, forming a cake layer or plugging membrane pores (completely or partially). Material can also be adsorbed within the membrane pores, increasing the resistance to the permeate flow (Fig. 2.2). The process of material accumulations, and the accumulated materials themselves is generally referred to as fouling and foulants, respectively. Biomass flocs in MBR bioreactors are generally much larger than the membrane pores, and therefore, tends to form a cake layer on the membrane surface.

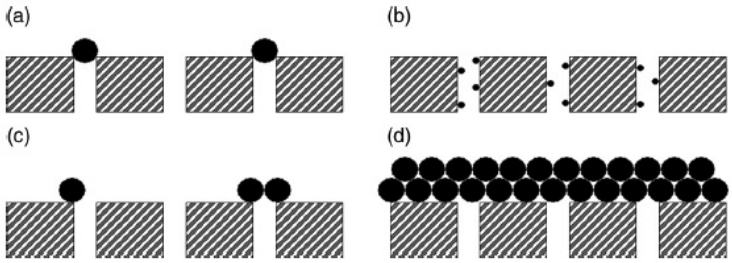

Figure 2.2: Membrane fouling processes: a) complete pore blocking, b) adsorption, c) partial pore blocking d) cake layer [16]).

Different types cleaning procedures can be used to reduce fouling. Hydraulic cleaning, such as air scouring or backwashing, can be used to remove loosely attached foulants on the membrane surface. Chemical cleaning can be used to remove adsorbed foulants. Irreversible fouling cannot be removed by either physical or chemical approaches [27].

2.1.4 Air scouring

Air scouring is a physical cleaning method used to prevent and reduce fouling on a membrane's surface. Aeration is applied at the bottom of the membrane module. As the bubbles rise, shear forces are induced on to the membrane's surface to remove accumulated foulants. Although very effective, membrane scouring has been identified as one of the largest contributors to the high energy consumption of MBRs [12].

The amount of air scouring required for fouling control has substantially decreased over the last two decades [11]. This evolution was made feasible by increasing membrane surface area per unit tank volume and improvement of the aeration method. This largely resulted from a shift from continuous aeration (1995) to cyclic aeration (2000), then sequential aeration (2006) and, more recently, large pulse bubble aeration (2011) [11, 21].

2.1.5 Benefits of MBRs

Compared to CAS systems, MBRs can achieve better treated water quality in a smaller footprint because membranes require less space than clarifiers and higher concentrations of mixed liquor can be maintained. MBRs can also be operated with a high degree of automation, which is beneficial if operator attention needs to be minimized, such as in remote treatment systems. In addition, MBRs can meet more stringent discharge requirements for a number of parameters such as suspended solids, organic matter, total phosphorus or total nitrogen compared to traditional CAS plants [40].

2.1.6 RAS

Concentrated solids in the membrane tank are usually pumped back to the bioreactor to maintain high biomass concentrations within the bioreactor tank. The flow of biomass from the membrane tank to the bioreactor, hereafter referred to as RAS can be calculated based on a mass balance around the membrane tank, which yields the relationship presented in Equation 2.1.1.

$$MLSS_{membranetank} = \frac{(R+1)}{R} MLSS_{bioreactor} \tag{2.1.1}$$

To maintain biomass concentrations of approximately 10,000 $^{mg}/_{L}$,expressed as MLSS), which is typical for MBRs, the recycle ratio should range from approximately 300 to 500% of the incoming flow.

2.1.7 Costs

Young et al. [43] developed energy consumption factors for MBRs and CAS plants with an average daily flow (ADF) rate of 5 MGD (18.925 $\frac{m^3}{d}$) and compared the life cycle costs between the two systems. Tertiary filtration was required following CAS treatment to produce an effluent quality comparable to that of an MBR. The results indicated that MBRs had higher operation and maintenance costs than CAS systems, mainly because of membrane replacement costs (approximately once every 10 years), costs associated with fouling control (such as recovery or chemical cleaning and generally higher level of pre-treatment of the feed), and RAS pumping costs. RAS pumping was assumed to be 1.0 and 4.0 times the AFD for the CAS system and the MBR plant, respectively. Nonetheless, the study determined that the higher operation and maintenance costs associated with MBR systems was

offset by their lower capital costs [43].

2.2 Airlift pumps

An airlift pump is a vertical riser tube which is partially submerged in liquid into which compressed air is injected near the bottom of the riser tube. The rising air in the riser tube entrains the water, causing a gas lift effect (Fig. 2.3). Airlift pumps are reliable and require limited maintenance compared to mechanical pumps. Airlift pumps are commonly used in nuclear fuel processing plants due to its robustness in handling corrosive, abrasive and radioactive fluids [9].

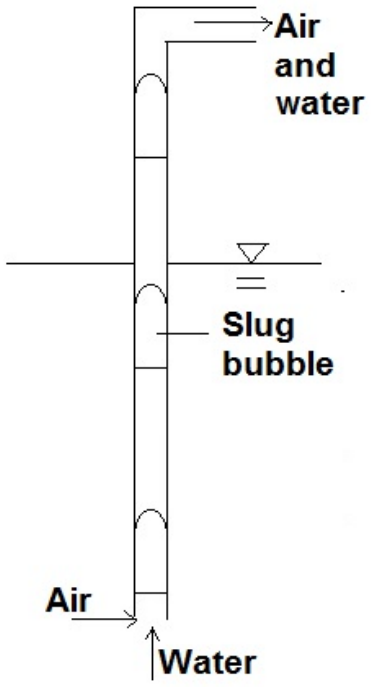

Figure 2.3: Illustration of an airlift pump.

Two-Phase Flow

The performance of an airlift pump depends the flow pattern or so called "flow regime" when gas and air flow up together in the vertical riser tube. The flow regime is a function of the fluxes of both phases, properties of various factors and dimensions and location of the channel [34]. The basic flow patterns are bubbly, slug, churn and annular, but definitions vary by authors (Fig. 2.2.1). A detailed description of flow maps can be found in [34]. Early but fundamental studies focusing on airlift pumps indicated that the slug flow regime (long round nosed bubbles, called "Taylor" bubbles), with the length of the bubbles ranging from roughly the diameter of the tube to several times this value [33], were the most efficient regime for airlift pumping [29]. Nicklin suggested that each flow-pattern needed a separate mathematical treatment [29]. All models investigated in this study assume the slug-flow regime, except the Chexal-Lellouche model, which is not flow specific.

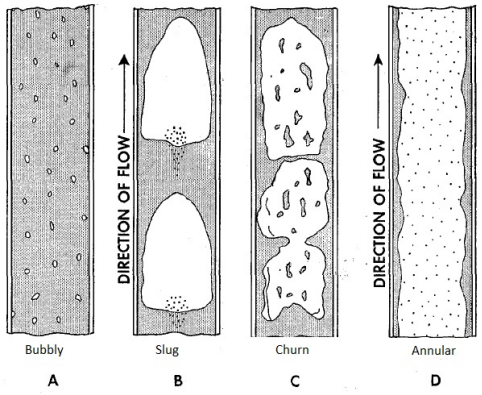

Figure 2.4: Flow regimes (modified from [31]).

2.2.1 Airlift pump models

The five semi-mechanistic models considered in the present study are discussed below. The models considered were previously compared in [42].

The governing equations, which are based on fluid properties, geometrical characteristics, and mass and momentum balances can be solved for velocities and hence, liquid flows. The equations for the different airlift models considered are dependent on the geometry of the airlift device. The equations presented below were developed for the experimental conditions used in the present study (i.e. vertical cylindrical riser tube partially submerged in water to which air is introduced at the base of the riser tube). The notation used in the equations is presented in Table 2.1, the indices "g" and "l" stand for gas and water, respectively.

Table 2.1: Two-Phase flow parameters as used in [42]

Parameter	Unit	Definition
D	m	Diameter of riser tube
P	Pa	Pressure
H	m	Submergence depth
L	m	Riser tube length
K		Nominal head loss coefficient
ρ_g	kg/m^3	Density of gas phase
ρ_l	kg/m^3	Density of liquid phase
ρ_h	kg/m^3	Homogenous density
ρ_{tp}	kg/m^3	Two-phase density
$A = \pi D^2/4$	m^2	Total cross sectional area of riser tube
A_g	m^2	Cross sectional area gas occupies
$A_l = A - A_g$	m^2	Cross sectional area liquid occupies
$\varepsilon = A_g/A$	-	Gas void fraction of the flow
ε_h		Homogenous void fraction (S=1)
ε_r	mm	Pipe roughness
$\dot{\forall}_g$	m^3/s	Gas volumetric flow rate
$\dot{\forall}_l$	m^3/s	Liquid volumetric flow rate
$\dot{\forall} = \dot{\forall}_g + \dot{\forall}_l$	m^3/s	Total volumetric flow rate
$j_g = \dot{\forall}_g/A$	m/s	Gas superficial velocity
$j_l = \dot{\forall}_l/A$	m/s	Liquid superficial velocity
$j = j_g + j_l$	m/s	Total average velocity of the flow
$V_m = j$	m/s	Velocity of mixture
$V_g = \mathrm{j_g}/\varepsilon$	m/s	Velocity of the gas
$V_l = \mathrm{j_l}/1-\varepsilon$	m/s	Velocity of the liquid
$\dot{m}_g$	kg/s	Mass flow rate of gas
$\dot{m}_l$	kg/s	Mass flow rate of liquid
$\dot{m}$	kg/s	Total mass flow rate
$x = \mathrm{\dot{m}_g}/\mathrm{\dot{m}}$	-	Quality
$S = \mathrm{V_g}/\mathrm{V_l}$	-	Slip between phases
$Re = \mathrm{jD}/\nu$		Reynolds number
f_{tp}		Two=phase friction factor
$f'_{tp} = \mathrm{f_{tp}}/4$		Fanning friction factor

Based on the momentum equation, the pressure at the inlet of the riser tube can be determined:

$$P_a = P_{sys} + \rho_l g H - \rho_l \frac{V_l^2}{2} \tag{2.2.1}$$

where P is the pressure, V is the velocity, g is gravity and the index "a" stands for the point of the air inlet.

Neglecting transition losses and assuming the water at the air inlet conserves its momentum as it mixes with the air yields:

$$P_{a2} = P_a + \rho_h V_l (V_m - V_l), \tag{2.2.2}$$

where the index "m" stands for the mixture of air and water, "a2" is the state at the air inlet after mixing. The velocities of both phases are assumed to be approximately equal, therefore a homogenous density (ρ_h) is used in the momentum equation [42]. It can be calculated with a conservation of mass between the state before and after mixing:

$$\rho_l A V_l + \dot{m}_g = \rho_h A V_m. \tag{2.2.3}$$

Rearranging yields:

$$\rho_h = \frac{\rho_l V_l A + \dot{m}_g}{A V_m} = \frac{\dot{m}_l + \dot{m}_g}{\frac{\pi}{4D^2} V_m}, \tag{2.2.4}$$

The velocity of the mixture describes the total average velocity of both phases and equals the total average velocity of the flow j:

$$V_m = \frac{\dot{\forall}_g + \dot{\forall}_l}{A} = \frac{\dot{\forall}}{A} = j. \tag{2.2.5}$$

Because the void fraction ε is defined as the average cross sectional area occupied by the gas divided by the total cross sectional area A_g/A, the average cross sectional area occupied by liquid divided by the total cross sectional area A_l/A must be $1-\varepsilon$.

Incorporating the above into the momentum equation in the riser tube (from inlet to outlet) yields:

$$P_{a2} = P_{sys} + \rho_l g L(1-\varepsilon) + f_{tp}\frac{(\rho_l j_l + \rho_g j_g)^2}{2\rho_{tp}}(\frac{L}{D}) \tag{2.2.6}$$

where f_{tp} is the two-phase friction factor, which will be discussed in Section 2.2.3, and ρ_{tp} is the two-phase density of the mixture. The third term of Equation 2.2.6 represents the head loss h_l in the riser tube, which is usually in the following form:

$$h_l = f\frac{\rho V^2}{2g}\frac{L}{D}. \tag{2.2.7}$$

The second represents the hydrostatic pressure along the riser tube. However, because the riser tube is only partially filled with water, the term needs to be multiplied with the fraction of water in the tube (1- ε).

Because there is slip between the two phases, the homogenous density cannot be used. The density of the two-phase fluid is:

$$\rho_{tp} = \rho_g \varepsilon + \rho_l(1-\varepsilon). \tag{2.2.8}$$

Combining Equations 2.2.2, 2.2.5, 2.2.6 and replacing V_l by j_l yields:

$$P_a + \rho_h j_l (j - j_l) = P_{sys} + f_{tp} \frac{(\rho_l j_l + \rho_g j_g)^2}{2\rho_{tp}} (\frac{L}{D}) + \rho_l g L (1 - \varepsilon), \tag{2.2.9}$$

adding Equation 2.2.1 yields:

$$P_{sys} + \rho_l g H - \rho_l \frac{j_l^2}{2} + \rho_h j_l (j - j_l) = P_{sys} + f_{tp} \frac{(\rho_l j_l + \rho_g j_g)^2}{2\rho_{tp}} (\frac{L}{D}) + \rho_l g L (1 - \varepsilon). \tag{2.2.10}$$

Solving Equation 2.2.10 for H/L results in a general equation that describes the submergence ratio, which is equivalent to the average pressure gradient along the riser tube ([29]). It is presented in Equation 2.2.11.

$$\frac{H}{L} = f_{tp} \frac{(\rho_l j_l + \rho_g j_g)^2}{2gD\rho_l \rho_{tp}} + \frac{j_l^2}{2gL} + \frac{(j_l \rho_h (j - j_l))}{\rho_l g L} + 1 - \varepsilon. \tag{2.2.11}$$

2.2.2 Modifications

The equations presented in the previous section assume, that entrance and exit losses are negligible. Considering the entrance and exit losses yields:

$$\frac{H}{L} = f_{tp} \frac{(\rho_l j_l + \rho_g j_g)^2}{2gD\rho_l \rho_{tp}} + \frac{j_l^2}{2gL} + \frac{(j_l \rho_h (j - j_l))}{\rho_l g L} + 1 - \varepsilon + K \frac{j_l^2}{2gD}, \tag{2.2.12}$$

where K is the nominal head loss coefficient. K is usually assumed to be 0.5 and 1 for entrance and exit losses, respectively [32].

2.2.3 Friction factor for two-phase flow

When modeling two-phase flows, predicting two-phase flow friction factors can be challenging. Reinemann et al. [33] and Cachard and Delhaye [6] calculate the friction factor using Equation 2.2.13.

$$f = \frac{0.316}{Re^{0.25}}, \tag{2.2.13}$$

with

$$Re = \frac{jD}{\nu}, \tag{2.2.14}$$

where ν is the kinematic fluid viscosity of the liquid in $^{m^2}/_{s}$, and Re is the Reynolds number. This is a friction factor for smooth pipes and Reynolds numbers between 3000 and 100 000 as suggested by Blasius [19].

White [42] uses an approach recommended by Beattie and Whalley [4], that uses the Colebrook equation to estimate friction factors. The Reynolds number is derived from a homogenous model but is calculated using two-phase properties, therefore one Reynolds number was used for modeling which was based on an average of each phase's properties:

$$\frac{1}{\sqrt{f'_{tp}}} = 3.48 - 4log_{10}\left[2\frac{\varepsilon_r}{D} + \frac{9.35}{Re_{tp}\sqrt{f'_{tp}}}\right], \tag{2.2.15}$$

where ε_r is the pipe roughness, 0.0015 mm was used for this study (value for PVC pipes [1]).

The difference between the two friction factors (i.e. Equations 2.2.13 and 2.2.15) was reported to be negligible. As the presented study was in part based on White's work, the Beattie and Whalley approach was chosen to calculate the friction factor. The parameters needed to solve Equation 2.2.15 are as follows.

$$f'_{tp} = \frac{f_{tp}}{4}, \tag{2.2.16}$$

where f'_{tp} is the fanning friction factor,

$$\varepsilon_h = \frac{x}{x + \frac{\rho_l}{\rho_g}(1-x)}, \tag{2.2.17}$$

where ε_h is the homogeneous void fraction (when S=1, no slip conditions),

$$\mu_{tp} = \varepsilon_h \mu_g + \mu_l(1-\varepsilon_h)(1+2.5\varepsilon_h), \tag{2.2.18}$$

where μ is the dynamic viscosity in Pas or $^{\mathrm{kg}}/_{\mathrm{ms}}$, and

$$Re_{tp} = \frac{(\rho_g j_g + \rho_l j_l)D}{\mu_{tp}}. \tag{2.2.19}$$

2.2.4 The drift-flux model

The velocity of a slug bubble in a riser tube can be described relative to a moving liquid as presented in Equation 2.2.20:

$$V_t = C_0 V_m + V_{gj}, \tag{2.2.20}$$

where V_t is the rise velocity of the bubble, C_0 is the liquid slug velocity coefficient

and V_{gj} is the rise velocity of the same bubble in still fluid in $^{m}/_{s}$, also called the drift velocity and can also be defined as:

$$V_{gj} = V_g - j. \tag{2.2.21}$$

Nicklin et al. [30] suggested that the velocity of the Taylor bubble could also be calculated using Equation 2.2.22.

$$V_t = \frac{\forall_g}{\varepsilon A}, \tag{2.2.22}$$

where ε is the gas void ratio [30].

Combining Equations 2.2.5, 2.2.20 and 2.2.22 results in the following relationship, that summarizes the drift flux model:

$$\varepsilon = \frac{j_g}{C_0(j_l + j_g) + V_{gj}}. \tag{2.2.23}$$

Zuber and Findlay [44] published the same result for the analysis of two-phase flows, but used a different approach. Their correlation is applicable to any two-flow regime and takes into account the effect of non-uniform flow and concentration profiles which is accounted for by the distribution parameter C_0. The effect of the local relative velocity is also taken into account by the correlation developed by Zuber and Findlay via the weighted mean drift velocity $^{\varepsilon V_{gj}}/_{\varepsilon}$, which is not readily apparent from Equation 2.2.23 as described above; further details can be found in [44]. Both effects depend on the flow regime and appropriate velocities and expressions for the drift velocity need to be inserted. For the present study, slug flow regime was considered as it was reported to be the most efficient regime to

pump water [29]. Note that the Chexal and Lellouche model is not only applicable to one flow regime. In the present study, the drift flux model was applied to all the models but the one by Delano.

2.2.5 Nicklin model

Nicklin et al. [30] formulated an equation to calculate the velocity of slugs in steady two-phase flow in 1962. The expression is equivalent to the denominator in the drift-flux model (i.e.$C_0(j_l + j_g) + V_{gj}$, in Equation 2.2.23). This model has been used so widely that it is often considered the original slug flow model [42]. Nicklin used an approach developed by Dumitrescu [15] and Davies and Taylor [13] to describe the drift velocity:

$$V_{gj} = 0.35\sqrt{\frac{g(\rho_l - \rho_g)D}{\rho_l}} \approx 0.35\sqrt{gD}. \tag{2.2.24}$$

In addition, Nicklin also assumed:

$$C_0 = 1.2. \tag{2.2.25}$$

It is argued that the bubble is transported faster than the average flow as it is located in a high-velocity region (i.e. at the centreline) of the riser tube. The value of 1.2 was chosen because it describes the maximum to average velocity fully developed turbulent flow regime in cylindrical tubes [44]. The equations were tested for air and water in tubes with riser tube diameter between 0.63 and 2.5 inches (1.6 - 6.35 cm), no minimum or maximum pipe length was given [30].

2.2.6 Reinemann model

White et al. [41] and Zukoski [45] suggested in 1962 and 1966, respectively, that the effects of surface tension on the vertical flow becomes increasingly important when the riser tube diameter is decreased below a certain point, without coming up with a model to predict the flow. In 1990, Reinemann et al. [33] published a correlation for airlift pumps with riser tube diameters between 3 and 25 mm. It was noted that previous studies had been performed with riser tube diameters bigger than 20 mm in which the effect of surface tension is small and can be neglected. Reinemann et al. [33] considered the effects of surface tension, altering the drift velocity term to Equation 2.2.26:

$$V_{gj} = 0.352(1 - 3.18\Sigma - 14.77\Sigma^2), \tag{2.2.26}$$

where Σ is the surface tension number, calculated with:

$$\Sigma = \frac{\sigma}{\rho g D^2}, \tag{2.2.27}$$

where σ is the surface tension in $^{\mathrm{N}}/_{\mathrm{m}}$. C_0 remained 1.2. Kouremenos and Staicos [25] also focused on small riser tube diameter airlift pumps (between 12 and 19 mm). Their model was not considered for the present study it is not relevant for the riser tube diameters considered in the present study.

2.2.7 De Cachard & Delhaye model

De Cachard & Delhaye [6] also developed a correlation for small riser tube diameter airlift pumps, still using C_0 =1.2, but taking surface tension into account by altering the drift velocity to:

$$V_{gj} = 0.345(1 - e^{\left(\frac{-0.01N_f}{0.345}\right)})(1 - e^{\left(\frac{3.37 - Bo}{m}\right)})\sqrt{gD}, \tag{2.2.28}$$

where Bo is the Bond number and N_f is the Archimedes number, defined as:

$$Bo = \frac{(\rho_l - \rho_g)gD^2}{\sigma}, and \tag{2.2.29}$$

$$N_f = \frac{\rho_l(\rho_l - \rho_g)gD^3}{\mu_l^2}, \tag{2.2.30}$$

respectively. m is defined for different ranges of N_f:

when $N_f > 250$:

$$m = 10, \tag{2.2.31a}$$

when $18 < N_f < 250$:

$$m = 69N_f^{-0.35}, and \tag{2.2.31b}$$

when $N_f < 18$:

$$m = 25. \tag{2.2.31c}$$

It should be noted that De Cachard & Delhaye also modelled an acceleration component that was added to the pressure gradient. The component is based on a thin liquid film falling around the Taylor bubble, without interfacial shear stress, inside a vertical cylinder. The acceleration component was calculated for the various experimental conditions used in this study and found to be negligible.

De Cachard & Delhaye suggest to use this model for the design of small diameter riser tubes (up to 40 mm) and tall airlifts, with a length-to-diameter ratio greater than 250 [6].

2.2.8 Chexal-Lellouche model

The Chexal-Lellouche correlation was developed for a wide range of pressures, flows, void fractions, fluid types (steam-water, air-water, hydrocarbons and oxygen) and is valid for riser tube diameters up to 450 mm [8]. It is continuous and does not depend on flow regimes. The drift flux parameters C_0 and V_{gj} are not related to the drift flux model and can be determined for both, cocurrent and countercurrent flows.

The liquid slug velocity coefficient is defined as presented in Equation 2.2.32.

$$C_0 = \frac{L_c}{K_0 + (1 - K_0)\varepsilon^r}, \tag{2.2.32}$$

where L_c is the Chexal-Lellouche fluid parameter. It varies for different fluids, but for an air-water mixture it is defined as

$$L_c = min(1.15\varepsilon^{0.45}, 1). \tag{2.2.33}$$

Equation 2.2.32 consists of many parameters, which are defined as follows:

$$K_0 = B_1 + (1 - B_1)\left(\frac{\rho_g}{\rho_l}\right)^{0.25}, \tag{2.2.34}$$

$$r = \frac{1 + 1.57\frac{\rho_g}{\rho_l}}{1 - B_1}, \tag{2.2.35}$$

$$B_1 = min(0.8, A_1), and \tag{2.2.36}$$

$$A_1 = \frac{1}{1 + e^{\left(\frac{-Re_v}{60000}\right)}}, \tag{2.2.37}$$

where Re_v varies with Re_g and Re_l.

If $Re_g > Re_l$:

$$Re_v = Re_g, \tag{2.2.38a}$$

and if $Re_g \leq Re_l$:

$$Re_v = Re_l. \tag{2.2.38b}$$

The drift velocity is defined as:

$$V_{gj} = 1.41 \left[\frac{(\rho_l - \rho_g)\sigma g}{\rho_l^2}\right]^{0.25} C_1 C_2 C_3 C_4, \tag{2.2.39}$$

where

$$C_1 = (1 - \varepsilon)^{B_1}. \tag{2.2.40}$$

C_2 varies with the liquid to gas density ratio; details can be found in [8]. As the

density of the gas and the liquid entering the riser tube are generally constant, C_2 can be calculated as follows:

$$C_2 = 1 - e^{\left(\frac{-C_5}{1-C_5}\right)}, \tag{2.2.41}$$

$$C_3 = max(0.5, 2e^{\left(\frac{-Re_l}{300000}\right)}), and \tag{2.2.42}$$

$$C_7 = \left(\frac{D_2}{D}\right)^{0.6}, \tag{2.2.43}$$

where D_2 = 0.09144 m is a reference diameter. If $C_7 < 1$ then:

$$C_4 = \frac{1}{1 - e^{-C_8}}, \tag{2.2.44a}$$

else:

$$C_4 = 1, \tag{2.2.44b}$$

where

$$C_8 = \frac{C_7}{1 - C_7}. \tag{2.2.45}$$

For both riser tube diameters considered in the present study, C_7 was found to be larger than 1, thus Equation 2.2.44b was used.

$$C_5 = \sqrt{\frac{150}{\frac{\rho_l}{\rho_g}}}. \tag{2.2.46}$$

2.2.9 Delano model

Delano models an airlift pump as part of the Einstein refrigeration model. Instead of injecting air at the bottom of the riser tube, the riser tube is heated at the bottom, causing vapour bubbles to form and rise. This application is called vapour-lift pump and is a two-phase flow in a vertical riser tube- like an airlift pump, therefore the same models can be used. Delano's approach was referenced by other studies related to vapour-lift pumps ([35]). Delano uses the analysis of Stenning and Martin [36]. As mentioned earlier, this model does not use the drift flux model, but the following definition for the void fraction instead:

$$\varepsilon = \frac{1}{1 + S\frac{j_l}{j_g}} \tag{2.2.47}$$

According to Stenning and Martin, the value for the slip (S) is normally between 1.5 and 2.5 for the range of flows which yield the best performance [36]. Delano calculates the head loss in the system using:

$$K = \frac{4fL}{D}. \tag{2.2.48}$$

White [42] suggested to use the constants 2.5 and 17 for S and K, respectively (which was done in this study as well). Instead of Equation 2.2.12, Delano used the following equation for the basis of his model [14]:

$$\frac{H}{L} = \frac{1}{1 + \left[\frac{\dot{\forall}_g}{\dot{\forall}_l S}\right]} + \frac{j_l^2}{2gL}\left[K\left(1 + \frac{\dot{\forall}_g}{\dot{\forall}_l}\right) + 2\frac{\dot{\forall}_g}{\dot{\forall}_l} + 1\right]. \tag{2.2.49}$$

For the remainder of the present study, the models will be referred to with the

names of the authors.

2.3 MBR model

When modeling the MBRs, 6 different plant sizes with capacities of 0.5, 0.75, 1, 2, 5 and 10 MGD were considered. Before the membrane tank could be modeled, assumptions about the biological parameters had to be made, as discussed below.

2.3.1 Bioreactor tank

Equation 2.3.1 presents a mass balance of biomass for the bioreactor and membrane tank of an MBR.

$$\frac{dX}{dt}V = Q_i X i - Q_e X_e + \left(\mu_g \frac{S}{k_s + S} X - bX\right) V, \tag{2.3.1}$$

where X is the biomass in $^{kg}/_{m^3}$, S is the substrate in $^{kg}/_{m^3}$, μ_g is the maximum specific growth rate in $^{1}/_{day}$, k_s is the half-saturation concentration in $^{mg}/_{l}$, b is the endogenous decay rate in $^{1}/_{day}$ and the indices i and e stand for influent and effluent, respectively.

Assuming steady state conditions, no biomass in the effluent and that the incoming and outgoing flow are equal, replacing X_e by X and after some rewriting, Equation 2.3.1 becomes:

$$\frac{Q}{V} = \frac{1}{\theta_c} = \mu_g \frac{S}{k_s + S} X - b, \tag{2.3.2}$$

where θ_c is the sludge retention ime (SRT) in days.

Similarly, Equation 2.3.3 presents a mass balance of substrate for the bioreactor and membrane tank of an MBR.

$$\frac{dS}{dt}V = Q_i Si - Q_e S_e - \left(\frac{\mu_g}{Y}\frac{S}{k_s + S}X\right)V, \tag{2.3.3}$$

where Y is the biomass yield.

Assuming steady state conditions, that the incoming and outgoing flow are equal, replacing S_e by S and after some rewriting, Equation 2.3.3 becomes:

$$\frac{S_i - S}{\theta} = \frac{\mu_g}{Y}\frac{S}{k_s + S}X, \tag{2.3.4}$$

where θ is the hydraulic retention time (HRT). Using Equations 2.3.2 and 2.3.4, the achievable substrate concentration and the required HRT can be calculated. For the assumed kinematic stoichiometric parameters presented in the Table 2.3, the HRT results in 0.049 days. This HRT was used to size the MBRs as presented in Chapter 6.

Table 2.3: Parameters assumed for MBR model

Parameter	Sign	Value assumed
Maximum specific growth rate [$^{1}/_{\text{day}}$]	μ_g	6
Half-saturation concentration [$^{\text{mg}}/_{\text{l}}$]	k_s	40
Yield (ratio of mass of microorganisms formed (measured as VSS), to the mass of substrate consumed [-] [40]	Y	0.4
Endogenous decay rate [$^{1}/_{\text{day}}$]	b	0.12
Substrate in Influent [28] [$^{\text{mg}}/_{\text{L}}$]	S_i	210

Values for the decay rate b for conventional activated sludge and aerobic processes is typically in the range of 0.04 to 0.075 $^{1}/_{\text{day}}$ [22]. Experiments by Huang et al. [20] suggested a slightly higher decay rate for MBRs, but the chosen value is still in the appropriate range. Huang et al. also calculated that the biomass yield in MBRs is in the same range as in conventional systems; therefore, the typical value for CAS was used [28]. The value chosen for μ_g is the typical value for CAS systems presented in [28], as well, and the value for k_s is within the presented range [28]. It was assumed that the latter two parameters can be used for MBRs as well.

Chapter 3

Knowledge gap and objectives

As discussed in Section 2.1.7, MBRs have higher operation and maintenance costs than conventional systems. Previous work focused on this issue by reducing the power requirement through an optimization of the air scouring [21]. However, after the air is used for cleaning purposes, it is essentially wasted as it escapes into the atmosphere. The objective of the present study is to determine whether the excess air (which otherwise escapes to the atmosphere), can be used to airlift and convey return activated sludge (RAS) within an MBR system. In addition, optimum geometries for the design of the application were sought. These included the collector angle, submergence ratio, shape of air collector (square or rectangular) and the water redirection system.

Replacing electrically driven pumps, even if only partially with airlift pumps, powered with escaping air, could result in a significant reduction in energy use. In order to determine the feasibility of this approach, several tasks had to be accomplished. The tasks that address the objectives are the following:

- Task 1: Model water flow of airlift pumps
  - Compare the results from exiting models to those obtained experimentally
  - Modify existing models as needed to reliably predict water flow in air lift pumps
- Task 2: Model the extent of which RAS can be pumped using waste air for MBR plants with treatment capacities ranging from 0.5 and 10 MGD
- Task 3: Design a pilot airlift RAS pump prototype
  - Design air collector
  - Design water redirection system
- Task 4: Compare results from pilot scale experiments to those obtained by modeling.

Chapter 4

Materials and methods

A bench and a pilot scale setup were build as part of this present study. These were used to validate the numerical model considered, and to confirm the feasibility of conveying return activated sludge (RAS) within an MBR system, using airlift pumps. Both setups consist of the following items:

- Riser tube
- Tank
- Air supply
- Water flow measurement

The different setups are presented in Figure 4.1 and are discussed below.

4.1 Bench scale system

The experimental setup consisted of a vertical cylindrical riser tube partially submerged in a plexiglas tank (Fig. 4.1 A)). The tank dimensions were 15 cm (W) *

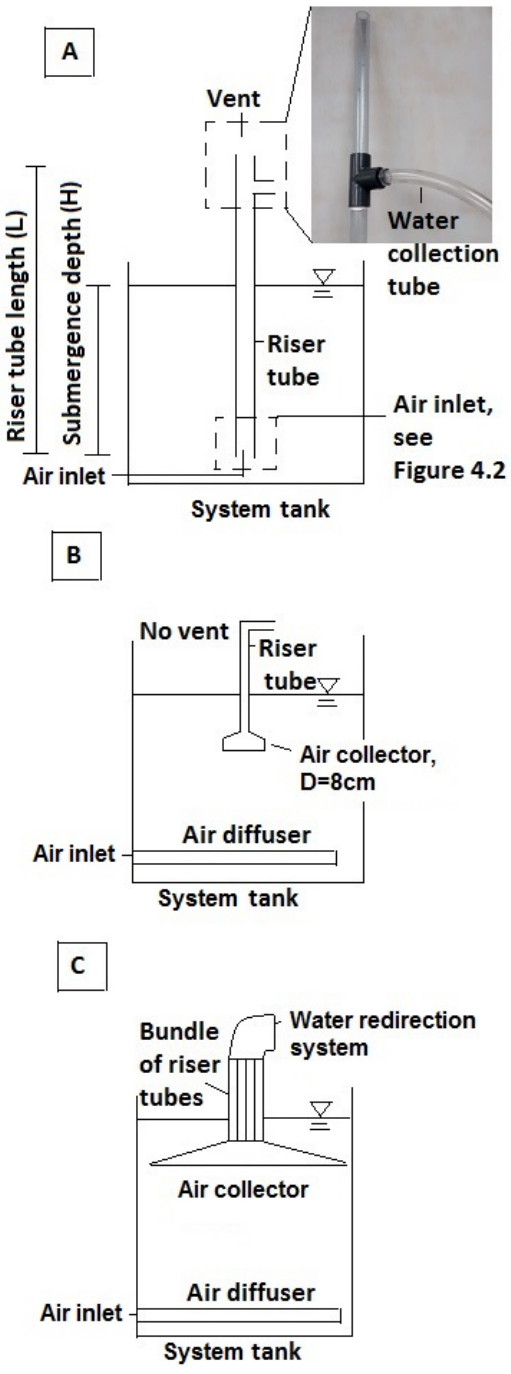

Figure 4.1: Experimental setups of the airlift pump.
A) bench scale setup, discussed in Section 4.1, B) setup for preliminary testing, discussed in Section 4.2.1, C) pilot scale setup, discussed in Section4.2.3

90 cm (L) * 150 cm (D). The riser tube was attached to the side of the tank. Poly vinyl chloride (PVC) riser tubes with lengths of 1 and 2 meter, and riser tube inner diameters of $^3/_4$ inch (1.905cm) and 1 inch (2.54 cm) were considered.

Air was injected through a nozzle located at the bottom of the riser tube (Fig. 4.2). The inner and outer diameter of the air inlet nozzle were 3.6 and 5.7 mm, respectively (additional dimensions are presented in Table 4.1). A valve and flowmeter with an accuracy of 3% (1G08R3, Key Instruments), with glass float was used to control and measure the air flow rate. Air flow rates of 6.0, 7.6, 9.1, 10.7, 12.3, 13.9, 15.5, 17.1, 18.7, 20.4, 22.1 $^{L}/_{min}$, corresponding to rates at standard atmospheric conditions, were considered.

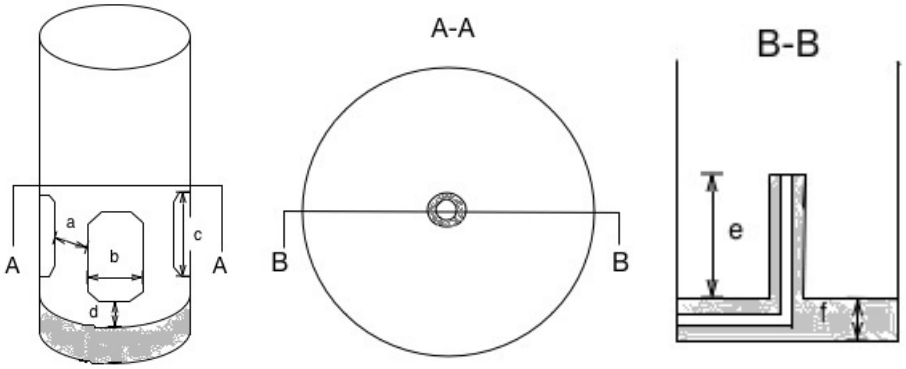

(a) (b) (c)

Figure 4.2: Water and air inlet of airlift pump.
The shaded areas correspond to the nozzle assembly which was also used to provide air. Dimensions can be found in Table 4.1; a) base of riser tube; b) horizontal cross section of riser tube nozzle; c) vertical cross section of riser tube and nozzle.

A T-connection with a side horizontal tube was placed at the height of the riser

Table 4.1: Dimensions of water and air inlet of airlift pump (see Fig. 4.2) in mm.

Riser tube diameter [inch]	Section					
	a	b	c	d	e	f
3/4	7	13	19.3	4	8	17.7
1	7	14.25	19.5	4	8	17.7

tube where water was to be collected (Fig 4.1 a). Water flow gas lifted through the riser tube was determined by measuring the volume of water collected from the tube connected to the T-connection over a period of 30 seconds. All water flow measurements were done in triplicate. Water collected to measure the flow was returned to the tank. A summary of the experimental conditions considered is presented in Table 4.2.

Table 4.2: Experimental conditions for the bench scale setup.

	Riser tube		
Experiment number	Length [m]	Diameter [inch]	Submergence ratio α
1	1	3/4	0.5
2			0.4
3			0.3
4		1	0.5
5			0.4
6			0.3
7	2	3/4	0.5
8			0.45
9			0.4
10		1	0.5
11			0.45
12			0.4

For each condition, air flow rates of 6.0, 7.6, 9.1, 10.7, 12.3, 13.9, 15.5, 17.1, 18.7, 20.4, 22.1 $^{L}/_{min}$ were considered. As mentioned in Section 2.2.1, the submergence ratio (α) is the ratio of the submergence depth to the riser tube length ($^{H}/_{L}$)

4.2 Scale-up from bench to pilot scale

4.2.1 Single riser tube system

The experimental setup consisted of a 54 cm long vertical cylindrical PVC riser tube, with a riser tube diameter of $^{3}/_{4}$ inch (1.905 cm) partially submerged in a

stainless steel tank (Fig. 4.1 B). The tank dimensions were 85 (D) cm *45 (W) cm *213 (H) cm. The tank provides space for a membrane cassette (ZW500, GE, Oakville, Canada). Note that no membrane cassette was present during any experiments. The riser tube was held vertically in the tank by hand.

The air was supplied to the tank through an air diffuser which was attached to an F-450 flowmeter (blue-white, USA). The diffuser consists of a one inch pipe with $1/4$ inch diameter holes drilled into it, each ten cm apart from each other, enabling an evenly distributed air supply in the tank. Air flow rates of 81.2, 142.5 and 203.7 L/min, corresponding to rates at standard atmospheric conditions, were considered. The air flow calibration will be discussed in Section 4.2.2. The air was not directly injected into the riser tube; it was collected over an area of 50.3 cm^2 using a cylindrical collector attached to the base of the riser tube (Fig. 4.1 B). Water flow gas lifted through the riser tube was determined by measuring the volume of water collected from the tube connected to the L-connection over a period of 30 seconds. All water flow measurements were done in triplicate. Water collected to measure the flow was returned to the tank.

4.2.2 Air flow calibration

The cross sectional distribution of air flow at the surface of the water in the tank was characterized using an inverted 2 L graduated cylinder filled with water. The air flow was determined based on the volume of air that accumulated in the inverted cylinder over a given time period at nine different locations in the tank (Fig. C.1). Air flow rates of 81.2, 142.5 and 203.7 L/min, corresponding to rates at standard atmospheric conditions, were considered. Measurements at each location were

taken in triplicate. The average air flow measured with the cross sectional area of the cylinder ($\approx 0.005 m^2$) was then extrapolated to the area in the tank.

4.2.3 Bundle of riser tubes

The tank, air addition and air flow rates when considering a bundle of riser tubes was identical to those for the single riser tube system, which was discussed in Section 4.2.1. However, the number of riser tubes, the area over which the air was collected, and the water flow measurements differed for the bundle of riser tubes and the single tube system.

A bundle of 19 tubes was considered as an alternative to multiple individual riser tubes. As discussed in Chapter 5, tube diameters of $3/4$ inch (1.905 cm) could more effectively lift liquid than 1 inch (2.54 cm) riser tubes. For this reason, $3/4$ inch tubes were used in the present study. A total bundle diameter of 10 inch (25.4 cm) was considered to be compatible with piping diameters commonly used at wastewater treatment plants. 19 thin walled aluminum riser tubes could be fit into a 10 inch diameter pipe. The space between the tubes was sealed using silicone. The riser tube at the centerline of the bundle was placed 0.5 cm higher than the ones next to it, while the ones on the perifory of the bundle were another 1 cm lower than the centerline tube (Fig. 4.3 a), allowing a better distribution of air to the tubes. For the calculations, the slight height differences between the riser tubes at the centerline and perifory were neglected. The riser tubes were all 46 cm long.

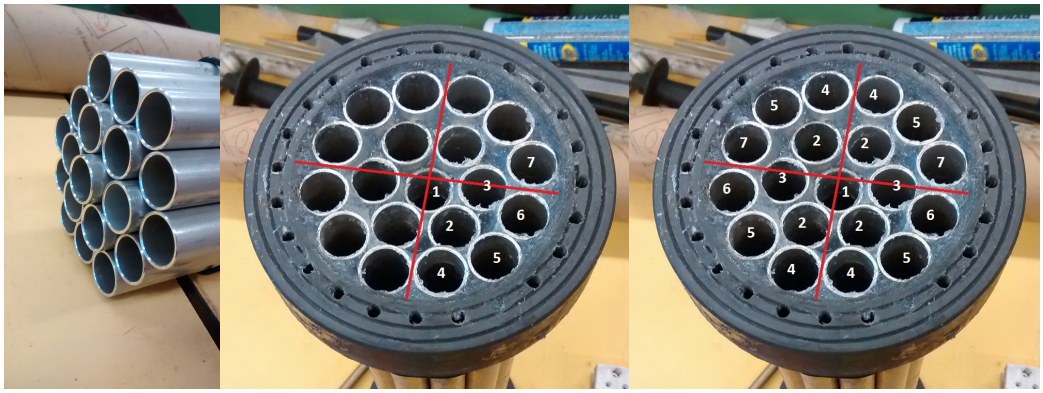

(a) Top view (b) Individually measured riser tubes and numbers they represent (c) Assumed distribution of riser tubes

Figure 4.3: Airlift riser tubes used in the air collection system.

The lower end of the riser tubes was attached to the air collection apparatus as presented in Figure 4.4. Two geometries were considered for the air collector. The first was rectangular in shape and was sized (83 cm * 43 cm) to be approximately equivalent to the surface area of the tank. The second had a square geometry (43 cm * 43 cm). The top of the air collector was made of a flexible material, enabling the angle of the base of the collector to be easily adjusted by lifting the bundle of riser tubes above the base of the air collector. Three base angles were considered, 0°, 6.7° and 13.2°. The collector angle corresponds to $\tan^{liftheight}/_{43/2}$, all dimensions in cm. Therefore, for the rectangular collector, only the short collector side will be reported (angles 3.2° & 6.7° for long and short side, respectively will be represented by 6.7°, while angles: 6.3° & 13.2° will be represented by 13.2°), as the short side of the rectangular collector equals the collector angle of the squared collector.

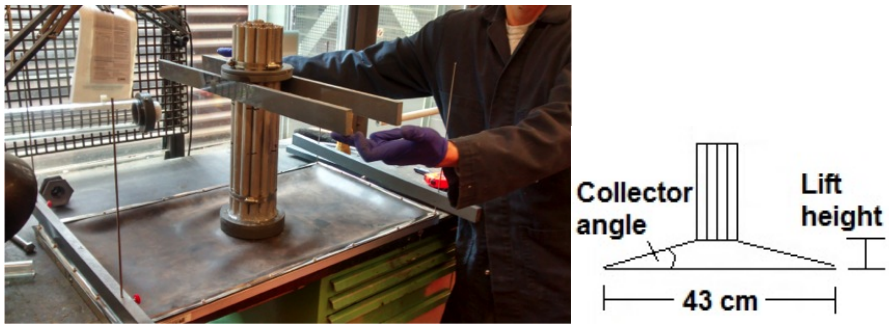

(a) (b)

Figure 4.4: Experimental setup of bundle of riser tubes attached to air collection apparatus
a) picture; b) illustration.

The rectangular collector was assumed to trap most of the air added to the base of the tank. Because the size of the collector was slightly smaller than the surface area of the tank, some air did escape along the sides of the frame. The amount of air trapped by the collector was assumed to be equal to 90% of the air added to the base of the tank. For the square collector, all of the air exiting the top of the tank, over the area occupied by the air collector, was trapped.

Because of symmetry, water flow measurements were only performed within one quadrant of the bundled riser tubes as illustrated in Figure 4.3 b), and the results extrapolated to all the tubes in the bundle (as illustrated in Figure 4.3 c)). To measure the water flow through an individual riser tube within the bundle, a section of flexible tubing was temporarily placed at the top end of the riser tube to direct the gas lifted water into a container. Note that the flexible tubing increased the length of the tube from 46 to 54 cm. This length difference was taken into account when water flows were modeled. Two submergence ratios, $\alpha = 0.44$ (L=54cm, H=24cm),

and α = 0.65 (L=0.54cm, H= 35 cm) were considered. Flow was determined based on the volume of liquid that accumulated in the container over a given time period. Water collected in the container was returned to the tank to maintain a constant liquid level. Flow measurements were done in triplicate.

A summary of the experimental conditions investigated is presented in Table 4.3. The experimental conditions that were considered are also illustrated in Figure 4.5.

Table 4.3: Experimental conditions for bundle of riser tube setup.

Experiment nr.	Air collection frame geometry	Riser tube diameter [inch]	Submergence ratio (α)	Collector angle [°]
1	rectangular	3/4	0.44	0
2				6.7
3				13.2
4			0.65	0
5				6.7
6				13.2
7	square	3/4	0.44	0
8				6.7
9				13.2
10			0.65	0
11				6.7
12				13.2

For each experiment, the air flow rates 81.2, 142.5 and 203.7 $^{L}/_{min}$ were considered.

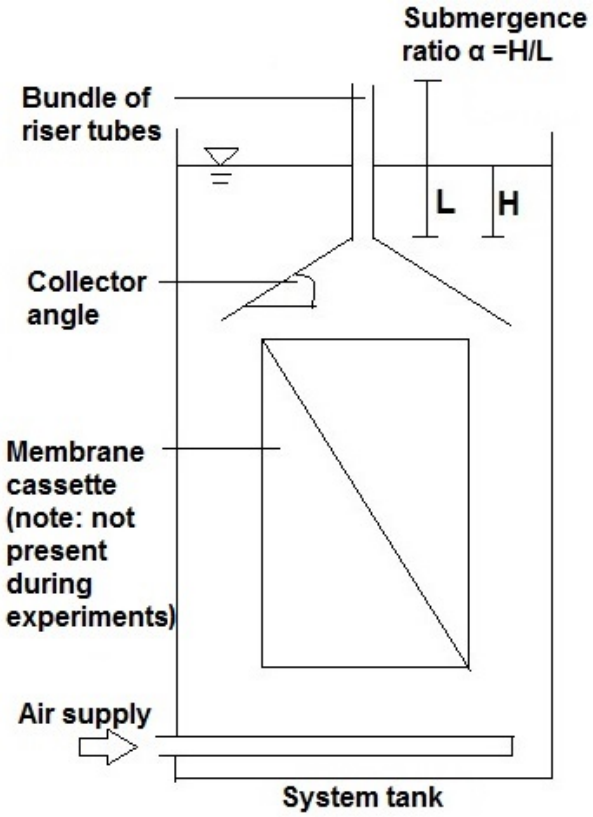

Figure 4.5: Illustration of experimental conditions for bundle of riser tubes that were varied for both, the rectangular and square collectors: submergence ratio α, collector angles and different air flows.

4.2.4 Water redirection system

The vertical flow through each of the riser tubes in the bundle must be redirected to flow horizontally. Four options to achieve this were considered:

1. a simple 90 degree elbow (D=4 inches, equivalent to 10.16cm) to redirect the bulk of the flow from the riser tube bundle (Fig. 4.6 a)),

2. a 90 degree elbow (D=4 inches (10.16 cm)) into which nine flexble tubes

were placed to redirect the flow from different sections of the riser tube bundle (note: the flexible tubes were not directly connected to the riser tubes),

3. flexible tubes joined to the top of each riser tube in a bundle, with approximately half of the flexible tubes grouped together and bent to one side, the other half grouped together and bent to the opposite side, effectively forming two bundles of 90° elbows pointing away from each other (Fig. 4.6 b)), and

4. flexible tubes joined to the top of each riser tube in a bundle, with all flexible tubes grouped together and bent to one side, effectively forming a bundle of 90° elbows (Fig. 4.6 c)).

These systems will from now on be referred to as configurations A through D, respectively.

(a) (b) (c)

Figure 4.6: Configurations A, C and D.

The water redirection experiments were examined using the square collector setup.

A comparison of these 4 alternative designs to redirect the vertical flow from the riser tubes was performed for a selected set of experimental conditions as presented

in Table 4.4.

Table 4.4: Experimental conditions for gas lifted water collection setup.

Experimental condition	Set-points considered
Length (L) [cm]	62.5
Submerged depth (H) [cm]	27.5
Submergence ratio (α)	0.44
Collector angle [°]	6.7, 13.2
Air flow [$^{L}/_{min}$]	81.2, 142.5, 203.7

4.2.5 MBR system and RAS piping

The present study considered pumping mixed liquor using airlift pumps above the membrane tank, enabling it to flow by gravity to the bioreactor tank. Therefore, in addition to bench and pilot scale equipment used, the present study also considered full scale MBR systems. Although full scale MBR systems were not built, it was necessary to size them (i.e. determine dimensions of system tanks) to address the research objectives.

Full scale MBR systems, with capacities of 0.5, 0.75, 1,2,5 and 10 MGD (1 MGD is equivalent to $3.785 * 10^6$ $^{L}/_{day}$), were considered. This range was selected because it corresponds to the capacities of most existing MBRs. The sizing was important because the longer the distance between the membrane tank and the bioreactor tank, the longer the pipe between these two tanks and therefore the greater the head loss. As a consequence, the elevation to which the mixed liquor from the membrane tank needs to be air lifted increases with the size of the MBR system. The design of MBRs is highly site, application, membrane type and manufacturer specific. For the present study, a number of assumptions were considered in deter-

mining the dimensions of the system tank.

Based on the biological parameters presented in Section 2.3.1, the tank sizes of the MBRs within the considered flow ranges had to be determined. The following configurations and constraints were used.

Configurations and constraints

The membrane area required for the MBRs was calculated using Equation 4.2.1.

$$A_{membrane} = \frac{\text{Flow capacity}}{\text{Flux}} \tag{4.2.1}$$

A flux of 25 lmh was assumed. Based on the required membrane area, the required number of membrane cassettes was determined. It was assumed that the membrane area in a module is of 31.2 m^2 [18] and a cassette consists of 48 modules [17], as is typical for ZW 500 MBRs (GE water and process technologies, Oakville, Canada). The cassettes were assumed to be placed next to each other without spacing between them in a "train". The maximum number of cassettes per train was assumed to be seven.

The following conventions were assumed in sizing the membrane tank component of an MBR.

- The foot print area of all cassettes in the tank is 50% of the total foot print area of the membrane tank (Fig. 4.7).
- The distance between the cassettes and the tank wall on the short sides is considered to be negligible (shaded area in Fig. 4.7). For example, the foot

print area of the three cassettes required in a 0.5 MGD plant is approximately 11 m^2, therefore the total foot print area of the membrane tank is approximately 22 m^2. Because the volume of the shorter side of the membrane tank is negligible, the longer side is 5.235 m long (which is equivalent the length of a cassette).

- The distance between the top of the cassette and the liquid level in the tank is 0.35 m.
- The distance between the bottom of the cassette and the bottom of the tank is 0.25 m.
- The height of the water in the tank is 3.145 m, which is the height of the cassette (2.545 m, [17]), plus the sum of 0.35 m and 0.25 m.
- The bioreactor tank wall is located next to the long side of the membrane tank, with both having the same length. Figure 4.7 presents the 0.5 MGD plant as an example, where the bioreactor would share the 5.2 m wall.

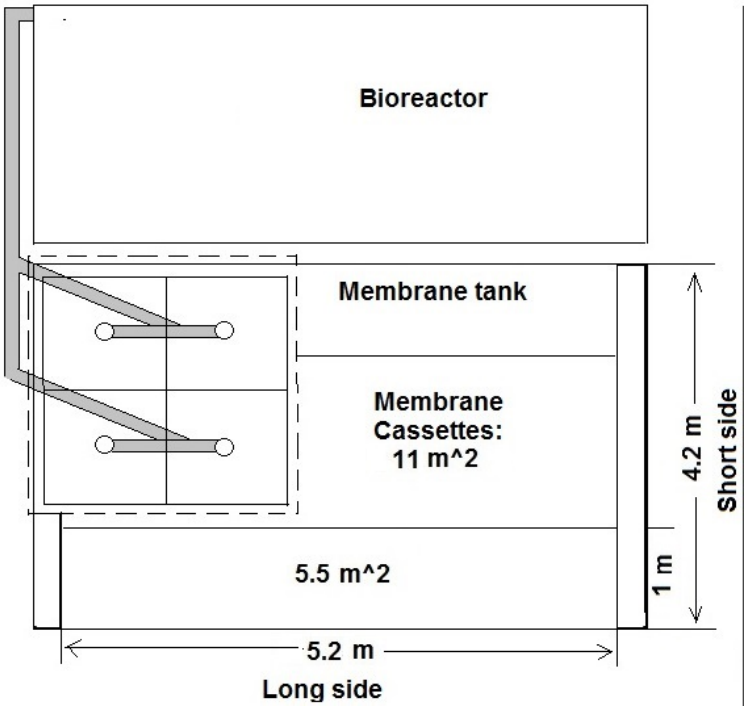

Figure 4.7: Top view of a 0.5 MGD plant according to assumptions made in the present study. The bundle of riser tubes setup is illustrated in the dashed lines, the shaded areas are RAS pipes.

The total volume of both, the bioreactor tank and the membrane tank was assumed to be:

$$V = \theta * \dot{V} \tag{4.2.2}$$

where V is the volume in m^3 and $\dot{V}$ is the incoming flow in $^{m^3}/_{d}$. θ is the Hydraulic Retention Time (HRT), it was calculated in Section 2.3.1.

Based on the dimensions of the system tank, it is possible to estimate the distance over which the RAS must be conveyed. The following assumptions were consid-

ered in determining the distance over which the RAS is conveyed for MBRs with different capacities.

- The length of the riser tube is based on the height required to provide enough head loss to let the wastewater flow back by gravity plus an additional 10 cm safety factor. This is discussed in Section 4.2.6.
- Head loss is calculated based on the length of the RAS conveyance pipe and assuming that two 90 degree elbows are located within the RAS pipe. The length of the pipes transporting the RAS was assumed to be width of the membrane and bioreactor tank, plus a safety factor of one meter.
- Several pipes convey the RAS to biological reactor (with D=10.16 cm). The number of pipes assumed differs for different treatment capacities and are presented in Table 6.2.
- RAS pipes are located on the side of the tanks providing easy access to membranes if required, as illustrated in Figure 4.7.

4.2.6 Calculation of achievable RAS

Water flow through an air lift pump generally increases as the air flow increases. However, a point of diminishing return occurs above which a further increase in air flow does not result in a proportional increase in water flow. The air flow to the individual riser tubes in the riser tube bundle was selected as the air flow at the point of diminishing return. This approach is consistent with that reported by Kassab et al. [23] who suggested that the maximum efficiency does not occur at the maximum water mass flow rate. The resulting total flow to all riser tubes in a

bundle was the sum of the air flow corresponding to the point of diminishing return for individual riser tubes. This will be further discussed in Section 6.3.

The distribution of the air in the membrane tank is not known. To investigate the potential effect of the distribution of the air flow, three different scenarios were considered.

1. 100% of the air can be collected from a location directly above the membrane cassettes
2. 90% of the air can be collected from a location directly above the membrane cassettes, 10% of the air can be collected from the sides
3. 75% of the air can be collected from a location directly above the membrane cassettes, 25% of the air can be collected from the sides

This will be further discussed in Section 6.3.

Chapter 5

Comparison of model and measured results for single riser tube in bench system

The models presented in Section 2.2.1 were solved using the program engineering equation solver (EES) for the conditions outlined in Section 4.1. The modeled results were compared with the measured results for the single riser tube experiments at bench-scale, to assess their validity.

5.1 Comparison of models to experimental results

The models generally overpredicted the water flow measured experimentally. A representative plot comparing the modeled and measured results is presented in Figure 5.1 . (Note: all model and experimental measurements for all conditions

investigated are presented in appendix B). The discrepancy between the modeled and measured results was lowest over the lower range of air flow considered (below 10 $^{L}/_{min}$), and increased as the air flow increased. The fit of the Delano model to the data was the poorest. This model overpredicted the liquid flow at low air flows and underpredicted the liquid flow at high air flows. Although the overall trend between modeled and measured data was better for the Reinemann and Chexal-Lellouche models, these models could not be solved for low flows (i.e. air flows lower than approximately 5 $^{L}/_{min}$). For these reasons, the Delano, Reinemann and Chexal-Lellouche models were not further considered.

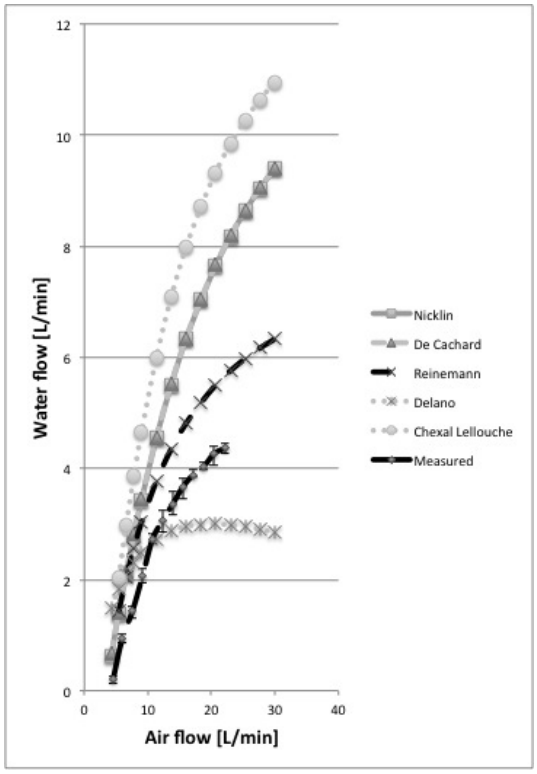

Figure 5.1: Compairison of model and measured results.
(Error bars correspond to minimum and maximum values. (D=3/4 inch, riser tube length 1m, lift 0.5m))

The results for the Nicklin and De Cachard & Delhaye models were similar over the range of air flows considered. The main difference between the two models is the the drift velocity V_{gj} calculation (see Section 2.2.1). Although the Nicklin Model overestimated the liquid flow at a given air flow, the overall trend of increase in liquid flow with air flow was consistent with the measured results. Also, the Nicklin model could be solved for low flow conditions, and is simpler than the De Cachard & Delhaye model. For these reasons, the Nicklin model was considered in the present study.

For the remainder of this study, only the smaller riser tube diameter ($^3/_4$ inch) was considered because it achieved higher water flows compared to larger riser tube diameters. For example, for a submergence ratio of 0.5, higher water flows were achieved compared to the riser tube with the one inch diameter (Fig. 5.2a) and B.3a)). Also, the smaller riser tube diameter achieved water flows up to a submergence ratio of α=0.7 (Fig. 5.2c), while 1 inch riser tubes barely lifted water when a low submergence ratio of 0.55 was used (Fig. B.3b)).

5.2 Modifications to the model

The Nicklin model (as well as the other models considered) were developed for long tubular configurations. For these conditions, entrance and exit losses can be ignored. However, when dealing with relatively short tubular configurations, as considered in the present study, entrance and exit losses can become significant.

The Nicklin model was modified to incorporate a head loss term as presented in Section 2.2.2. Because of the nature of the entrance and exit of the tubular config-

uration considered, the specific entrance or exit loss constant K was unknown. The value of the sum of the entrance and exit loss constant K for the setup considered was determined by fitting the modified Nicklin model to the measured results.

Estimated best fit values for the different experimental conditions investigated are summarized in Table 5.1. As indicated, no single K-value could be used to match the modeled to the measured results over the entire range of air flows considered. This was unexpected because K-values associated with entrance and exit losses are considered to be constants. It is likely that in addition to entrance and exit losses, other mechanisms, which are not accounted for in the models considered, affect behaviour of the airlift riser tubes.

Table 5.1: K-values for D= $^3/_4$ inch.

n.a.: Model did not fit data for any K-value considered.

Riser tube length [m]	Submergence ratio α		
	0.5	0.4	0.3
1	0.7	1	1
	Submergence ratio α		
	0.5	0.45	0.4
2	Approximately between 0.2 and 0.4	1	n.a.

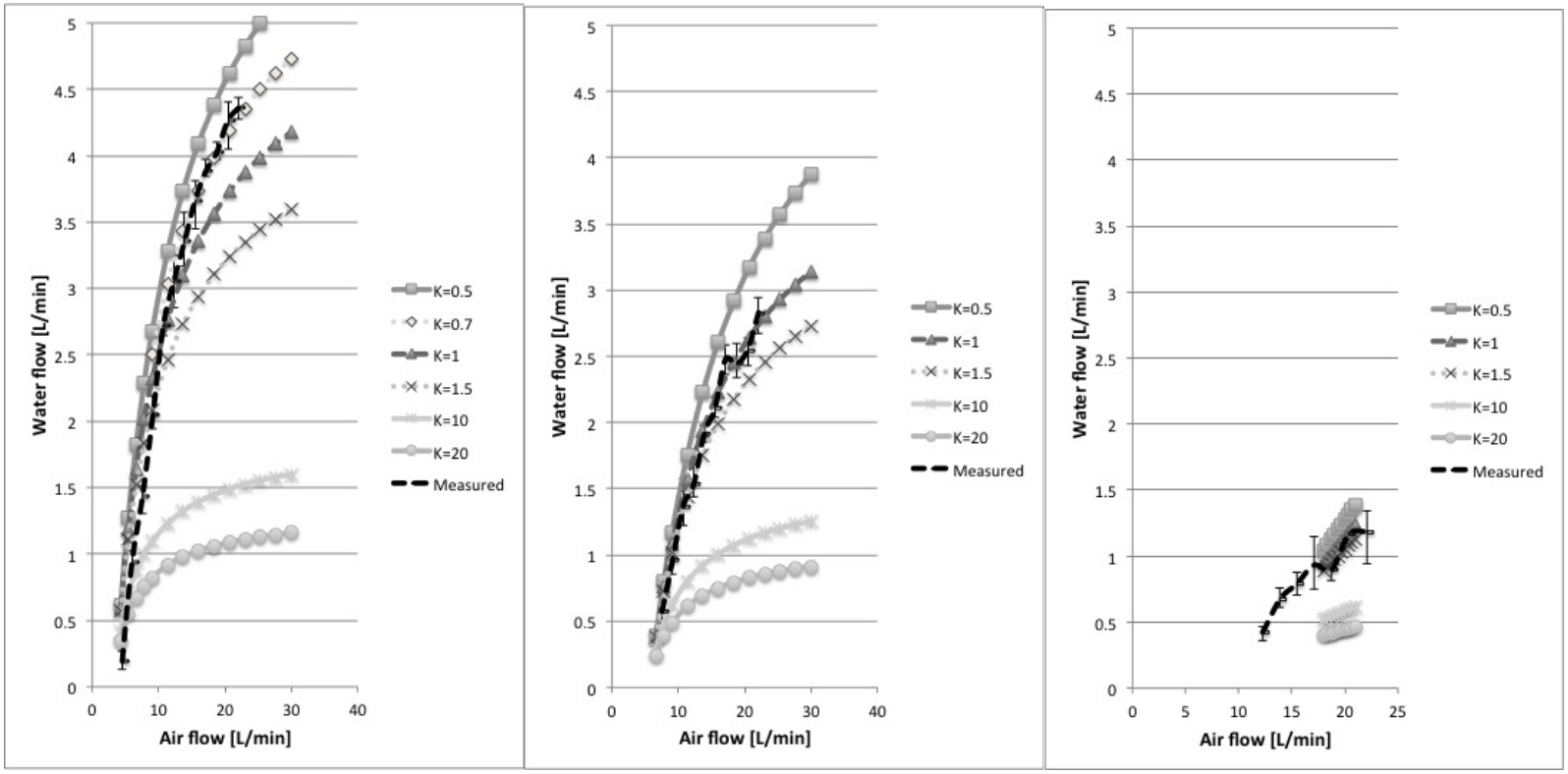

Figure 5.2: Evaluation of head loss coefficient using riser tubes with D=3/4 inch, 1m long.
(Error bars correspond to minimum and maximum values. (a: Lift 0.5m, b: Lift 0.6m, c: Lift 0.7m))

To identify the best K-value to apply, a range of values, corresponding to those in Table 5.1 were considered for the different experimental conditions investigated. As illustrated in Figure 5.2 a), no single head loss coefficient could be used to accurately model the measured results over the entire range of air flows considered. At low air flow, the K value had limited effect on model results. This was expected because the head loss associated with entrance and exit losses is proportional to the square of the flow. However, at higher flows, the modeled and measured results were similar, when a K-value of approximately 1 was assumed.

For the remainder of this present study, the K-value associated with entrance and exit losses was assumed to be 1. As illustrated in Figure 5.3, assuming a K-value of 1 generates results that are consistently similar to measured results (i.e. 1:1 slope of Figure 5.3).

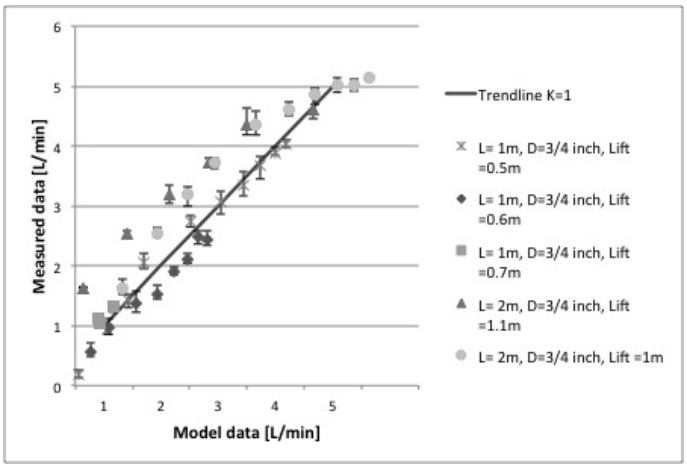

Figure 5.3: Experimental vs. modeled data for K=1.
(Error bars correspond to minimum and maximum values.)

Chapter 6

Theoretical energy savings for different scenarios

The modified Nicklin model (i.e. including entrance and exit losses, see Section 5.2) was used to estimate the amount of mixed liquor in an MBR that could be pumped from the membrane tank to the head of the biological tank, (i.e. the RAS flow).

6.1 Plant footprint, RAS pumping distance and available air for pumping

The RAS flow is expressed as a percentage of the influent flow to the MBR. Six plant sizes with different capacities were considered (0.5, 0.75, 1, 2, 5 and 10 MGD; 1 MGD is equivalent to $3.785 * 10^6$ $^{L}/_{day}$). The range of sizes was selected because the most common treatment plants are able to treat 1 to 5 MGD, and installations of sizes of 10 MGD or more are expected to increase [40]. To estimate the distance over which the RAS needed to be pumped, the footprint of an MBR

was estimated using the configurations and constraints outlined in Section 4.2.5.

All of the air introduced for fouling control was assumed to be available for air lifting. As presented in Section 4.2.6, the air present in the tank was assumed to be 0.12 m^3/m^2hr [11]. Thus, the membrane area per MBR size was determined using Equation 4.2.1. Reactor dimensions, membrane area, supplied air per reactor and distances over which the RAS must be pumped for the different MBR plant sizes considered are summarized in Table 6.1.

Table 6.1: MBR dimensions and RAS piping distances.

	MBR system size [MGD] (1 MGD is equivalent to 3.785 $^{L}/_{day}$)					
	0.5	0.75	1	2	5	10
Volume [m^3]	93.0	139.5	186.0	372.0	930.0	1860.1
Volume membrane tank [m^3]	69.4	92.8	116.2	232.1	608.9	973.9
Volume bioreactor tank [m^3]	23.6	46.7	69.8	140.0	321.1	886.2
Width membrane tank [m]	4.2	4.2	4.2	8.5	12.2	12.2
Length membrane tank [m]	5.2	7.0	8.7	8.7	15.8	25.3
Height water level [m]	3.1	3.1	3.1	3.1	3.1	3.1
Height tank wall [m]	4.0	4.0	4.0	4.0	4.0	4.0
Calculated width of bioreactor tank [m]	1.4	2.1	2.5	5.1	6.4	11.1
Length RAS pipe [m]	9.5	10.2	10.7	20.3	30.4	32.7
Membrane area [m^2]	3154.2	4731.3	6308.3	12616.7	31541.7	63083.3
Air supplied in tank [$^{m^3}/_{h}$]	378.5	567.8	757.0	1514.0	3785.0	7570.0

6.2 Head loss for RAS pumping

In order to be conservative, the diameter of the transporting pipes was assumed to be 4 inches (10.16 cm), and a high average wall roughness height of e= 0.00026 m [32] was assumed. Friction factors were determined using a Moody diagram. Results are presented in Table 6.2.

Table 6.2: Head loss calculations for RAS pipes.

Multiple pipes were considered in order to reduce head loss.

	MBR system size [MGD] (1 MGD is equivalent to 3.785 $^{L}/_{day}$)					
	0.5	0.75	1	2	5	10
Single pipe transporting sludge						
Velocity [$^{m}/_{s}$]	0.86	1.29	1.72	3.45	8.62	17.25
Reynolds	87266.7	130900.0	174533.3	349066.7	872666.7	1745333.5
f factor	0.036	0.032	0.030	0.028	0.026	0.025
Head loss [m]	0.13	0.29	0.50	3.55	30.90	128.11
Multiple pipes transporting sludge						
Number of pipes	2	2	2	3	9	
RAS per pipe [$^{L}/_{min}$]	2628.5	3942.7	5256.9	7009.3	8761.6	11682.1
Velocity [$^{m}/_{s}$]	0.43	0.65	0.86	1.15	1.45	1.91
Reynolds	43633.3	65450.0	87266.7	116355.6	145444.5	193925.9
f factor	0.045	0.037	0.035	0.032	0.031	0.030
Head loss [m]	0.06	0.13	0.22	0.59	1.23	2.27

6.3 RAS pumping

The height to which the activated sludge had to be lifted included the head loss generated when RAS flowed from the top of the riser tube bundle (total length (L) - submerged depth (H)) to the head of the biological tank and two 90° elbows, plus a 10 cm safety factor. This sum was calculated for all 6 MBR sizes considered.

As discussed in Section 4.2.5, the depth of the liquid above the cassettes in a membrane tank is approximately 35 cm. Two different riser tube submergence depths (both ending above the membrane cassette) were considered: 20 cm (scenario A and B, see Table 6.3) and 30 cm (scenario C, see Table 6.3). These two submerged lengths allow for either 15 or 5 cm between the cassette and riser tubes, to accommodate an air collector.

Table 6.3: Scenarios considered for RAS pumping for air that can be collected from directly above the membrane cassettes.

	Scenario		
Parameter	A	B	C
Submerged depth (H) [cm]	20	20	30
Head loss (h_l) cm	Depends on MBR size, see Table 6.2		
Safety factor (SF)	20	10	10
Length (L) [cm]	20 + h_l +20	20 +h_l + 10	30 + h_l +10

The Length (L) of the riser tubes of each scenario is based on the sum H + h_l + SF.

In the experiments to study the pilot scale application, a setup with a bundle of riser tubes was built to investigate scenario C in a 0.5 MGD plant. This setup had a total

length ‘L’ of 30 cm + 6 cm (h_l for 0.5 MGD, see Section 6.2) + 10 cm = 46 cm. This setup was then repurposed with a shorter submerged depth of 20 cm, scenario A. Since the riser tube setup was the same in scenarios A and C, the effective safety factor in scenario a is 20 cm.

In order to model the scenarios presented in Table 6.3, the experimental riser tube configuration (H + SF = 40 cm) was considered for or all six plant sizes (i.e. values of h_l), including the 0.5 MGD size from the experiment.

As discussed in Section 4.2.6, it is not known where on the surface of an MBR tank the air escapes. Table 6.4 presents three possible distributions of air in the different tank sizes, corresponding to the assumptions made. The fate of the escaping air was modeled using scenarios A, B and C for air escaping directly above the cassette. The fate of the escaping air was modeled using options I and II for air escaping at the sides of the cassette (either submergence of 50 or 60 cm, respectively). Options I and II allow for deeper submergence of the riser tube, as there is no cassette in the way. Thus, for each air distribution and plant size, all possible combinations of scenarios A,B,C and options I and II were modeled, as summarized in Table 6.5.

A range of air flows per riser tube was considered (i.e. discrete values between 2.5 and 15 $^{\mathrm{L}}/_{\mathrm{min}}$). By applying the modified Nicklin model to this range of air flows and the riser tube lengths and submergence ratios from scenarios A, B and C, 10 values of water flows for individual riser tubes were determined at equal intervals. The air available per condition (see Table 6.4) was then divided by the respective considered air flows per riser tube, resulting in the number of riser tubes required

Table 6.4: Available air flow [L/min] from membranes.

Distribution of air	Plant size [MGD]					
	0.5	0.75	1	2	5	10
	Air flow [$^{L}/_{min}$]					
100% above module	6308	9613	12617	25233	63083	126167
90% above module,	5678	8651	11355	22710	56775	113550
10% on side	631	961	1262	2523	6308	12617
75% above module,	4731	7209	9463	18925	47313	94625
25% on side	1577	2403	3154	6308	15770	31542

Table 6.5: Scenarios and options considered for assumptions made about location of escaping air.

Distribution of air	All plant sizes considered
100% above module	Scenario A, B and C
90% above module, 10% on side	Scenario A, B and C Option I and II
75% above module, 25% on side	Scenario A, B and C Option I and II

for the tank in each scenario. The calculated water flows were then multiplied by the respective number of riser tubes to find the total water flow for each condition and scenario. Optimum conditions were those which generated the highest RAS flow. Results for scenario a in 0.5 MGD plant are presented in Tables 6.6 to 6.8. The results of the other treatment plant sizes and scenarios considered are presented in Appendix D. In the tables, optimal conditions are identified.

Table 6.6: Scenario A, 0.5 MGD ($1.89 * 10^6$ L/day), 100% of air above module.

	L [m]	H [m]	Air above module, air per riser tube [L/min]						
	0.46	0.2	6.00	7.00	8.00	9.00	**10.00**	11.00	12.00
Water flow per riser tube [L/min]			0.77	1.12	1.42	1.67	**1.89**	2.07	2.24
Number of riser tubes			1051.00	901.00	788.00	700.00	**630.00**	573.00	525.00
Total RAS flow above module [L/min]			807.77	1008.39	1115.42	1167.61	**1187.75**	1188.50	1175.89

The optimum is presented in bold.

Table 6.7: Scenario A, 0.5 MGD ($1.89 * 10^6$ L/day), 90% of air above module, 10% on sides.

	L [m]	H [m]	Air above module, air per riser tube [L/min]						
	0.46	0.2	6.00	7.00	8.00	9.00	10.00	**11.00**	12.00
Water flow per riser tube [L/min]			0.77	1.12	1.42	1.67	1.89	**2.07**	2.24
Number of riser tubes			946.00	811.00	709.00	630.00	567.00	**517.00**	473.00
Total RAS flow above module [L/min]			727.07	907.66	1003.60	1050.85	1068.98	**1072.35**	1059.42
			Air on sides, option I, air per riser tube [L/min]						
	0.76	0.5	1.80	**2.93**	4.07	5.20	6.33	7.47	8.60
Water flow per riser tube [L/min]			1.63	**2.68**	3.32	3.78	4.13	4.41	4.64
Number of riser tubes			350.00	**215.00**	155.00	121.00	99.00	84.00	73.00
Total RAS flow from sides [L/min]			569.58	**575.16**	515.27	457.92	409.35	370.77	338.94
			Air on sides, option II, air per riser tube [L/min]						
	0.86	0.6	**1.80**	2.93	4.07	5.20	6.33	7.47	
Water flow per riser tube [L/min]			**2.02**	3.01	3.63	4.08	4.41	4.69	
Number of riser tubes			**350.00**	215.00	155.00	121.00	99.00	84.00	
Total RAS flow from sides [L/min]			**706.87**	647.73	563.12	493.19	437.08	393.62	
Total RAS option I [L/min]			**1647.50**						
Total RAS option II [L/min]			**1779.22**						

The optimum is presented in bold. Total RAS flows were calculated by adding the optimum water flow above the module and the optimum water flow in the side for option I and II, respectively.

Table 6.8: Scenario A, 0.5 MGD ($1.89 * 10^6$ L/day), 75% of air above module, 25% on sides.

	L [m]	H [m]	Air above module, air per riser tube [L/min]					
	0.46	0.2	6.00	7.00	8.00	9.00	10.00	**11.00**
Water flow per riser tube [L/min]			0.77	1.12	1.42	1.67	1.89	**2.07**
Number of riser tubes			788.00	675.00	591.00	525.00	473.00	**430.00**
Total RAS flow above module [L/min]			605.64	755.45	836.57	875.71	891.76	**891.89**
			Air on sides, option I, air per riser tube [L/min]					
	0.76	0.5	**1.80**	2.93	4.07	5.20	6.33	
Water flow per riser tube [L/min]			**1.63**	2.68	3.32	3.78	4.13	
Number of riser tubes			**876.00**	537.00	387.00	303.00	249.00	
Total RAS flow from sides [L/min]			**1425.58**	1436.56	1286.51	1146.69	1029.59	
			Air on sides, option II, air per riser tube [L/min]					
	0.86	0.6	**2.00**	3.00	5.00			
Water flow per riser tube [L/min]			**2.02**	3.06	4.00			
Number of riser tubes			**788.00**	525.00	315.00			
Total RAS flow from sides [L/min]			**1591.47**	1604.61	1258.74			
Total RAS option I [L/min]			**2317.48**					
Total RAS option II [L/min]			**2483.36**					

The optimum is presented in bold. Total RAS flows were calculated by adding the optimum water flow above the module and the optimum water flow in the side for option I and II, respectively.

Even though the present study focuses on pumping mixed liquor in an MBR, the fluid properties of water were used for calculations. The density and viscosity of water and mixed liquor are relatively similar for MLSS concentrations less than approximately 10,000 mg/L, which is typical for MBRs. However, even at higher MLSS concentrations, the results of the present study are valid as discussed in the Appendix (A).

6.4 RAS pumping capacity for MBRs of different sizes

For all scenarios, the achievable RAS, as a percentage of the incoming flow, decreased as the size of the MBR system increased. The RAS must be transported over longer distances as the capacities (i.e. size) of the MBR system increases.

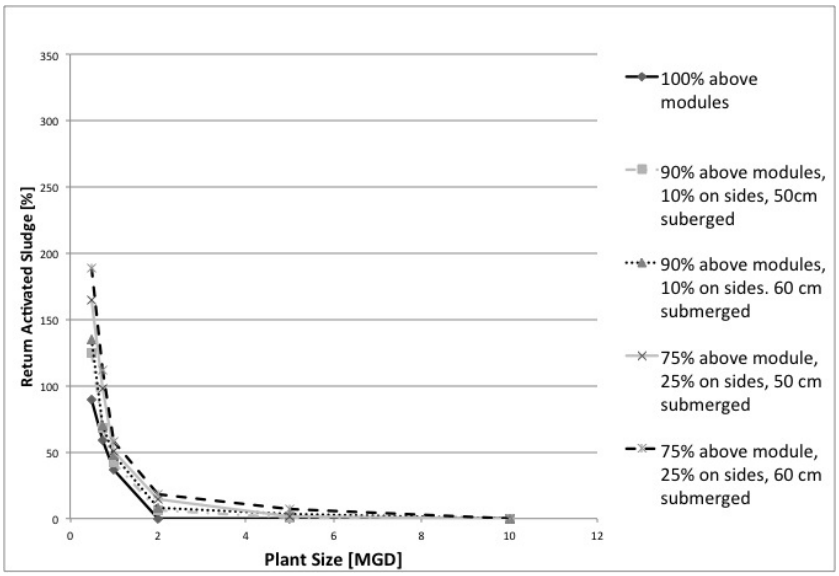

Figure 6.1: Achievable RAS vs plant size, 20 cm submerged, scenario A (see Section 6.3)

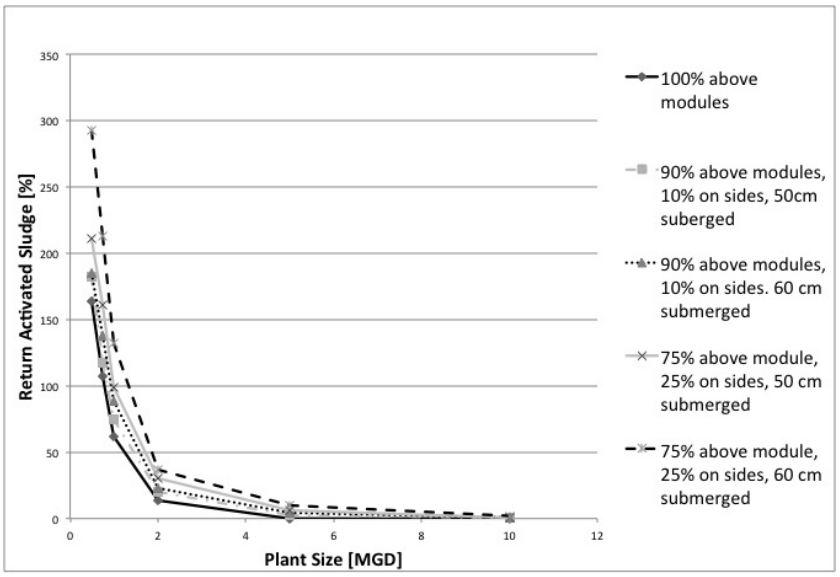

Figure 6.2: Achievable RAS vs plant size, 20 cm submerged, scenario B (see Section 6.3)

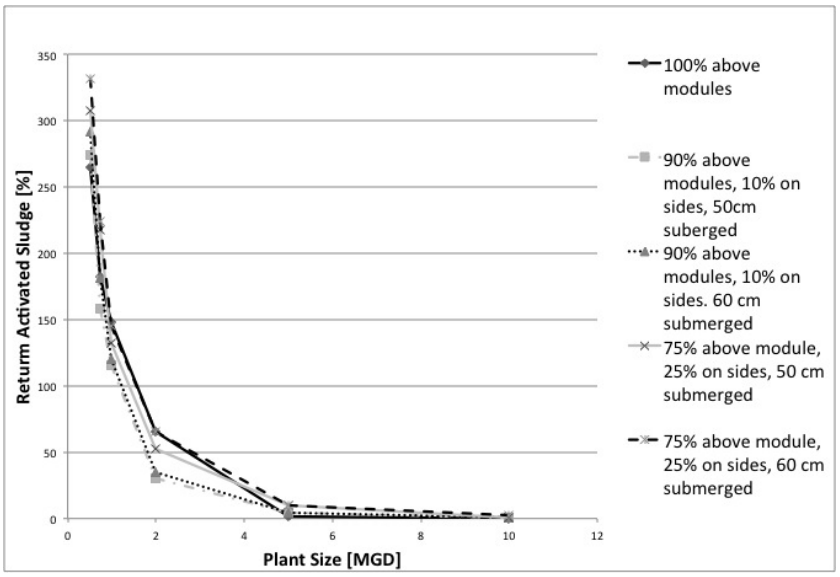

Figure 6.3: Achievable RAS vs plant size, 30 cm submerged, scenario C (see Section 6.3)

As illustrated in Figures 6.1, 6.2 and 6.3, the higher the submergence ratio, the greater the extent to which RAS can be pumped. The model predicts scenario a, with the lowest submergence ratio, will perform the poorest. For 0.5 MGD plants in scenario a, RAS flows between 90 and 189 % can be achieved, depending on where the air is located. For scenarios b and c, RAS flows between 163 and 293 % and 265 and 332 % can be achieved, respectively. This outcome is promising as most MBR installations have capacities less than 1 MGD (3.8 $\frac{ML}{d}$) [40]. Increasing the submergence depth (i.e. liquid level above the membrane) increases the amount of RAS that can be pumped for a given air flow.

As mentioned in Section 2.1.6, the RAS in MBRs is usually between 300 and 500% of the incoming flow. This means that in small plants the pumping costs for water conveyance can be significantly decreased or even completely eliminated by using air escaping from the membrane tank for RAS pumping.

Chapter 7

Comparison of model and measured results for multiple riser tubes in a pilot system

The following chapter presents water flow data observed in the pilot system. As done for bench-scale conditions, the Nicklin model was used to model liquid flows at pilot scale. To confirm the validity of the Nicklin model, a pilot-scale single riser tube experiment was performed (as discussed in Section 4.2.1).

7.1 Bundle of riser tubes

The water flows for experiments performed with the riser tube bundle for different collectors (rectangular and square), collector angles, submergence ratios (α) and air flows are discussed in the following sections. Results of the air flow calibration are discussed in the Appendix (C).

7.1.1 Influence of experimental conditions on square and rectangular collector geometry

As discussed in Section 4.2.3, the experimental conditions investigated were two submergence ratios (0.44 and 0.65), three collector angles (0°, 6.7° and 13.2°) and three air flow rates (81.2, 142.5 and 203.7 $^{L}/_{min}$).

Figures 7.1 and 7.2 present the estimates of the total flow for a bundle of 19 riser tubes, for the 2 submergence ratios tested. The total measured flow was calculated based on an extrapolation of the water flows measured from the 7 individual riser tubes in the representative quadrant (see Section 4.2.3). The total modeled flow was calculated as the sum of the modeled flow determined using the Nicklin model, from each of the 19 individual riser tubes in a bundle, assuming that each riser tube receives $^{1}/_{19}th$ of the total air to the collector.

Note that for the experiments performed with the rectangular collector at the highest air flow rate and the low collector angle (0 °), excessive amounts of air escaped between the frame and the tank, causing the setup to shake. For these conditions, no measurements were taken and are, therefore, not considered in the analysis. A similar behaviour was observed for higher collector angles (6.7 ° and 13.2 °); however, the setup did not shake to the same extent and therefore measurements were taken and used in the analysis.

As expected, for both, the square and the rectangular collector, the low submergence ratio resulted in a lower water flow at a given air flow rate than the high submergence ratio. This trend is consistent with the observations made at bench

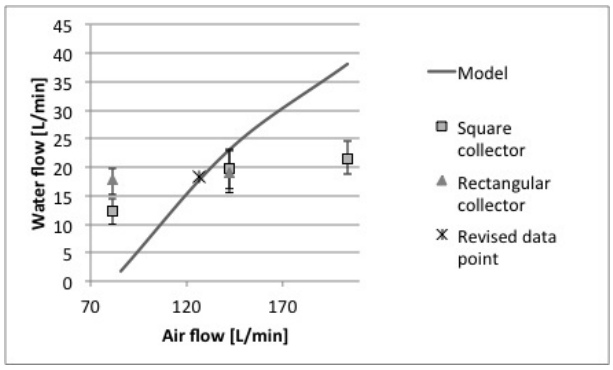

(a)

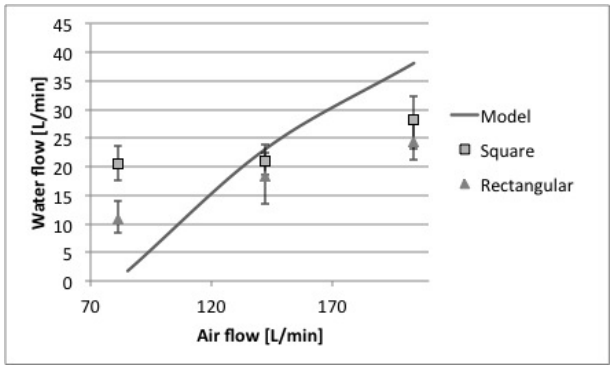

(b)

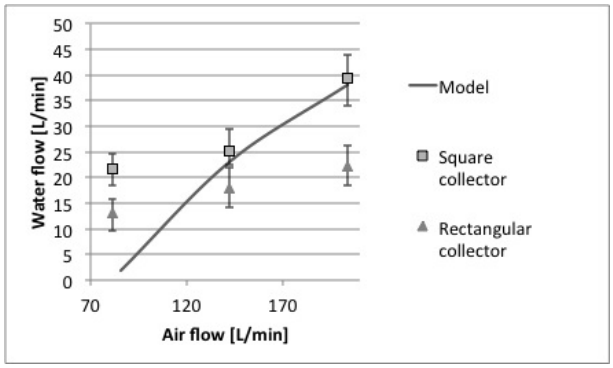

(c)

Figure 7.1: Estimated total flow for bundle of riser tubes for rectangular and square collector.
(Error bars correspond to estimated minimum and maximum values; a: low angle (0°), b: medium angle (6.7°), c: large angle (13.2°), Alpha = 0.44; the revised data point is based on calculations presented in Section 7.1.3; model results based in Nicklin model)

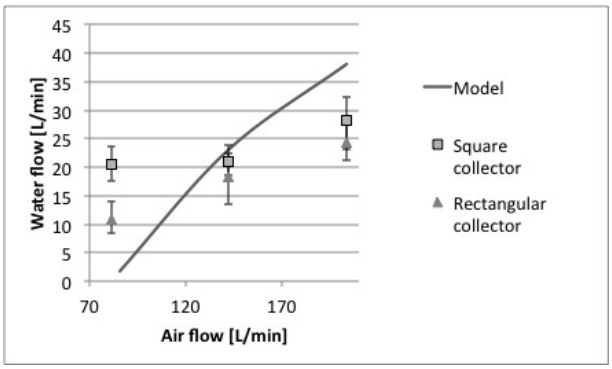

(a)

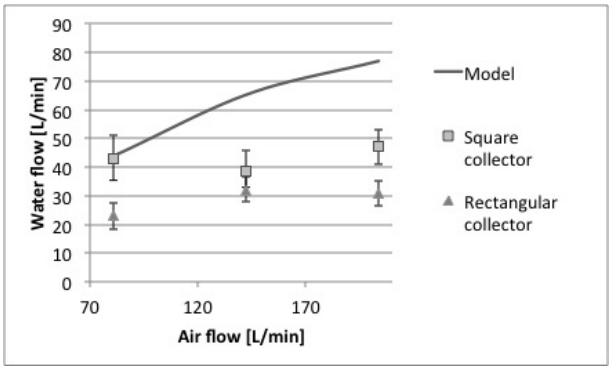

(b)

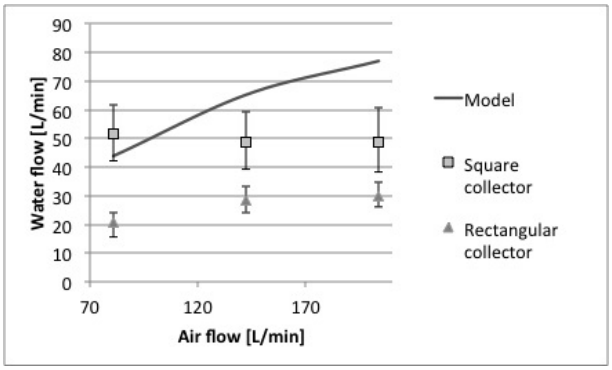

(c)

Figure 7.2: Estimated total flow for bundle of riser tubes for rectangular and square collector.
(Error bars correspond to estimated minimum and maximum values; a: low angle (0°), b: medium angle (6.7°), c: large angle (13.2°), Alpha = 0.65; model results based in Nicklin model)

scale (see Chapter 5).

For the system with a square collector, the total water flow was affected by the collector angle. Generally, as the collector angle increased, so did the total water flow. For the system with a rectangular collector, the collector angle did not substantially affect the water flow for different air flows or submergence ratios, except for the lower submergence ratio and low air flow. Under these conditions, the water flow was highest when considering a low collector angle.

For the lower submergence ratio considered, increasing the air flow generally resulted in an increase of the total water flow. This was observed for both collectors. However, the modeled increase was much greater than that which was measured. Also, no such correlation between air and water flow was observed for the higher submergence ratio considered.

In general, at a given air flow rate, higher water flows can be achieved with the square collector than with the rectangular collector.

7.1.2 Evaluation of the model, comparison of square and rectangular collector geometry

In order to assess whether the asymmetrical geometry of the rectangular collector contributed to an uneven distribution of air flow in the bundle of riser tubes, possibly affecting the fit of measured to modeled data, results of experiments of a square and a rectangular collector were compared to the modeled data.

In general, the model more accurately predicts the measurements of the square collector, than those of the rectangular collector. For the lower submergence ratio considered, there was better agreement between the modeled and measured results for the system with a square collector, especially at the higher air flows and collector angles considered. For the higher submergence ratio considered, the measured results were also closer to the modeled results for the system with a square collector. However, there was never consistent agreement between measured and modeled results. At high submergence ratios, the model generally overpredicted the water flows for both collectors. This trend is not consistent with the observations made at bench scale (see Chapter 5), and will be discussed later in this section.

For both collectors, at low submergence ratios and low air flow rates, the measured water flows were greater than the modeled water flows. This was not observed at the higher submergence ratio. This may have resulted from the upflow of water entrained by rising bubbles in the tank. This upward water flow contributes to the momentum of water entering and rising through the tubes, resulting in an increased flow. At lower submergence ratio, there would be greater opportunity for the upflow of entrained water than at a higher submergence ratio.

As discussed in Section 7.1.1, the water flow increases with increasing submergence ratio for both collectors. However, the measured water flow rates for the high submergence ratio were significantly lower than what the model predicted for both collectors. This suggests that a higher submergence ratio does increase the water flow; however, the extent of increase cannot be predicted with the model

considered.

The model results assume that the air flow is equally distributed to all riser tubes, and therefore, the flow from all riser tubes is the same. However, if this is not the case, then some tubes could be receiving more or less air, which could be out of the optimum range (as discussed in Section 6.3). To gain insight into the discrepancy between the model and measured results, the distribution of water flows of the riser tubes in the bundles was investigated in two ways, as described in the following sections.

7.1.3 Revised air flow based on water flow

To determine if the discrepancy between the model and measured results was due to the uneven distribution of air flow into the different riser tubes in a bundle, the air flows of the different riser tubes were estimated based on the measured liquid flow of each tube (see Fig. 7.3). This was done for the measurements collected from the setup with the rectangular collector frame at an air flow rate of 142.5 $^{L}/_{min}$ and a low collector angle.

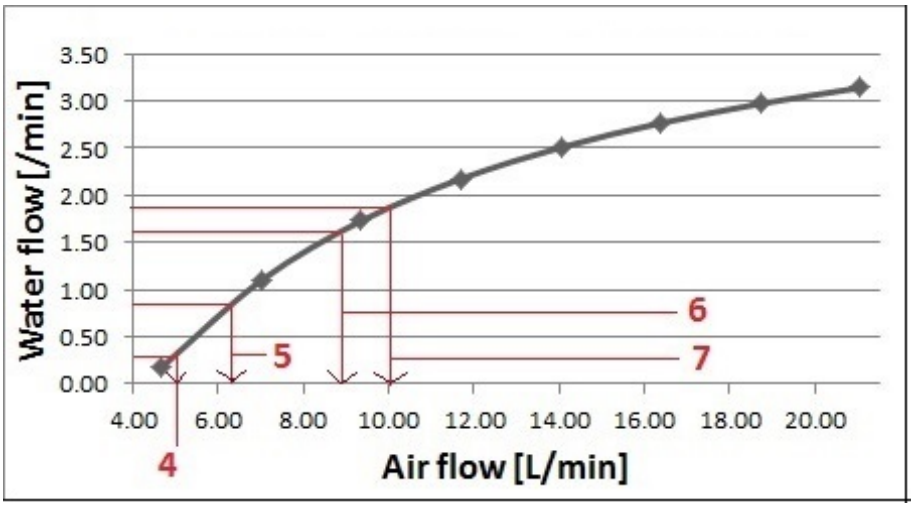

Figure 7.3: Water vs. air flow according to Nicklin model.
(D=$^3/_4$ inch, length =0.54cm, lift = 0.3m; the numbers next to the lines represent riser tube numbers.)

Table 7.1: Extrapolation for air flow per riser tube in a bundle based on measured results of rectangular setup, using the Nicklin model.

Riser tube number (see Fig. 4.3)	Assumed to be representative of "n" riser tubes in the system [n]	Estimated air flow per riser tube from Figure 7.3 [$^L/_{min}$]
1	1	5
2	4	6
3	2	6.8
4	4	5
5	4	6.5
6	2	9
7	2	10
total:	19	126.6

As presented in Table 7.1, the total air flow corresponding to the measured water

flow was estimated to be 126.6 $^{L}/_{min}$. The estimated total air flow is slightly lower than the measured flow of air added to the tank (142.5 $^{L}/_{min}$). The discrepancy is likely due to the gas that escapes the system between the collector angle frame and the tank walls.

When taking into account the uneven distribution of air flow into each riser tube, the model and measured results are in better agreement, as illustrated with an "x" in Figure 7.1.

7.1.4 Distribution of water flow

In order to determine whether the shape of the collector had an impact on the distribution of the water flow, water flows of individual riser tubes of both setups were characterized. As discussed in Section 4.2.3, two submergence ratios (0.44 and 0.65), three collector angles (0°, 6.7° and 13.2°) and three air flow rates (81.2, 142.5 and 203.7 $^{L}/_{min}$) were investigated at pilot scale.

Figures 7.4 and 7.5 present water flows of the 7 individual riser tubes in the representative quadrant (see Section 4.2.3), for the rectangular and square collector, respectively, at the low submergence ratio (α =0.44), similar results were observed for the high submergence ratio (α = 0.65) and are presented in the Appendix B.7.

As expected, the measured water flows were more evenly distributed for the square collector than the rectangular collector.

Although the flow distribution was more homogenous for the square collector than

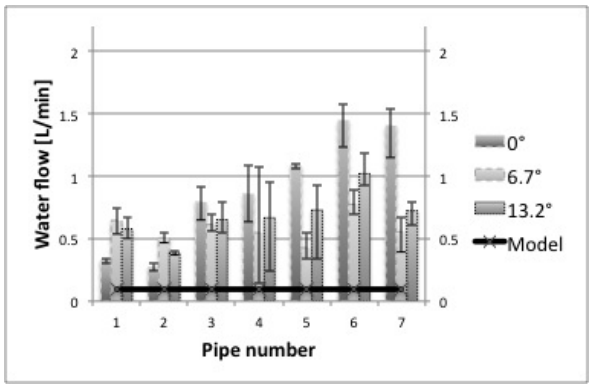

(a)

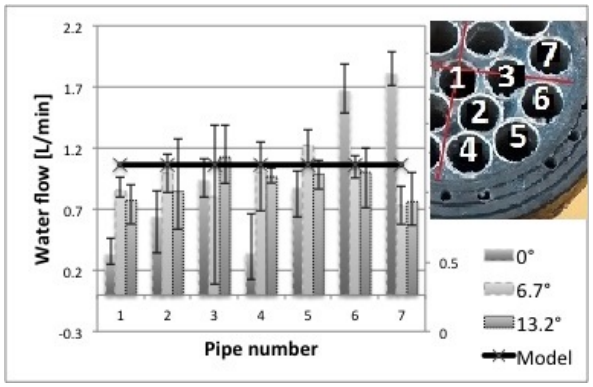

(b)

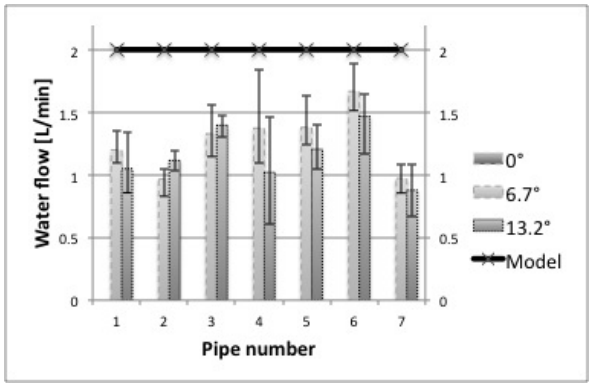

(c)

Figure 7.4: Water flow distribution of individual riser tubes for the rectangular collector (alpha =0.44).
(Error bars correspond to minimum and maximum values; air flows of a: 81.2 L/min; b: 142.5 L/min; c: 203.7 L/min)

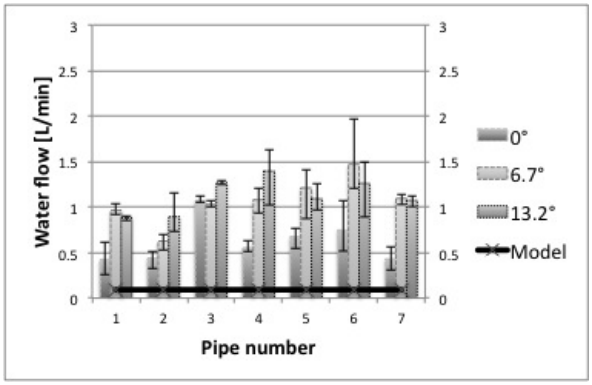

(a)

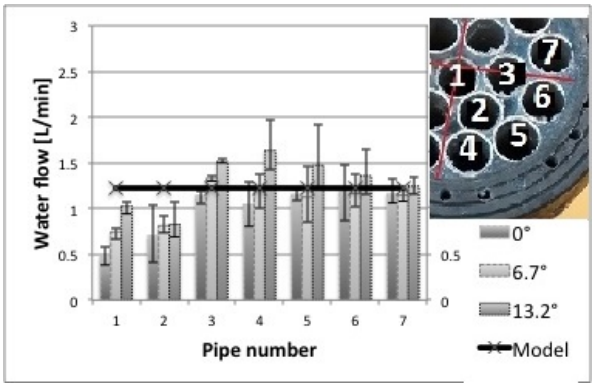

(b)

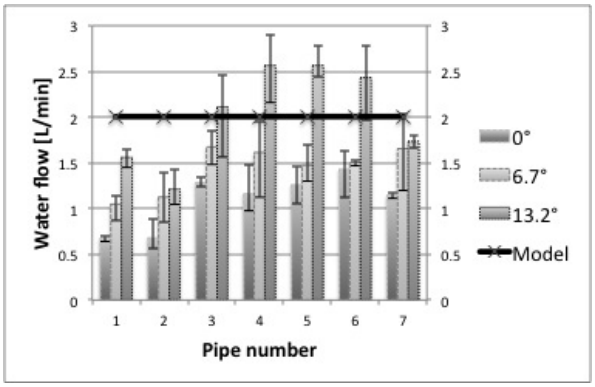

(c)

Figure 7.5: Water flow distribution of individual riser tubes for the square collector (alpha =0.44).
(Error bars correspond to minimum and maximum values; air flows of a: 81.2 L/min; b: 142.5 L/min; c: 203.7 L/min)

for the rectangular collector, the flow of some of the riser tubes (i.e. number 1 and 2) were still less than expected based on the average and the model prediction, for both submergence ratios. For both collectors, the submergence ratio had no impact on the flow distribution.

As discussed in Section 7.1.1, the lowest collector angle resulted in the highest total water flow for low and medium air flow ranges for the rectangular collector. However, as presented in Figure 7.4 a, this configuration had the least homogenous distribution of flows of individual riser tubes. In general, a higher collector angle results in a better flow distribution for the rectangular collector. When the square collector was used, the largest collector angle resulted in the highest water flow independent of the air flow and submergence ratio. The air flow rate did not affect the distribution of air in the individual riser tubes for either collector.

The results confirm that the shape of the collector has an impact on the distribution of the flow. The square collector resulted in a better distribution and, therefore, generally higher water flows than the rectangular collector. The results also indicate that, although the uneven distribution of air flow to the riser tubes contributes to the discrepancy between the measured and modeled results, other mechanisms also likely contribute to this discrepancy. Further research is required to identify the mechanisms responsible for the observed results.

7.2 Water redirection system

After the water is lifted to the required height, it must be transferred into the RAS pipes that transport it back to the head of the bioreactor tank. Four different ap-

proaches were investigated to direct the water flow from the vertical riser tubes to the RAS pipes. The redirection of the lifted water flow was investigated for only two conditions (i.e. two collector angles (6.7 and 13.2°) for one submergence ratio $\alpha = 0.44$) and for the square collector.

As illustrated in Figures 7.6 a and b, the geometry of the flow redirection system had a significant effect on the total water flow. The total flow collected when using a simple 90° elbow was the lowest of the different options considered. This is likely because some of the lifted water simply hit the top of the elbow and was redirected downward, rather than horizontally (see Fig. 7.6 a). Inserting flexible tubes in a standard 90° elbow to more effectively redirect the flow did increase the total collected flow. However, the total flow was much lower than expected. When the elbow was filled with flexible tubes that were not directly connected to the riser tubes, the water likely hit the hoses and was directed back into the riser tubes, instead of carried out (Fig.7.7 b).

Configuration C and D , where curved tubes are fitted to each riser tube in a bundle, resulted in the highest total water flows. The total water flow measured for configurations C and D are similar to the total expected water flow (i.e. estimated from the 19 individual riser tubes in a bundle).

Although configurations C and D can provide similar water flows, the RAS piping network is expected to be simpler, and therefore, less costly to build and maintain using configuration D. This reflects the fact that the flow from a bundle of riser tubes is redirected and collected at one side of the bundle, as opposed to configu-

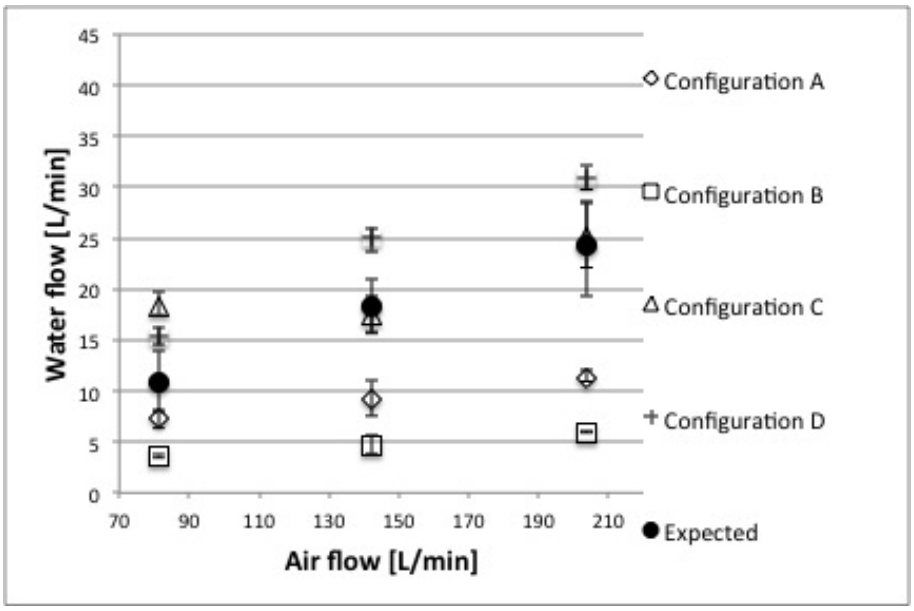

(a)

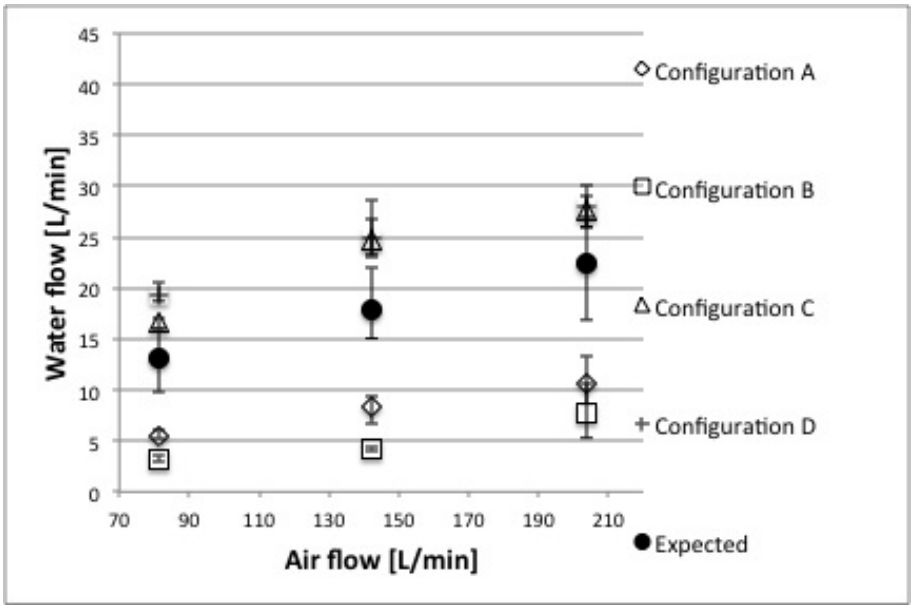

(b)

Figure 7.6: Effect of water collecting methods.
(Error bars correspond to minimum and maximum values; a: medium ; b: large angle. The expected value is based on an extrapolation from 7 individual riser tubes as discussed in Section 7.1.1)

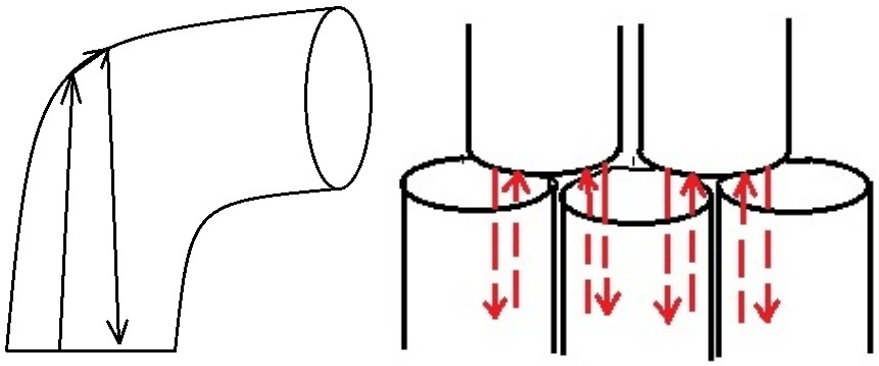

(a) Elbow (b) Tubes within elbow on top of riser tubes

Figure 7.7: Illustrations of losses in water collection system.

ration C, for which the water flow is redirected and collected at both sides of the bundle (therefore requiring more piping).

Chapter 8

Conclusions and engineering significance of work

8.1 Conclusions

An existing airlift pump model was modified, so that it accurately predicted water flows for single riser tubes.

Using the assumptions for the investigated conditions in the present work, the modified model predicts that airlift pumps, using waste air, can convey RAS (return ativated sludge) flows of up to 332 % of the influent flow, indicating that waste air from membrane sparging can be used to convey liquid within MBR (membrane bioreactor) systems, using airlift pumps.

Existing airlift pump models can provide an approximate estimate of the RAS flow that can be achieved. However, they cannot be used to accurately predict the water

flow that can be achieved.

The higher submergence ratio resulted in higher water flows. However, the extent of increase could not be accurately modeled.

In general, better flow distribution in a bundle of riser tubes was observed at higher collector angles. However, there was no significant difference in water flows achieved in systems with small and the large collector angle. .

The collector with a square geometry resulted, not only in a better flow distribution in a bundle of riser tubes, but also in higher total water flows than the collector with a rectangular geometry.

When redirecting the water from the top of the bundle of riser tubes to the RAS piping network pipes, fitting curved tubes to each riser tube in a bundle resulted in the highest collected water flows.

8.2 Engineering significance

It was concluded that air exiting to the atmosphere from an MBR can be used to convey RAS within MBR systems. However, existing airlift pump models could not accurately predict water flows that can be achieved.

If electrically driven pumps can be completely replaced by airlift pumps, energy costs for an MBR can be decreased by up to 26% (If electrically driven pumps can be replaced completely, see Fig. 1.1). Replacing electrically driven pumps by

airlift pumps in MBRs would result in lower operating costs.

Since both, energy and water demand will increase in the future, solutions that decrease the energy demand for water treatment need to be identified. The present study presented an opportunity to do so. However, it is crucial to have accurate models that can be used to design air lift RAS pumps. Such models should include factors like the submergence ratio α, which will likely be given for each MBR due to a limited space to submerge the riser tubes, and a required height that the water needs to be lifted to.

8.3 Future work

The outcomes of the present study are specific to the conditions investigated and were only intended to determine the feasibility of using air escaping from the membrane tank to lift and convey RAS. Although the results from the present study are promising, additional research is required before airlift pumping can be implemented at commercial scale for RAS conveyance. The requirements of each individual MBR will be the key element of the design process, which can be addressed once a model for this kind of application exists. Limitations can be addressed in future work, as listed below.

1. Further research is needed to develop models that can accurately predict the achievable water flow.

2. Build and test several airlift pump applications with varying parameters, such as the optimum number of riser tubes in a bundle, or the increments between the heights of the individual riser tubes.

3. Different types of aeration should be included in the experimental plan such as cyclic or intermittent aeration.

4. Sludge clogging in riser tubes and RAS transportation pipes can be a potential problem. An investigation in to long term maintenance requirements for airlift pumping of RAS needs to be undertaken.

5. The potential effect of the mixed liquor solids content/viscosity on the airlifting of RAS should be addressed.

Bibliography

[1] Engineeringtoolbox.com. URL http://www.engineeringtoolbox.com/surface-roughness-ventilation-ducts-d_209.html,May2014.

[2] Meeting the challenges of the water-energy nexus: the role of reuse and wastewater treatment. Water 21, Magazine of the International Water Association, April 2012.

[3] Water and energy: conflicts and connections. Water 21, Magazine of the International Water Association, October 2012.

[4] D. R. H. Beattie and P. Whalley. A simple two-phase frictional pressure drop calculation method. Int. J. Multiphase Flow, 8:83–87, 1982.

[5] T. Buer and J. Cumin. Mbr module design and operation. Desalination, 250: 1073–1077, 2010.

[6] F. D. Cachard and J. M. Delhaye. A slug-churn flow model for small-diameter airlift pumps. Int. J. Multiphase Flow, 22(4):627–649, 1996.

[7] L. D. Chabalina, J. B. Ruiz, M. R. Pastor, and D. P. Rico. Influence of eps and mlss concentrations on mixed liquor physical parameters of two membrane bioreactors. Desalination and water treatment, 46:46–59, 2012.

[8] L. Chexal, G. Lellouche, G. Horowitz, and J. Haelzer. A void fraction correlation for generalized applications. Progress in Nuclear Energy, 27(4): 255–295, 1992.

[9] N. Clark and R. Dabolt. A general design equation for air lift pumps operating in slug flow. American Institue of Chemical Engineers, 32:56–64, 1986.

[10] R. Clift, J. Grace, and M. Weber. Bubbles, Drops and Particles. Academic Press, INC., 1978.

[11] P. Côté, Z. Alam, and J. Penny. Hollow fibre membrane life in membrane bioreactors (mbr). Desalination, 288:145–151, 2012.

[12] P. Côté, T. Young, S. Smoot, and J. Peeters. Energy consumption of mbr for municipal wastewater treatment: Current situation and potential. In Proceedings of the Water Environment Federation, volume 14, pages 479–492(14), 2013.

[13] R. Davies and G. Taylor. The mechanics of large bubbles rising through extended liquids and through liquids in tubes.pdf. Proceedings of the Royal Society of London, 200A(1062):375–390, 1950.

[14] A. D. Delano. Design Analysis of the Einstein Refrigeration Cycle. PhD thesis, Georgia Institute of Technology, June 1998.

[15] D. Dumitrescu. Stroemung an einer luftblase im senkrechten rohr. Zeitschrift fuer angewandte Mathematik und Mechanik, 23:139–149, 1943.

[16] R. Field. Fundamentals of Fouling, in Membrane Technology: Membranes for Water Treatment, volume 4 (eds K.-V. Peinemann and S. Pereira Nunes). Wiley-VCH Verlag GmbH und Co. KGaA, Weinheim, Germany, 2010.

[17] GE Power and Water. Zeeweed 500d casette specification sheet. Technical report, General Electric Company, 2006.

[18] GE Power and Water. Zeeweed* 500d module fact sheet. Technical report, General Electric Company, 2013.

[19] R. Giles, J. Evett, and C. Liu. Theory and Problems of Fluid Mechanics and Hydraulics. McGraw-Hill, Schaum's Outline Series, third edition, 1994.

[20] X. Huang, P. Gui, and Y. Qian. Effect of sludge retention time on microbial behaviour in a submerged membrane bioreactor. Process Biochemistry, (36): 1001–1006, 2001.

[21] S. Jankhah. Effect of Bubble Size and Sparging Frequency on the Power Transferred onto Membranes for Fouling Control. PhD thesis, University of British Columbia, December 2013.

[22] S. Judd and C. Judd. MBR Book - Principles and Applications of Membrane Bioreactors for Water and Wastewater Treatment. Butterworth-Heinemann, 2nd edition, 2011.

[23] S. Kassab, H. Kandil, H. Wards, and W. Ahmed. Air-lift pumps characteristics under two-phase flow conditions. International Journal of Heat and Fluid Flow, 30:88–98, 2009.

[24] W. Khongnakorn, C. Wisniewski, L. Pottier, and L. Vachoud. Physical properties of activated sludge in a submerged membrane bioreactor and relation with membrane fouling. Separation and purification technology, 55: 125–131, 2007.

[25] D. Kouremenos and J. Staicos. Performance of a small air-lift pump. International Journal of Heat and Fluid Flow, 6:217–222, 1985.

[26] R. Liu, X. Huang, Y. F. Sun, and Y. Quian. Hydrodynamic effect on sludge accumulation over membrane surfaces in a submerged membrane bioractor. Process Biochemistry, 39:157–163, 2003.

[27] F. Meng, S. Chae, M. Kraume, A. Drews, F. Yang, and H. Shin. Recent advances in membrane bioreactors (mbrs): Membrane fouling and membrane material. Water research, 43(6):1489–1512, 2009.

[28] Metcalf and Eddy. Wastewater Engineering Treatment and Reuse. McGraw-Hill, fourth edition, 2003.

[29] D. Nicklin. The air-lift pump: Theory and optimization. Trans. Instn. Chem. Engrs., 41:29–39, 1963.

[30] D. Nicklin, J. Wilkes, and D. J.F. Two-phase flow in vertical tubes. Trans. Instn. Chem. Engrs., 40:62–68, 1962.

[31] J. Orkiszewski. Predicting two-phase pressure drops in vertical pipe. Journal of Petroleum Technology, pages 829–838, 1967.

[32] M. C. Potter, D. C. Wiggert, and B. H. Ramadan. Mechanics of Fluids. Cengage learning, 4th si edition, 2012.

[33] D. Reinemann, J. Parlange, and T. M.B. Theory of small-diameter airlift pumps. Int. J. Multiphase Flow, 16(1):113–122, 1990.

[34] V. Samaras and D. Margaris. Two-phase flow regime maps for air-lift pump vertical upward gas–liquid flow. International Journal of Multiphase Flow, 31:757–766, 2005.

[35] L. A. Schaefer. Single pressure absorption heat pump analysis. PhD thesis, Georgia Institute of Technology, 2000.

[36] A. Stenning and C. Martin. An analytical and experimental study of air-lift pump performance. ASME Journal of Engineering for Power, pages 106–110, 1968.

[37] N. Trixier, G. Guibaud, and M. Baudu. Determination of some rheological parameters for the characterization of activated sludge. Bioresource technology, 90:215–220, 2003.

[38] R. S. Trussella, R. P. Merlob, S. W. Hermanowiczc, and D. Jenkinsc. Influence of mixed liquor properties and aeration intensity on membrane fouling in a submerged membrane bioreactor at high mixed liquor suspended solids concentrations. Water research, 41:947–958, 2007.

[39] VDI Association. VDI-Waermeatlas. Springer, 10th edition, 2006.

[40] Water Environment Federation. Membrane Bioreactors WEF Manual of Pratice No.36. Mc Graw Hill, 2011.

[41] E. White and R. Beardmore. Velocity of rise of single cylindrical air bubbles through liquids contained in vertical tubes. Chemical Engineering Science, 17:351–361, 1962.

[42] S. J. White. Bubble pump design and performance. Master's thesis, Georgia Institute of Technology, August 2001.

[43] T. Young, M. Muftugil, S. Smoot, and J. Peeters. Mbr vs. cas- capital and operation cost evaluation. Water Practice and Technology, 7(04), 2012.

[44] N. Zuber and J. Findlay. Average volumentric concentration in two-phase flow systems. Journal of Heat Transfer, 87:453–468, 1965.

[45] E. Zukoski. Influence of viscosity, surface tension and inclination angle on motion of long bubbles in closed tubes. Journal of Fluid Mechanics, 25: 821–832, 1966.

Appendix A

Sludge viscosity calculations

As the MLSS concentration in the membrane tank was assumed to be between 8000 and 12000 $^{mg}/_{L}$, these two values were considered as the boundaries for the viscosity calculations. To calculate the viscosity, a correlation by Liu et al. [26] was used:

$$\eta = 1.61e^{0.07MLSS}. \tag{A.0.1}$$

Note that while for MLSS concentrations below 9 $^{g}/_{L}$, similar correlations were found [7, 37]. However, for MLSS concentrations greater than 10 $^{g}/_{L}$, viscosities in a wider range were reported (i.e. viscosities up to 46 mPas at 10 $^{g}/_{L}$ [38], or as low as 5 mPas at 15 $^{g}/_{L}$ [24]). When an MBR is run at the upper boundary MLSS concentration, the viscosity in the membrane tank should be investigated. Since the viscosity does not only depend on the MLSS concentration but also on the composition of the sludge, the floc size and shape and bound water [24, 37], the appropriateness of the sludge viscosity for the application of the present study

should be investigated.

Using Equation A.0.1, the viscosity is between approximately 280 to 370% higher than the viscosity of pure water (see Table A.1), which was assumed when modelling the airlift pump (assuming the viscosity of water is 1.0016 mPas (at 20 °C) [39]).

Clift et al. [10] presented a correlation between the Eötvös number Eo, the Froude number Fr and the Morton number M, which is presented in Figure A.1. The parameters needed for this correlation for the lower and upper boundaries assumed can be found in Table A.1.

Table A.1: Parameters to determine the impact of the sludge viscosity on bubble behaviour.

Parameter	Unit	Lower Boundary	Upper Boundary
MLSS	$^{mg}/_{L}$	8000	12000
Mo	-	$1.6 * 10^{-9}$	$4.9 * 10^{-9}$
η	mPas	2.82	3.73

Eo, Fr and M defined as follows:

$$Eo = \frac{g\Delta\rho D^2}{\sigma} \tag{A.0.2}$$

$$Fr = V_g \sqrt{\frac{\rho}{\Delta\rho} gD} \tag{A.0.3}$$

$$Mo = \frac{g\eta^4\Delta\rho}{\rho^2\sigma^3} \tag{A.0.4}$$

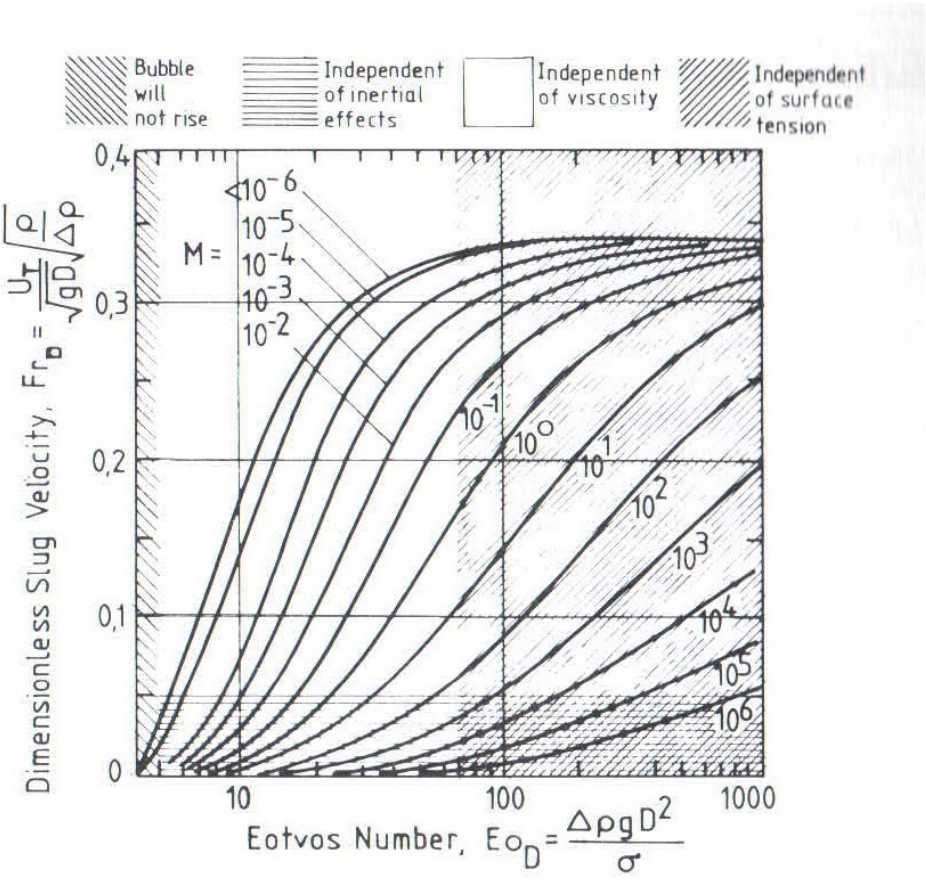

Figure A.1: Froude number vs. Eötvös number [10].

For surface tension, the value of water and air at 20°C was assumed ($72.74 * 10^{-3}\mathrm{N/m}$ [39]). The Eötvös number results in $Eo = 48.9$ for both, the lower and upper boundary. For calculated values for the Morton number of $1.6 * 10^{-9}$ and $4.9 * 10^{-9}$, respectively, Figure A.1 suggests, that bubbles form independently of viscosity in this range; hence, the assumption of the viscosity of water is justified.

Appendix B

Results

Results Models Before Modification

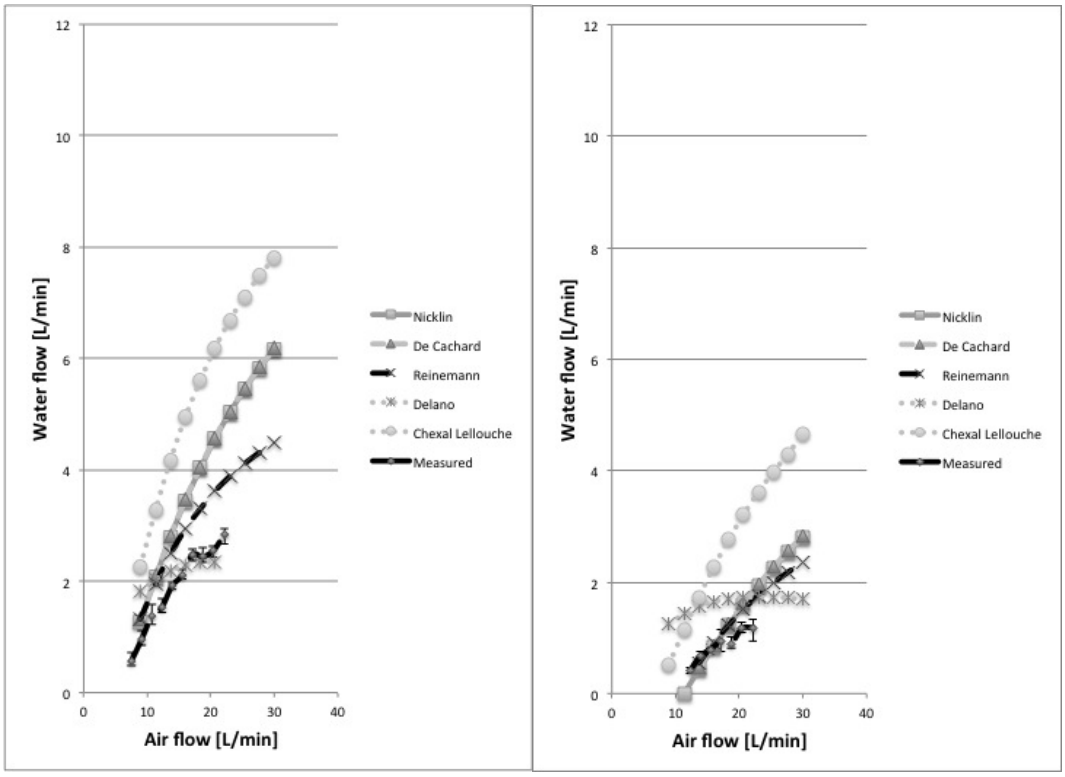

Figure B.1: Results using riser tubes with D=3/4 inch, 1m long, before modification.
(Error bars correspond to minimum and maximum values; a: Lift 0.6m; b: Lift 0.7m)

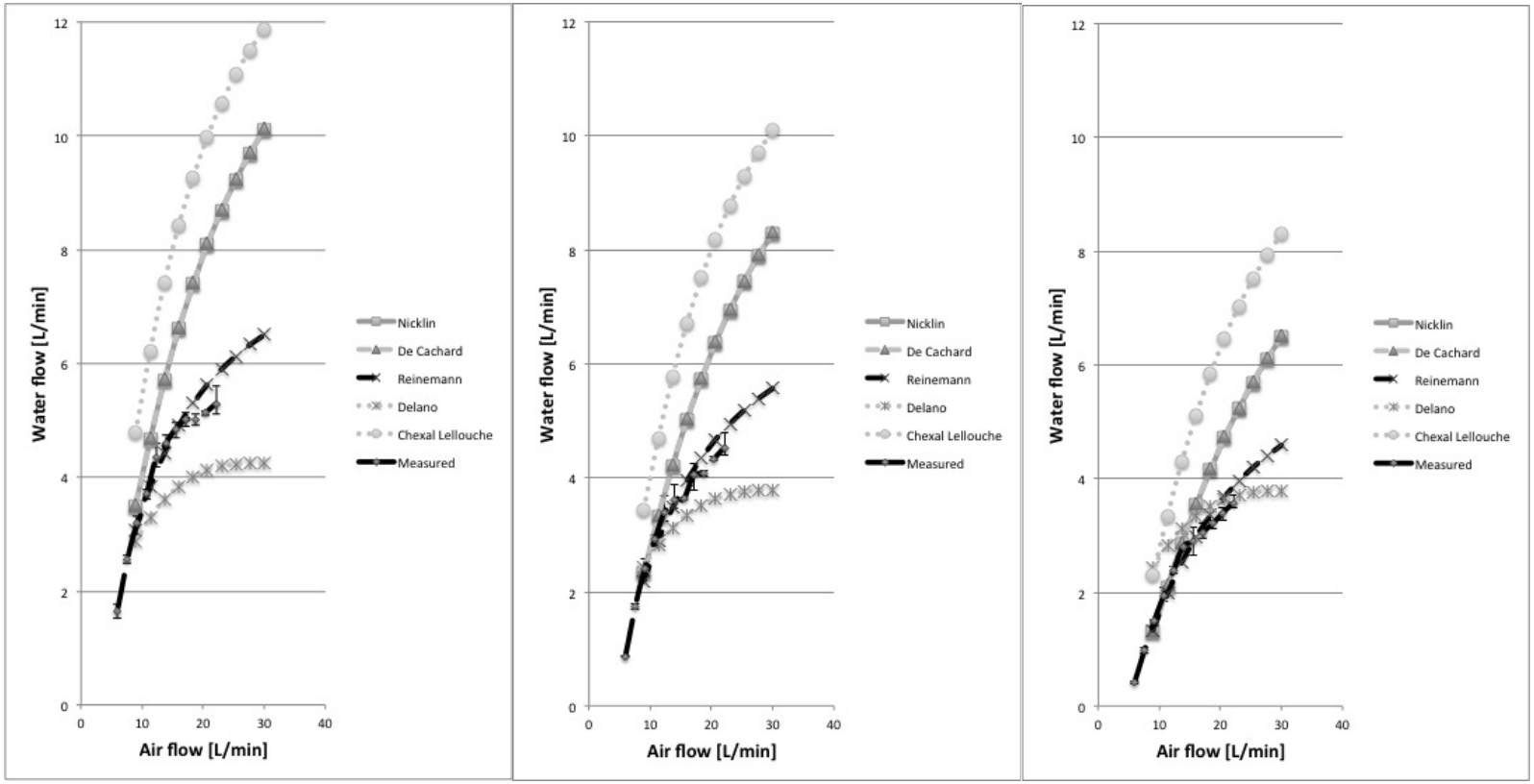

Figure B.2: Results using riser tubes with D=3/4 inch, 2m long, before modification.
(Error bars correspond to minimum and maximum values; a: Lift 1m; b: Lift 1.1m; c: Lift 1.2m)

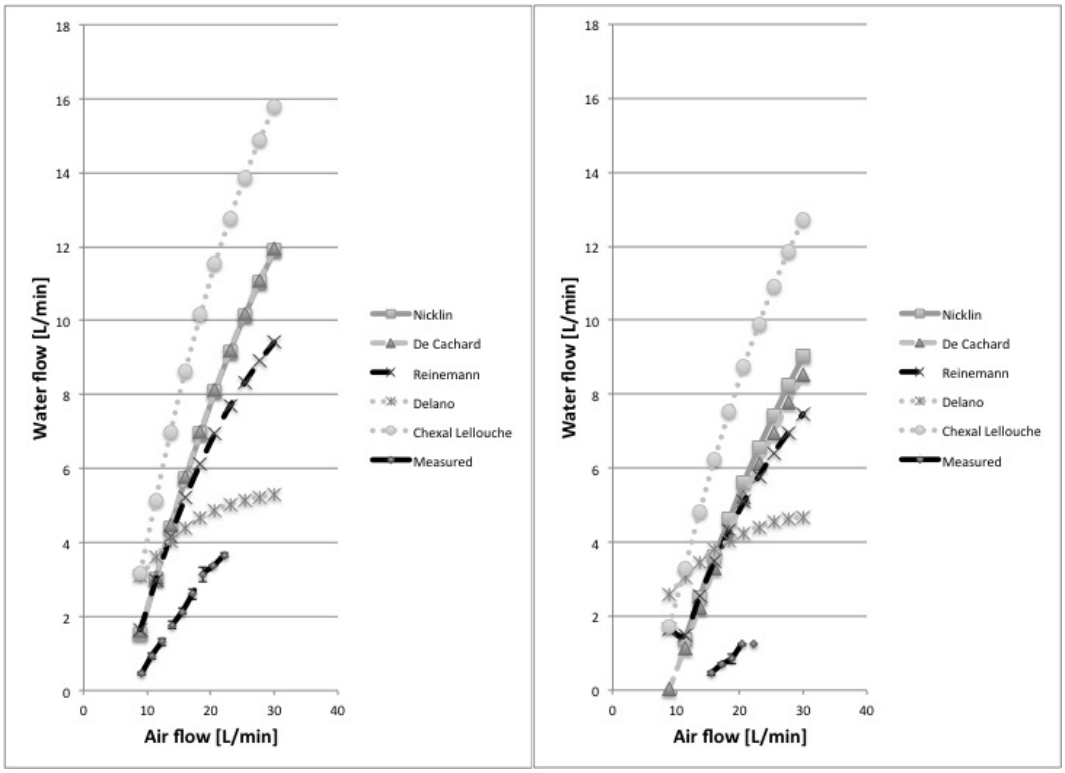

(a) (b)

Figure B.3: Results using riser tubes with D=1 inch, 1m long, before modification. (Error bars correspond to minimum and maximum values; a: Lift 0.5m; b: Lift 0.55m)

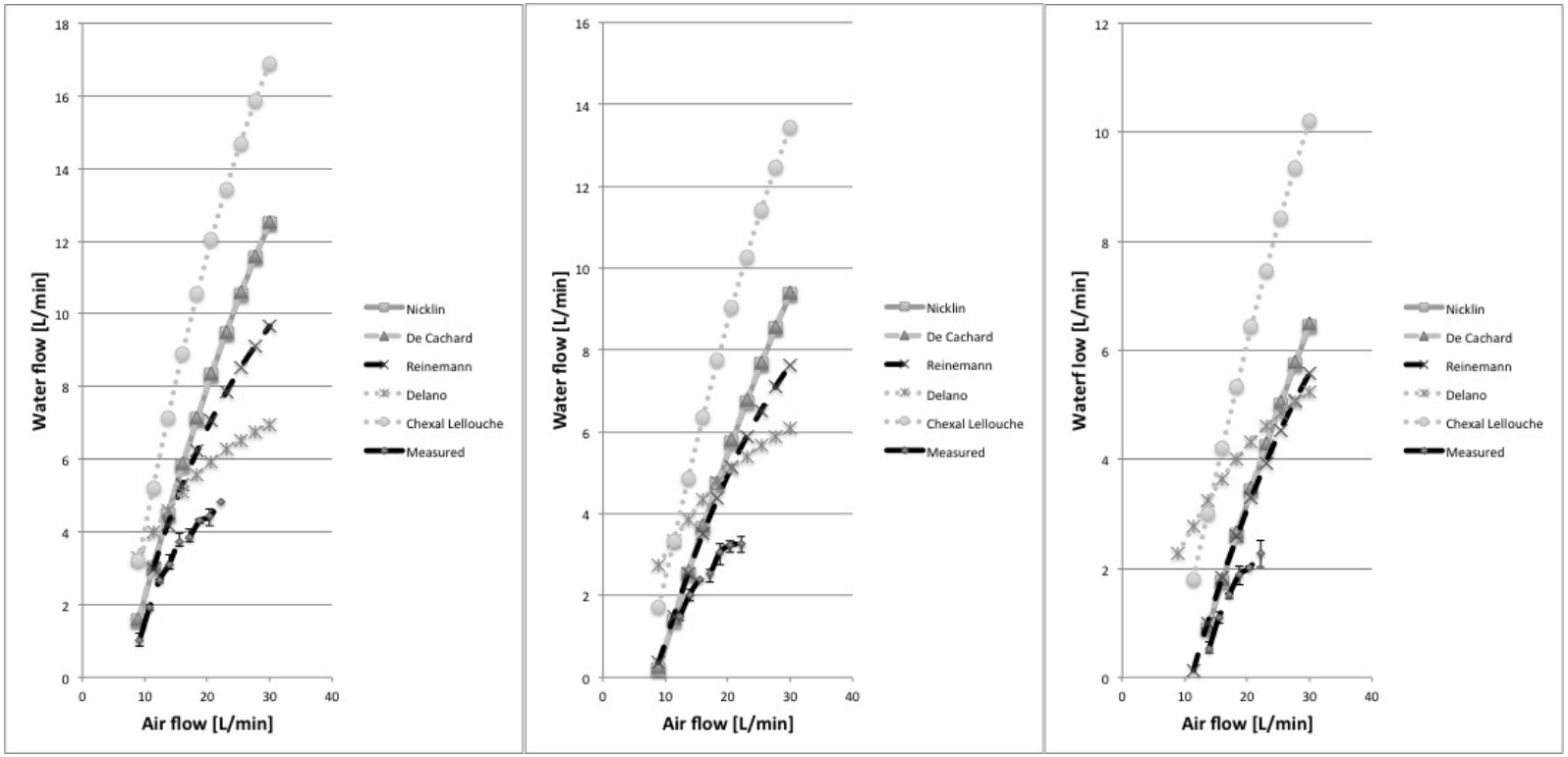

(a) (b) (c)

Figure B.4: Results using riser tubes with D=1 inch, 2m long, before modification.
(Error bars correspond to minimum and maximum values; a: Lift 1m; b: Lift 1.1m; c: Lift 1.2m)

Results of Evaluation of Head Loss Coefficient

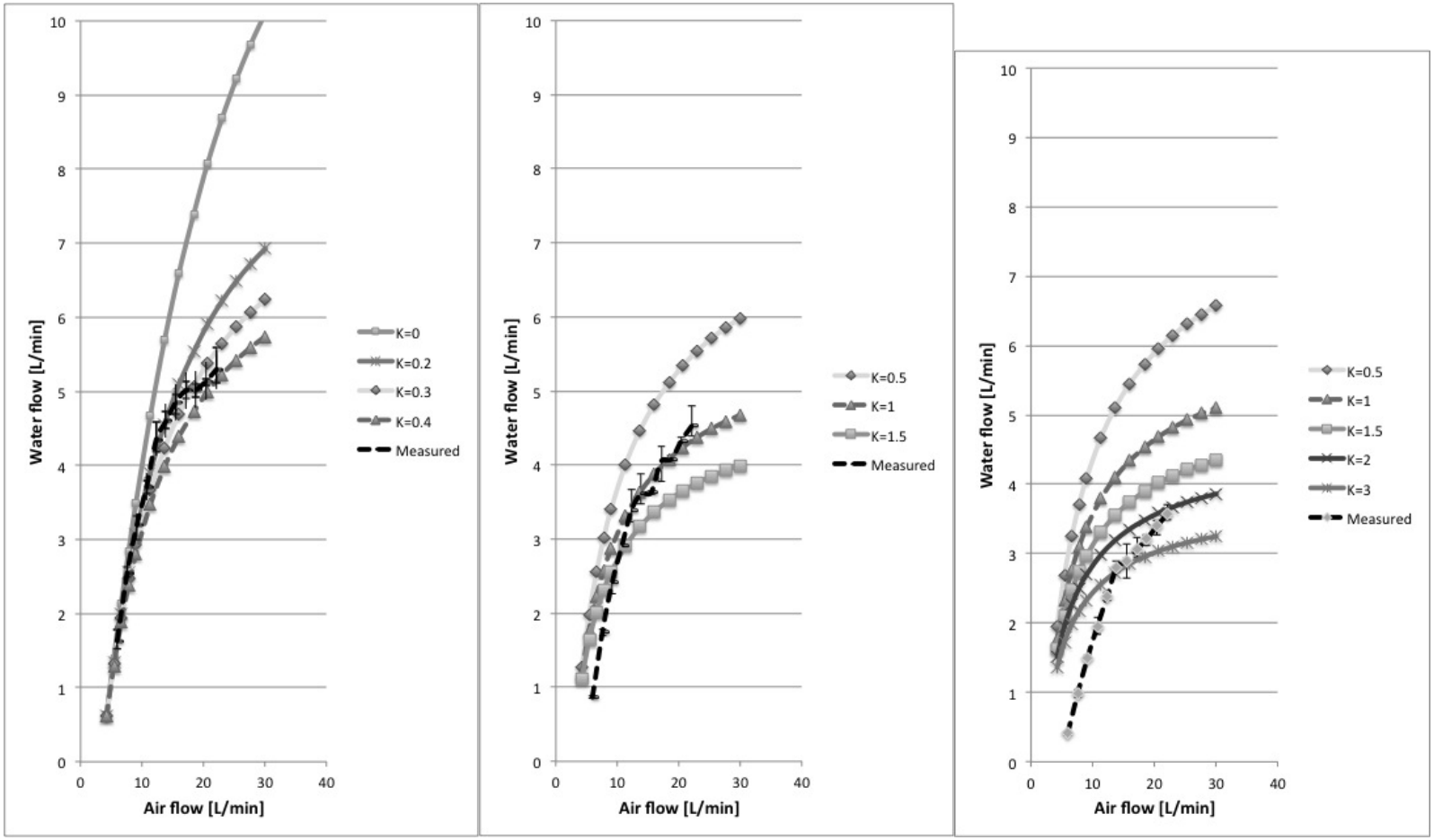

(a) (b) (c)

Figure B.5: Evaluation of head loss coefficient using riser tubes with D=3/4 inch, 2m long.
(Error bars correspond to minimum and maximum values; a: Lift 1m; b: Lift 1.1m; c: Lift 1.2m)

Water Distribution

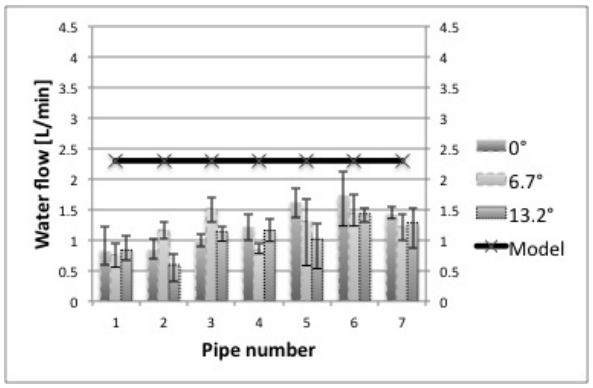

(a)

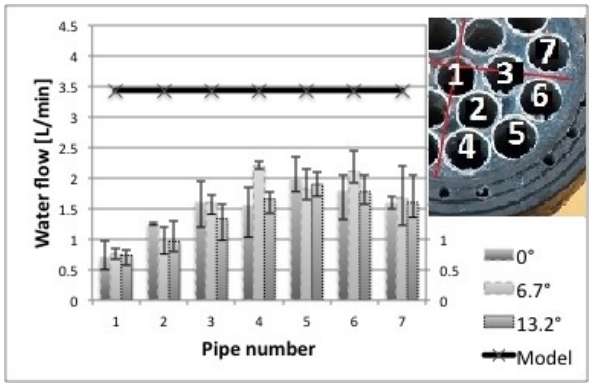

(b)

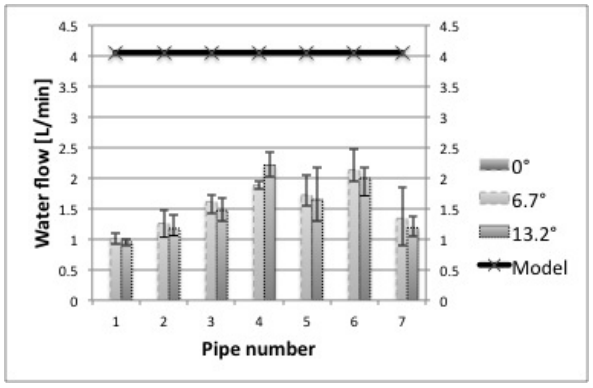

(c)

Figure B.6: Water flow distribution of individual riser tubes for the rectangular setup (alpha =0.64).
(Error bars correspond to minimum and maximum values; air flows of a: 81.2 L/min; b: 142.5 L/min; c: 203.7 L/min)

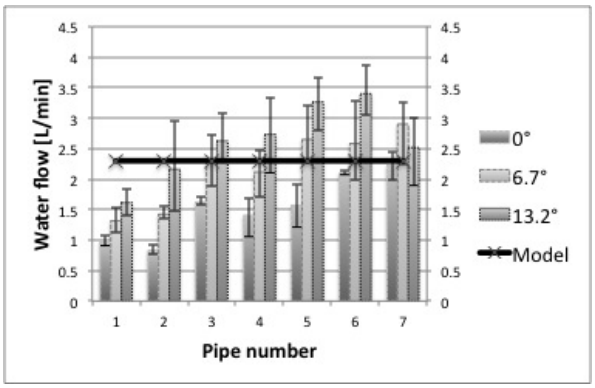

(a)

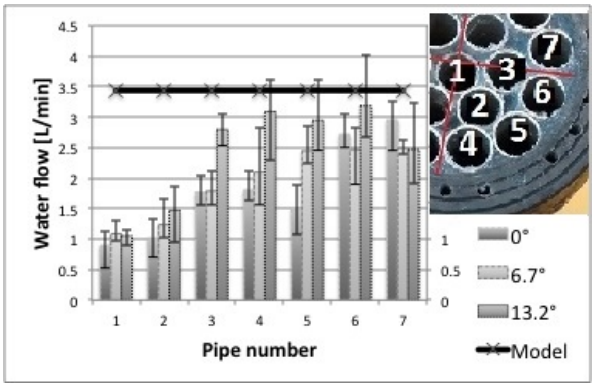

(b)

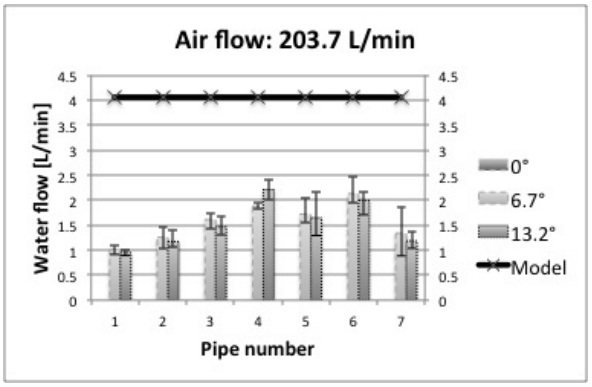

(c)

Figure B.7: Water flow distribution of individual riser tubes for the square setup (alpha =0.64).
(Error bars correspond to minimum and maximum values; air flows of a: 81.2 L/min; b: 142.5 L/min; c: 203.7 L/min)

Appendix C

Air flow calibration in tank used for water collection system

Air flow was calibrated as described in Section 4.2.2. Figure C.1 illustrates where air flow measurements were taken. Detailed results can be found in Figure C.1 and the calibration curve is presented in Figure C.2.

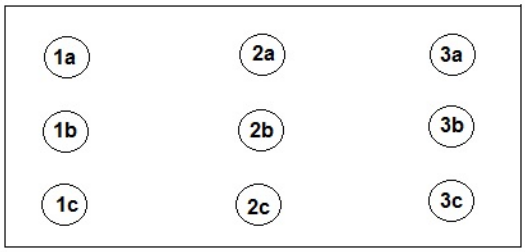

Figure C.1: Representative locations of air flow measurements (top view of tank).

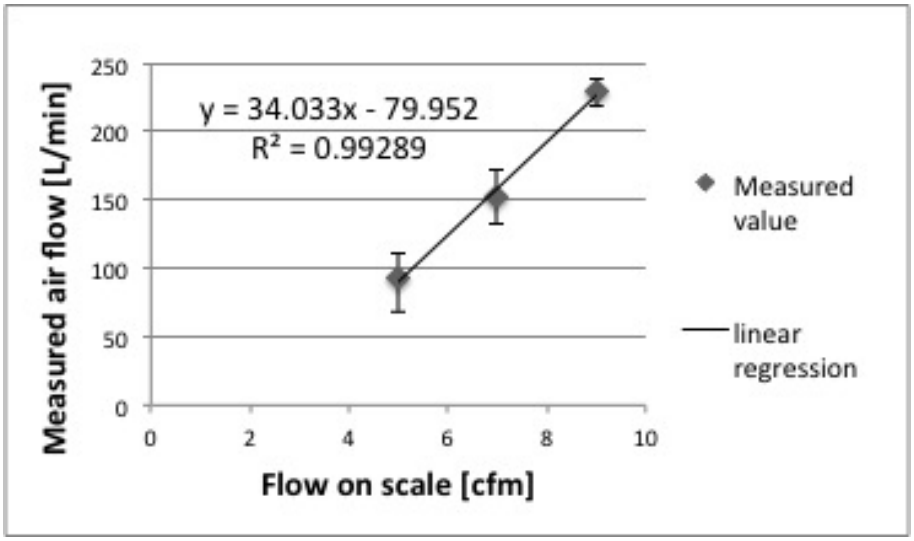

Figure C.2: Calibration curve for the air flowmeter attached to the tank used for the water collection system.
(Error bars correspond to average minimum and maximum values.)

Table C.1: Air flow measurements for calibration of pilot scale tank

Flow on scale cfm	Air measured [L]	Location 1a	1b	1c	2a	2b	2c	3a	3b	3c		
5	0.5	25	28	28	25	17	25	21	24	32		
		28	29	27	23	21	20	25	25	26		Total air
		27	27	23	26	18	22	20	35	23	Average	
	Average [s]	26.67	28.00	26.00	24.67	18.67	22.33	22	28	27	[L/min]	[L/min]
	Air flow [L/min]	1.13	1.07	1.15	1.22	1.61	1.34	1.36	1.07	1.11	1.23	93.54
7	0.5	17.5	17	17	14	13	14	13	15	10		
		16	13	18	14	12	14	17	12.5	13		Total air
		18	20	16	18	15	13	16	20	15	Average	
	Average [s]	17.17	16.67	17.00	15.33	13.33	13.67	15.33	15.83	12.67	[L/min]	[L/min]
	Air flow [L/min]	1.75	1.80	1.76	1.96	2.25	2.20	1.96	1.89	2.37	1.99	151.63
9	1	18	22	18	17	26	23	15	22	20		
		20	26	17	18	22	20	20	26	17		Total air
		18	20	20	20	22	23	17	23	15	Average	
	Average [s]	18.67	22.67	18.33	18.33	23.33	22.00	17.33	23.67	17.33	[L/min]	[L/min]
	Air flow [L/min]	3.21	2.65	3.27	3.27	2.57	2.73	3.46	2.54	3.46	3.02	229.67

Appendix D

Achievable RAS flows for all MBR treatment capacities, scenarios and options considered

Table D.1: Scenario A, 0.75 MGD ($2.84 * 10^6$ L/day), 100% of air above module.

	L [m]	H [m]	Air above module, air per riser tube [L/min]						
	0.53	0.2	7.00	8.00	9.00	10.00	11.00	12.00	**18.00**
Water flow per riser tube [L/min]			0.28	0.58	0.84	1.07	1.27	1.45	**2.19**
Number of riser tubes			1373.00	1201.00	1068.00	961.00	873.00	801.00	**534.00**
Total RAS flow above module [L/min]			390.81	697.82	898.32	1027.55	1108.70	1159.42	**1167.54**

The optimum is presented in bold.

Table D.2: Scenario A, 0.75 MGD ($2.84 * 10^6$ L/day), 90% of air above module, 10% on sides.

	L [m]	H [m]	Air above module, air per riser tube [L/min]					
	0.53	0.2	8.00	9.00	10.00	11.00	12.00	**18.00**
Water flow per riser tube [L/min]			0.58	0.84	1.07	1.27	1.45	**2.19**
Number of riser tubes			948.00	843.00	759.00	690.00	633.00	**421.00**
Total RAS flow above module [L/min]			550.82	709.07	811.56	876.29	916.25	**920.47**
			Air on sides, option I, air per riser tube [L/min]					
	0.83	0.5	4.07	**5.20**	6.33	7.47	8.60	9.73
Water flow per riser tube [L/min]			1.76	**2.32**	2.74	3.07	3.34	3.57
Number of riser tubes			236.00	**184.00**	151.00	128.00	111.00	98.00
Total RAS flow from sides [L/min]			416.43	**426.96**	413.90	393.32	371.06	349.65
			Air on sides, option II, air per riser tube [L/min]					
	0.93	0.6	2.00	**3.00**	5.00	7.00	13.66	24.45
Water flow per riser tube [L/min]			0.32	**1.48**	2.24	2.77	3.17	3.49
Number of riser tubes			480.00	**320.00**	192.00	137.00	70.00	39.00
Total RAS flow from sides [L/min]			155.80	**474.14**	429.18	379.23	221.92	136.03
Total RAS option I [L/min]			**1347.43**					
Total RAS option II [L/min]			**1394.61**					

The optimum is presented in bold. Total RAS flows were calculated by adding the optimum water flow above the module and the optimum water flow in the side for option I and II, respectively.

Table D.3: Scenario A, 0.75 MGD ($2.84 * 10^6$ L/day), 75% of air above module, 25% on sides.

	L [m]	H [m]	Air above module, air per riser tube [L/min]					
	0.53	0.2	7.00	8.00	9.00	10.00	11.00	**12.00**
Water flow per riser tube [L/min]			0.28	0.58	0.84	1.07	1.27	**1.45**
Number of riser tubes			1029.00	901.00	801.00	720.00	655.00	**600.00**
Total RAS flow above module [L/min]		[L/min]	292.89	523.51	673.74	769.86	831.84	**868.48**
			Air on sides, option I, air per riser tube [L/min]					
	0.83	0.5	2.93	4.07	**5.20**	6.33	7.47	
Water flow per riser tube [L/min]			0.99	1.76	**2.32**	2.74	3.07	
Number of riser tubes			819.00	590.00	**462.00**	379.00	321.00	
Total RAS flow from sides [L/min]			810.29	1041.08	**1072.05**	1038.85	986.38	
			Air on sides, option II, air per riser tube [L/min]					
	0.93	0.6	2.00	3.00	**4.00**	5.00	6.00	
Water flow per riser tube [L/min]			0.32	1.48	**2.24**	2.77	3.17	
Number of riser tubes			1201.00	801.00	**600.00**	480.00	400.00	
Total RAS flow from sides [L/min]			389.83	1186.82	**1341.19**	1328.68	1268.13	
Total RAS option I [L/min]			**1940.53**					
Total RAS option II [L/min]			**2209.67**					

The optimum is presented in bold. Total RAS flows were calculated by adding the optimum water flow above the module and the optimum water flow in the side for option I and II, respectively.

Table D.4: Scenario A, 1 MGD ($3.79 * 10^6$ L/day), 100% of air above module.

	L [m]	H [m]	Air above module, air per riser tube [L/min]							
	0.62	0.2	11.33	13.67	16.00	18.33	**20.67**	23.00	25.33	27.67
Water flow per riser tube [L/min]			0.45	0.84	1.16	1.41	**1.61**	1.78	1.93	2.05
Number of riser tubes			1113.00	923.00	788.00	688.00	**610**	548	498	456
Total RAS flow above module [L/min]			504.92	779.91	910.43	966.90	**982.27**	975.96	958.71	934.10

The optimum is presented in bold.

Table D.5: Scenario A, 1 MGD ($3.79 * 10^6$ L/day), 90% of air above module, 10% on sides.

	L [m]	H [m]	Air above module, air per riser tube [L/min]							
	0.62	0.2	11.33	13.67	16.00	18.33	**20.67**	23.00	25.33	27.67
Water flow per riser tube [L/min]			0.45	0.84	1.16	1.41	**1.61**	1.78	1.93	2.05
Number of riser tubes			1001.00	830.00	709.00	619.00	**549.00**	493.00	448.00	410.00
Total RAS flow above module [L/min]			454.11	701.33	819.15	869.93	**884.05**	878.01	862.46	839.87
			Air on sides, option I, air per riser tube [L/min]							
	0.92	0.5	5.00	6.00	7.00	8.00	9.00	**10.00**	11.00	
Water flow per riser tube [L/min]			0.38	0.80	1.15	1.45	1.71	**1.93**	2.13	
Number of riser tubes			252.00	210.00	180.00	157.00	140.00	**126.00**	114.00	
Total RAS flow from sides [L/min]			94.72	167.17	207.33	228.20	239.58	**243.64**	242.50	
			Air on sides, option II, air per riser tube [L/min]							
	1.02	0.6	2.00	**3.00**	5.00	7.00	13.66	24.45		
Water flow per riser tube [L/min]			0.41	**0.93**	1.36	1.71	2.00	2.25		
Number of riser tubes			630.00	**420.00**	252.00	180.00	92.00	51.00		
Total RAS flow from sides [L/min]			255.36	**389.77**	341.71	307.53	184.25	114.85		
Total RAS option I [L/min]			**1127.68**							
Total RAS option II [L/min]			**1273.81**							

The optimum is presented in bold. Total RAS flows were calculated by adding the optimum water flow above the module and the optimum water flow in the side for option I and II, respectively.

Table D.6: Scenario A, 1 MGD ($3.79 * 10^6$ L/day), 75% of air above module, 25% on sides.

	L [m]	H [m]	Air above module, air per riser tube [L/min]						
	0.62	0.2	11.33	13.67	16.00	18.33	**20.67**	23.00	25.33
Water flow per riser tube [L/min]			0.45	0.84	1.16	1.41	**1.61**	1.78	1.93
Number of riser tubes			834.00	692.00	591.00	516.00	**457.00**	411.00	373.00
Total RAS flow above module [L/min]			378.35	584.72	682.82	725.18	**735.90**	731.97	718.07
			Air on sides, option I, air per riser tube [L/min]						
	0.92	0.5	5.00	6.00	7.00	8.00	9.00	**10.00**	
Water flow per riser tube [L/min]			0.38	0.80	1.15	1.45	1.71	**1.93**	
Number of riser tubes			630.00	525.00	450.00	394.00	350.00	**315.00**	
Total RAS flow from sides [L/min]			236.80	417.92	518.31	572.68	598.95	**609.09**	
			Air on sides, option II, air per riser tube [L/min]						
	1.02	0.6	4.00	5.00	6.00	7.00	**8.00**		
Water flow per riser tube [L/min]			0.41	0.93	1.36	1.71	**2.00**		
Number of riser tubes			788.00	630.00	525.00	450.00	**394.00**		
Total RAS flow from sides [L/min]			319.40	584.65	711.90	768.83	**789.09**		
Total RAS option I [L/min]			**1344.99**						
Total RAS option II [L/min]			**1524.99**						

The optimum is presented in bold. Total RAS flows were calculated by adding the optimum water flow above the module and the optimum water flow in the side for option I and II, respectively.

Table D.7: Scenario A, 2 MGD ($7.57 * 10^6$ L/day), 100% of air above module.

	L [m]	H [m]	Air above module, air per riser tube [L/min]
	0.99	0.2	
Water flow per riser tube [L/min]			Submergence ratio is too high to pump water
Number of riser tubes			
Total RAS flow above module [L/min]			

Table D.8: Scenario A, 2 MGD ($7.57 * 10^6$ L/day), 90% of air above module, 10% on sides.

	L [m]	H [m]	Air above module, air per riser tube [L/min]						
	0.99	0.2							
Water flow per riser tube [L/min]			Submergence ratio is too high to pump water						
Number of riser tubes									
Total RAS flow above module [L/min]									
			Air on sides, option I, air per riser tube [L/min]						
	1.29	0.5	**18.33**	18.67	19.00	19.33	19.67	20.00	20.33
Water flow per riser tube [L/min]			**2.40**	2.43	2.46	2.49	2.52	2.54	2.57
Number of riser tubes			**137.00**	135.00	132.00	130.00	128.00	126.00	124.00
Total RAS flow from sides [L/min]			**329.19**	328.34	324.80	323.48	321.95	320.23	318.31
			Air on sides, option II, air per riser tube [L/min]						
	1.39	0.6	**18.33**	18.67	19.00	19.33	19.67	20.00	
Water flow per riser tube [L/min]			**2.93**	2.96	2.99	3.01	3.04	3.07	
Number of riser tubes			**137.00**	135.00	132.00	130.00	128.00	126.00	
Total RAS flow from sides [L/min]			**401.91**	399.81	394.50	391.95	389.20	386.26	
Total RAS option I [L/min]			**329.19**						
Total RAS option II [L/min]			**401.91**						

The optimum is presented in bold. Total RAS flows were calculated by adding the optimum water flow above the module and the optimum water flow in the side for option I and II, respectively.

Table D.9: Scenario A, 2 MGD ($7.57 * 10^6$ L/day), 75% of air above module, 25% on sides.

	L [m]	H [m]	Air above module, air per riser tube [L/min]					
	0.99	0.2						
Water flow per riser tube [L/min]			Submergence ratio is too high to pump water					
Number of riser tubes								
Total RAS flow above module [L/min]								
			Air on sides, option I, air per riser tube [L/min]					
	1.29	0.5	**18.33**	18.67	19.00	19.33	19.67	
Water flow per riser tube [L/min]			**2.40**	2.43	2.46	2.49	2.52	
Number of riser tubes			**344.00**	337.00	332.00	326.00	320.00	
Total RAS flow from sides [L/min]			**826.57**	819.63	816.92	811.19	804.88	
			Air on sides, option II, air per riser tube [L/min]					
	1.39	0.6	**18.33**	18.67	19.00	19.33	19.67	20.00
Water flow per riser tube [L/min]			**2.93**	2.96	2.99	3.01	3.04	3.07
Number of riser tubes			**344.00**	337.00	332.00	326.00	320.00	315.00
Total RAS flow from sides [L/min]			**1009.18**	998.04	992.23	982.89	973.00	965.66
Total RAS option I [L/min]			**826.57**					
Total RAS option II [L/min]			**1009.18**					

The optimum is presented in bold. Total RAS flows were calculated by adding the optimum water flow above the module and the optimum water flow in the side for option I and II, respectively.

Table D.10: Scenario A, 5 MGD ($18.93 * 10^6$ L/day), 100% of air above module.

	L [m]	H [m]	Air above module, air per riser tube [L/min]
	1.63	0.2	
Water flow per riser tube [L/min]			Submergence ratio is too high to pump water
Number of riser tubes			
Total RAS flow above module [L/min]			

Table D.11: Scenario A, 5 MGD ($18.93 * 10^6$ L/day), 90% of air above module, 10% on sides.

	L [m]	H [m]	Air above module, air per riser tube [L/min]						
	1.63	0.2							
Water flow per riser tube [L/min]			Submergence ratio is too high to pump water						
Number of riser tubes									
Total RAS flow above module [L/min]									
			Air on sides, option I, air per riser tube [L/min]						
	1.93	0.5	18.00	18.33	18.67	19.00	19.33	19.67	**20.00**
Water flow per riser tube [L/min]			0.22	0.26	0.30	0.33	0.37	0.40	**0.43**
Number of riser tubes			350.00	344.00	337.00	332.00	326.00	320.00	**315.00**
Total RAS flow from sides [L/min]			77.26	88.90	99.46	109.88	119.28	127.98	**136.45**
			Air on sides, option II, air per riser tube [L/min]						
	2.03	0.6	18.00	18.33	18.67	19.00	19.33	**19.67**	
Water flow per riser tube [L/min]			0.98	1.02	1.05	1.09	1.12	**1.15**	
Number of riser tubes			350.00	344.00	337.00	332.00	326.00	**320.00**	
Total RAS flow from sides [L/min]			344.59	350.64	354.90	360.56	364.50	**367.78**	
Total RAS option I [L/min]			**136.45**						
Total RAS option II [L/min]			**367.78**						

The optimum is presented in bold. Total RAS flows were calculated by adding the optimum water flow above the module and the optimum water flow in the side for option I and II, respectively.

Table D.12: Scenario A, 5 MGD ($18.93 * 10^6$ L/day), 75% of air above module, 25% on sides.

	L [m]	H [m]	Air above module, air per riser tube [L/min]				
	1.63	0.2					
Water flow per riser tube [L/min]			Submergence ratio is too high to pump water				
Number of riser tubes							
Total RAS flow above module [L/min]							
			Air on sides, option I, air per riser tube [L/min]				
	1.93	0.5	18.00	18.33	18.67	19.00	**19.33**
Water flow per riser tube [L/min]			0.22	0.26	0.30	0.33	**0.37**
Number of riser tubes			876.00	860.00	844.00	830.00	**815.00**
Total RAS flow from sides [L/min]			193.38	222.24	249.10	274.69	**298.19**
			Air on sides, option II, air per riser tube [L/min]				
	2.03	0.6	18.00	18.33	**18.67**		
Water flow per riser tube [L/min]			0.98	1.02	**1.05**		
Number of riser tubes			876.00	860.00	**844.00**		
Total RAS flow from sides [L/min]			862.46	876.59	**888.83**		
Total RAS option I [L/min]			**298.19**				
Total RAS option II [L/min]			**888.83**				

The optimum is presented in bold. Total RAS flows were calculated by adding the optimum water flow above the module and the optimum water flow in the side for option I and II, respectively.

Table D.13: Scenario A, 10 MGD ($37.85 * 10^6$ $^{L}/_{day}$), 100% of air above module.

	L [m]	H [m]	Air above module, air per riser tube [L/min]
	2.67	0.2	
Water flow per riser tube [L/min]			Submergence ratio is too high to pump water
Number of riser tubes			
Total RAS flow above module [L/min]			

Table D.14: Scenario A, 10 MGD ($37.85 * 10^6$ L/day), 90% of air above module, 10% on sides.

	L [m]	H [m]	Air above module, air per riser tube [L/min]				
	2.67	0.2					
Water flow per riser tube [L/min]			Submergence ratio is too high to pump water				
Number of riser tubes							
Total RAS flow above module [L/min]							
			Air on sides, option I, air per riser tube [L/min]				
	2.97	0.5	67.35	78.10	88.85	**99.60**	
Water flow per riser tube [L/min]			0.09	0.31	0.47	**0.58**	
Number of riser tubes			187.00	161.00	141.00	**126.00**	
Total RAS flow from sides [L/min]			16.72	50.48	66.01	**73.51**	
			Air on sides, option II, air per riser tube [L/min]				
	3.07	0.6	**56.61**	67.35	78.10	88.85	99.6
Water flow per riser tube [L/min]			**1.03**	1.20	1.33	1.43	1.509892
Number of riser tubes			**222.00**	187.00	161.00	141.00	126
Total RAS flow from sides [L/min]			**227.71**	225.24	214.84	202.04	190.2464
Total RAS option I [L/min]			**73.51**				
Total RAS option II [L/min]			**227.71**				

The optimum is presented in bold. Total RAS flows were calculated by adding the optimum water flow above the module and the optimum water flow in the side for option I and II, respectively.

Table D.15: Scenario A, 10 MGD ($37.85 * 10^6$ L/day), 75% of air above module, 25% on sides.

	L [m]	H [m]	Air above module, air per riser tube [L/min]			
	2.67	0.2				
Water flow per riser tube [L/min]	Submergence ratio is too high to pump water					
Number of riser tubes						
Total RAS flow above module [L/min]						
			Air on sides, option I, air per riser tube [L/min]			
	2.97	0.5	67.35	78.10	88.85	**99.60**
Water flow per riser tube [L/min]			0.09	0.31	0.47	**0.58**
Number of riser tubes			468.00	403.00	354.00	**316.00**
Total RAS flow from sides [L/min]			41.85	126.35	165.74	**184.35**
			Air on sides, option II, air per riser tube [L/min]			
	3.07	0.6	**56.61**	67.35	78.10	
Water flow per riser tube [L/min]			**1.03**	1.20	1.33	
Number of riser tubes			**557.00**	468.00	403.00	
Total RAS flow from sides [L/min]			**571.33**	563.71	537.78	
Total RAS option I [L/min]			**184.35**			
Total RAS option II [L/min]			**571.33**			

The optimum is presented in bold. Total RAS flows were calculated by adding the optimum water flow above the module and the optimum water flow in the side for option I and II, respectively.

Table D.16: Scenario B, 0.5 MGD ($1.83 * 10^6$ L/day), 100% of air above module.

	L [m]	H [m]	Air above module, air per riser tube [L/min]							
	0.36	0.2	3.90	5.13	**6.35**	7.57	8.79	10.01	11.24	12.46
Water flow per riser tube [L/min]			1.07	1.70	**2.17**	2.53	2.82	3.06	3.26	3.43
Number of riser tubes			1615.00	1230.00	**993.00**	833.00	717.00	629.00	561.00	506.00
Total RAS flow above module [L/min]			1734.00	2093.07	**2153.66**	2108.02	2022.13	1923.61	1827.55	1734.38

The optimum is presented in bold.

Table D.17: Scenario B, 0.5 MGD ($1.83 * 10^6$ L/day), 90% of air above module, 10% on sides.

	L [m]	H [m]	Air above module, air per riser tube [L/min]						
	0.36	0.2	2.68	3.90	5.13	**6.35**	7.57	8.79	10.01
Water flow per riser tube [L/min]			0.20	1.07	1.70	**2.17**	2.53	2.82	3.06
Number of riser tubes			2116.00	1454.00	1107.00	**894.00**	749.00	647.00	566.00
Total RAS flow above module [L/min]			427.98	1561.14	1883.77	**1938.94**	1895.45	1824.71	1730.94
			Air on sides, option I, air per riser tube [L/min]						
	0.66	0.5	**2.68**	3.90	5.13	6.35	7.57	8.79	10.01
Water flow per riser tube [L/min]			**2.49**	3.25	3.76	4.14	4.44	4.68	4.88
Number of riser tubes			**235.00**	161.00	123.00	99.00	83.00	71.00	62.00
Total RAS flow from sides [L/min]			**585.11**	522.53	462.27	409.75	368.24	332.13	302.46
			Air on sides, option II, air per riser tube [L/min]						
	0.76	0.6	**2.68**	3.90	5.13	6.35	7.57	8.79	
Water flow per riser tube [L/min]			**2.84**	3.56	4.05	4.42	4.71	4.94	
Number of riser tubes			**235.00**	161.00	123.00	99.00	83.00	71.00	
Total RAS flow from sides [L/min]			**666.58**	572.75	498.24	437.47	390.77	350.96	
Total RAS option I [L/min]			**2524.05**						
Total RAS option II [L/min]			**2605.52**						

The optimum is presented in bold. Total RAS flows were calculated by adding the optimum water flow above the module and the optimum water flow in the side for option I and II, respectively.

Table D.18: Scenario B, 0.5 MGD ($1.83 * 10^6$ L/day), 75% of air above module, 25% on sides.

	L [m]	H [m]	Air above module, air per riser tube [L/min]					
	0.36	0.2	2.68	3.90	5.13	**6.35**	7.57	8.79
Water flow per riser tube [L/min]			0.20	1.07	1.70	**2.17**	2.53	2.82
Number of riser tubes			1764.00	1211.00	922.00	**745.00**	624.00	538.00
Total RAS flow above module [L/min]			356.78	1300.23	1568.95	**1615.79**	1579.12	1517.30
			Air on sides, option I, air per riser tube [L/min]					
	0.66	0.5	**2.68**	3.90	5.13	6.35	7.57	
Water flow per riser tube [L/min]			**2.49**	3.25	3.76	4.14	4.44	
Number of riser tubes			**588.00**	403.00	307.00	248.00	208.00	
Total RAS flow from sides [L/min]			**1464.02**	1307.94	1153.80	1026.45	922.82	
			Air on sides, option II, air per riser tube [L/min]					
	0.76	0.6	**2.00**	3.00	5.00			
Water flow per riser tube [L/min]			**2.84**	3.06	4.00			
Number of riser tubes			**788.00**	525.00	315.00			
Total RAS flow from sides [L/min]			**2235.17**	1604.61	1258.74			
Total RAS option I [L/min]			**3079.80**					
Total RAS option II [L/min]			**3850.96**					

The optimum is presented in bold. Total RAS flows were calculated by adding the optimum water flow above the module and the optimum water flow in the side for option I and II, respectively.

Table D.19: Scenario B, 0.75 MGD ($2.84 * 10^6$ L/day), 100% of air above module.

	L [m]	H [m]	Air above module, air per riser tube [L/min]							
	0.43	0.2	3.90	5.13	6.35	7.57	**8.79**	10.01	11.24	12.46
Water flow per riser tube [L/min]			0.12	0.74	1.23	1.62	**1.94**	2.20	2.42	2.61
Number of riser tubes			2462.00	1875.00	1514.00	1269.00	**1093.00**	959.00	855.00	771.00
Total RAS flow above module [L/min]			299.59	1388.52	1864.67	2059.22	**2120.03**	2111.11	2070.15	2011.28

The optimum is presented in bold.

Table D.20: Scenario B, 0.75 MGD ($2.84 * 10^6$ L/day), 90% of air above module, 10% on sides.

	L [m]	H [m]	Air above module, air per riser tube [L/min]						
	0.43	0.2	3.90	5.13	6.35	7.57	**8.79**	10.01	
Water flow per riser tube [L/min]			0.12	0.74	1.23	1.62	**1.94**	2.20	
Number of riser tubes			1944.00	1481.00	1195.00	1002.00	**865.00**	758.00	
Total RAS flow above module [L/min]			236.55	1096.74	1471.78	1625.96	**1677.79**	1668.63	
			Air on sides, option I, air per riser tube [L/min]						
	0.73	0.5	2.68	**3.90**	5.13	6.35	7.57	8.79	10.01
Water flow per riser tube [L/min]			1.75	**2.58**	3.14	3.56	3.88	4.14	4.35
Number of riser tubes			358.00	**246.00**	187.00	151.00	126.00	109.00	95.00
Total RAS flow from sides [L/min]			626.41	**635.38**	587.99	537.21	488.75	451.04	413.47
			Air on sides, option II, air per riser tube [L/min]						
	0.83	0.6	**2.00**	3.00	5.00	7.00	13.66	24.45	
Water flow per riser tube [L/min]			**2.18**	2.97	3.51	3.90	4.21	4.46	
Number of riser tubes			**480.00**	320.00	192.00	137.00	70.00	39.00	
Total RAS flow from sides [L/min]			**1045.32**	950.84	673.49	534.90	294.98	174.11	
Total RAS option I [L/min]			**2313.17**						
Total RAS option II [L/min]			**2723.11**						

The optimum is presented in bold. Total RAS flows were calculated by adding the optimum water flow above the module and the optimum water flow in the side for option I and II, respectively.

Table D.21: Scenario B, 0.75 MGD ($2.84 * 10^6$ L/day), 75% of air above module, 25% on sides.

	L [m]	H [m]	Air above module, air per riser tube [L/min]					
	0.43	0.2	3.90	5.13	6.35	7.57	**8.79**	10.01
Water flow per riser tube [L/min]			0.12	0.74	1.23	1.62	**1.94**	2.20
Number of riser tubes			1846.00	1406.00	1135.00	952.00	**819.00**	719.00
Total RAS flow above module [L/min]			224.63	1041.20	1397.88	1544.82	**1588.56**	1582.78
			Air on sides, option I, air per riser tube [L/min]					
	0.73	0.5	2.68	**3.90**	5.13	6.35	7.57	
Water flow per riser tube [L/min]			1.75	**2.58**	3.14	3.56	3.88	
Number of riser tubes			896.00	**615.00**	468.00	378.00	317.00	
Total RAS flow from sides [L/min]			1567.78	**1588.46**	1471.56	1344.81	1229.63	
			Air on sides, option II, air per riser tube [L/min]					
	0.83	0.6	**2.00**	3.00	4.00			
Water flow per riser tube [L/min]			**2.18**	2.97	3.51			
Number of riser tubes			**1201.00**	801.00	600.00			
Total RAS flow from sides [L/min]			**2615.48**	2380.08	2104.65			
Total RAS option I [L/min]			**3177.03**					
Total RAS option II [L/min]			**4204.05**					

The optimum is presented in bold. Total RAS flows were calculated by adding the optimum water flow above the module and the optimum water flow in the side for option I and II, respectively.

Table D.22: Scenario B, 1 MGD ($3.79 * 10^6$ L/day), 100% of air above module.

	L [m]	H [m]	Air above module, air per riser tube [L/min]							
	0.52	0.2	6.35	7.57	8.79	10.01	11.24	12.46	**13.68**	15.00
Water flow per riser tube [L/min]			0.14	0.53	0.86	1.14	1.38	1.59	**1.77**	1.94
Number of riser tubes			1987.00	1666.00	1435.00	1259.00	1122.00	1012.00	**922.00**	841.00
Total RAS flow above module [L/min]			279.49	884.18	1237.74	1440.67	1553.78	1610.95	**1633.38**	1631.88

The optimum is presented in bold.

Table D.23: Scenario B, 1 MGD ($3.79 * 10^6$ L/day), 90% of air above module, 10% on sides.

	L [m]	H [m]	Air above module, air per riser tube [L/min]							
	0.52	0.2	6.35	7.57	8.79	10.01	11.24	12.46	**13.68**	15.00
Water flow per riser tube [L/min]			0.14	0.53	0.86	1.14	1.38	1.59	**1.77**	1.94
Number of riser tubes			1788.00	1499.00	1291.00	1133.00	1010.00	911.00	**830.00**	757.00
Total RAS flow above module [L/min]			251.50	795.55	1113.54	1296.49	1398.68	1450.17	**1470.40**	1468.88
			Air on sides, option I, air per riser tube [L/min]							
	0.82	0.5	2.68	3.90	**5.13**	6.35	7.57	8.79	10.01	
Water flow per riser tube [L/min]			0.84	1.73	**2.34**	2.80	3.15	3.43	3.67	
Number of riser tubes			470.00	323.00	**246.00**	198.00	166.00	143.00	125.00	
Total RAS flow from sides [L/min]			392.51	558.17	**576.76**	554.16	523.01	490.94	458.25	
			Air on sides, option II, air per riser tube [L/min]							
	0.92	0.6	2.00	**3.00**	5.00	7.00	13.66	24.45		
Water flow per riser tube [L/min]			1.33	**2.20**	2.79	3.22	3.56	3.83		
Number of riser tubes			630.00	**420.00**	252.00	180.00	92.00	51.00		
Total RAS flow from sides [L/min]			835.76	**923.08**	702.71	580.12	327.51	195.38		
Total RAS option I [L/min]			**2047.16**							
Total RAS option II [L/min]			**2393.48**							

The optimum is presented in bold. Total RAS flows were calculated by adding the optimum water flow above the module and the optimum water flow in the side for option I and II, respectively.

Table D.24: Scenario B, 1 MGD ($3.79 * 10^6$ L/day), 75% of air above module, 25% on sides.

	L [m]	H [m]	Air above module, air per riser tube [L/min]					
	0.52	0.2	6.35	7.57	8.79	11.24	12.46	**13.68**
Water flow per riser tube [L/min]			0.14	0.53	0.86	1.38	1.59	**1.77**
Number of riser tubes			1490.00	1249.00	1076.00	842.00	759.00	**691.00**
Total RAS flow above module [L/min]			209.58	662.87	928.09	1166.03	1208.21	**1224.15**
			Air on sides, option I, air per riser tube [L/min]					
	0.82	0.5	2.68	3.90	**5.13**	6.35	7.57	
Water flow per riser tube [L/min]			0.84	1.73	**2.34**	2.80	3.15	
Number of riser tubes			1176.00	807.00	**615.00**	496.00	416.00	
Total RAS flow from sides [L/min]			982.12	1394.57	**1441.91**	1388.21	1310.67	
			Air on sides, option II, air per riser tube [L/min]					
	0.92	0.6	2.00	**3.00**	4.00			
Water flow per riser tube [L/min]			1.33	**2.20**	2.79			
Number of riser tubes			1577.00	**1051.00**	788.00			
Total RAS flow from sides [L/min]			2092.06	**2309.90**	2197.37			
Total RAS option I [L/min]			**2666.06**					
Total RAS option II [L/min]			**3534.05**					

The optimum is presented in bold. Total RAS flows were calculated by adding the optimum water flow above the module and the optimum water flow in the side for option I and II, respectively.

Table D.25: Scenario B, 2 MGD ($7.57 * 10^6$ L/day), 100% of air above module.

	L [m]	H [m]	Air above module, air per riser tube [L/min]							
	0.89	0.2	24.36	35.11	**45.86**	56.61	67.35	78.10	88.85	99.60
Water flow per riser tube [L/min]			0.32	0.94	**1.29**	1.51	1.66	1.78	1.86	1.93
Number of riser tubes			1035.00	718.00	**550.00**	445.00	374.00	323.00	283.00	253.00
Total RAS flow above module [L/min]			334.56	674.12	**708.04**	671.94	622.31	573.77	526.91	488.00

The optimum is presented in bold.

Table D.26: Scenario B, 2 MGD ($2.84 * 10^6$ L/day), 90% of air above module, 10% on sides.

	L [m]	H [m]	Air above module, air per riser tube [L/min]						
	0.89	0.2	24.36	35.11	**45.86**	56.61	67.35	78.10	88.85
Water flow per riser tube [L/min]			0.32	0.94	**1.29**	1.51	1.66	1.78	1.86
Number of riser tubes			932.00	646.00	**495.00**	401.00	337.00	290.00	255.00
Total RAS flow above module [L/min]			301.26	606.52	**637.24**	605.50	560.75	515.15	474.78
			Air on sides, option I, air per riser tube [L/min]						
	1.19	0.5	6.35	7.57	8.79	10.01	**11.24**	12.46	13.68
Water flow per riser tube [L/min]			0.68	1.08	1.41	1.69	**1.93**	2.13	2.31
Number of riser tubes			397.00	333.00	287.00	251.00	**224.00**	202.00	184.00
Total RAS flow from sides [L/min]			268.27	359.21	405.57	424.98	**432.39**	430.99	424.99
			Air on sides, option II, air per riser tube [L/min]						
	1.29	0.6	3.90	5.13	6.35	7.57	**8.79**	10.01	
Water flow per riser tube [L/min]			0.12	0.75	1.25	1.65	**1.97**	2.24	
Number of riser tubes			646.00	492.00	397.00	333.00	**287.00**	251.00	
Total RAS flow from sides [L/min]			78.70	366.85	494.42	548.14	**566.03**	562.88	
Total RAS option I [L/min]			**1069.62**						
Total RAS option II [L/min]			**1203.27**						

The optimum is presented in bold. Total RAS flows were calculated by adding the optimum water flow above the module and the optimum water flow in the side for option I and II, respectively.

Table D.27: Scenario B, 2 MGD ($2.84 * 10^6$ L/day), 75% of air above module, 25% on sides.

	L [m]	H [m]	Air above module, air per riser tube [L/min]						
	0.89	0.2	24.36	35.11	**45.86**	56.61	67.35	78.10	88.85
Water flow per riser tube [L/min]			0.32	0.94	**1.29**	1.51	1.66	1.78	1.86
Number of riser tubes			776.00	539.00	**412.00**	334.00	280.00	242.00	212.00
Total RAS flow above module [L/min]		[L/min]	250.84	506.06	**530.39**	504.33	465.90	429.89	394.72
			Air on sides, option I, air per riser tube [L/min]						
	1.19	0.5	6.35	7.57	8.79	10.01	**11.24**		
Water flow per riser tube [L/min]			0.68	1.08	1.41	1.69	**1.93**		
Number of riser tubes			993.00	833.00	717.00	629.00	**561.00**		
Total RAS flow from sides [L/min]			671.01	898.58	1013.22	1064.98	**1082.90**		
			Air on sides, option II, air per riser tube [L/min]						
	1.29	0.6	3.90	5.13	6.35	7.57	**8.79**	10.01	
Water flow per riser tube [L/min]			0.12	0.75	1.25	1.65	**1.97**	2.24	
Number of riser tubes			1615.00	1230.00	993.00	833.00	**717.00**	629.00	
Total RAS flow from sides [L/min]			196.75	917.13	1236.68	1371.17	**1414.10**	1410.57	
Total RAS option I [L/min]			**1613.29**						
Total RAS option II [L/min]			**1944.49**						

The optimum is presented in bold. Total RAS flows were calculated by adding the optimum water flow above the module and the optimum water flow in the side for option I and II, respectively.

Table D.28: Scenario B, 5 MGD ($18.93 * 10^6$ $^{L}/_{day}$), 100% of air above module.

	L [m]	H [m]	Air above module, air per riser tube [L/min]
	2.67	0.2	
Water flow per riser tube [L/min]			Submergence ratio is too high to pump water
Number of riser tubes			
Total RAS flow above module [L/min]			

Table D.29: Scenario B, 5 MGD ($18.93 * 10^6$ L/day), 90% of air above module, 10% on sides.

	L [m]	H [m]	Air above module, air per riser tube [L/min]						
	1.53	0.2							
Water flow per riser tube [L/min]			Submergence ratio is too high to pump water						
Number of riser tubes									
Total RAS flow above module [L/min]									
			Air on sides, option I, air per riser tube [L/min]						
	1.83	0.5	13.61	**24.36**	35.11	45.86	56.61	67.35	78.10
Water flow per riser tube [L/min]			0.33	**1.43**	1.95	2.25	2.44	2.57	3.21
Number of riser tubes			463.00	**258.00**	179.00	137.00	111.00	93.00	80.00
Total RAS flow from sides [L/min]			151.12	**368.27**	348.60	307.64	270.58	239.12	256.61
			Air on sides, option II, air per riser tube [L/min]						
	1.93	0.6	13.61	**24.36**	35.11	45.86	56.61	67.35	
Water flow per riser tube [L/min]			1.02	**2.06**	2.54	2.82	2.99	3.12	
Number of riser tubes			463.00	**258.00**	179.00	137.00	111.00	93.00	
Total RAS flow from sides [L/min]			472.17	**530.75**	454.54	385.74	332.32	289.95	
Total RAS option I [L/min]			**368.27**						
Total RAS option II [L/min]			**530.75**						

The optimum is presented in bold. Total RAS flows were calculated by adding the optimum water flow above the module and the optimum water flow in the side for option I and II, respectively.

Table D.30: Scenario B, 5 MGD ($18.93 * 10^6$ L/day), 75% of air above module, 25% on sides.

	L [m]	H [m]	Air above module, air per riser tube [L/min]				
	1.53	0.2					
Water flow per riser tube [L/min]			Submergence ratio is too high to pump water				
Number of riser tubes							
Total RAS flow above module [L/min]							
			Air on sides, option I, air per riser tube [L/min]				
	1.83	0.5	13.61	**24.36**	35.11	45.86	56.61
Water flow per riser tube [L/min]			0.33	**1.43**	1.95	2.25	2.44
Number of riser tubes			1158.00	**647.00**	449.00	343.00	278.00
Total RAS flow from sides [L/min]			377.96	**923.53**	874.43	770.21	677.66
			Air on sides, option II, air per riser tube [L/min]				
	1.93	0.6	13.61	**24.36**	35.11		
Water flow per riser tube [L/min]			1.02	**2.06**	2.54		
Number of riser tubes			1158.00	**647.00**	449.00		
Total RAS flow from sides [L/min]			1180.93	**1331.00**	1140.17		
Total RAS option I [L/min]			**923.53**				
Total RAS option II [L/min]			**1331.00**				

The optimum is presented in bold. Total RAS flows were calculated by adding the optimum water flow above the module and the optimum water flow in the side for option I and II, respectively.

Table D.31: Scenario B, 10 MGD ($37.85 * 10^6$ L/day), 100% of air above module.

	L [m]	H [m]	Air above module, air per riser tube [L/min]
	2.67	0.2	
Water flow per riser tube [L/min]			Submergence ratio is too high to pump water
Number of riser tubes			
Total RAS flow above module [L/min]			

Table D.32: Scenario B, 10 MGD ($37.85 * 10^6$ L/day), 90% of air above module, 10% on sides.

	L [m]	H [m]	Air above module, air per riser tube [L/min]				
	2.57	0.2					
Water flow per riser tube [L/min]			Submergence ratio is too high to pump water				
Number of riser tubes							
Total RAS flow above module [L/min]							
			Air on sides, option I, air per riser tube [L/min]				
	2.87	0.5	67.35	78.10	88.85	**99.60**	
Water flow per riser tube [L/min]			0.09	0.31	0.47	**0.58**	
Number of riser tubes			187.00	161.00	141.00	**126.00**	
Total RAS flow from sides [L/min]			16.72	50.48	66.01	**73.51**	
			Air on sides, option II, air per riser tube [L/min]				
	2.97	0.6	**56.61**	67.35	78.10	88.85	99.60
Water flow per riser tube [L/min]			**1.03**	1.20	1.33	1.43	1.51
Number of riser tubes			**222.00**	187.00	161.00	141.00	126.00
Total RAS flow from sides [L/min]			**227.71**	225.24	214.84	202.04	190.25
Total RAS option I [L/min]			**73.51**				
Total RAS option II [L/min]			**227.71**				

The optimum is presented in bold. Total RAS flows were calculated by adding the optimum water flow above the module and the optimum water flow in the side for option I and II, respectively.

Table D.33: Scenario B, 10 MGD (37.85 $*10^6$ $^{L}/_{day}$), 75% of air above module, 25% on sides.

	L [m]	H [m]	Air above module, air per riser tube [L/min]			
	2.57	0.2				
Water flow per riser tube [L/min]			Submergence ratio is too high to pump water			
Number of riser tubes						
Total RAS flow above module [L/min]						
			Air on sides, option I, air per riser tube [L/min]			
	2.87	0.5	67.35	78.10	88.85	**99.60**
Water flow per riser tube [L/min]			0.09	0.31	0.47	**0.58**
Number of riser tubes			468.00	403.00	354.00	**316.00**
Total RAS flow from sides [L/min]			41.85	126.35	165.74	**184.35**
			Air on sides, option II, air per riser tube [L/min]			
	2.97	0.6	**56.61**	67.35	78.10	
Water flow per riser tube [L/min]			**1.03**	1.20	1.33	
Number of riser tubes			**557.00**	468.00	403.00	
Total RAS flow from sides [L/min]			**571.33**	563.71	537.78	
Total RAS option I [L/min]			**184.35**			
Total RAS option II [L/min]			**571.33**			

The optimum is presented in bold. Total RAS flows were calculated by adding the optimum water flow above the module and the optimum water flow in the side for option I and II, respectively.

Table D.34: Scenario C, 0.5 MGD ($1.83 * 10^6$ L/day), 100% of air above module.

	L [m]	H [m]	Air above module, air per riser tube [L/min]							
	0.46	0.3	2.00	3.00	**4.00**	6.00	8.00	10.00	13.66	24.45
Water flow per riser tube [L/min]			0.61	1.56	**2.21**	3.05	3.58	3.97	4.45	5.16
Number of riser tubes			3154.00	2102.00	**1577.00**	1051.00	788.00	630.00	461.00	258.00
Total RAS flow above module [L/min]			1928.36	3269.03	**3481.07**	3205.34	2824.03	2502.74	2049.69	1331.28

The optimum is presented in bold.

Table D.35: Scenario C, 0.5 MGD ($1.83 * 10^6$ L/day), 90% of air above module, 10% on sides.

	L [m]	H [m]		Air above module, air per riser tube [L/min]					
	0.46	0.3	**4.00**	7.00	10.00	13.66	17.00	24.45	
Water flow per riser tube [L/min]			**2.21**	3.35	3.96	4.45	4.74	5.16	
Number of riser tubes			**1419.00**	811.00	567.00	415.00	334.00	232.00	
Total RAS flow above module [L/min]			**3132.30**	2713.28	2247.02	1845.17	1583.16	1196.77	
				Air on sides, option I, air per riser tube [L/min]					
	0.66	0.5	**2.00**	3.00	4.00	5.00	7.00	13.66	24.45
Water flow per riser tube [L/min]			**1.84**	2.72	3.29	3.71	4.31	4.55	5.45
Number of riser tubes			**315.00**	210.00	157.00	126.00	90.00	46.00	25.00
Total RAS flow from sides [L/min]			**579.29**	571.41	516.88	467.74	387.99	209.15	136.29
				Air on sides, option II, air per riser tube [L/min]					
	0.76	0.6	**2.00**	3.00	5.00	7.00	13.66	24.45	
Water flow per riser tube [L/min]			**2.22**	3.06	4.00	4.59	5.57	6.38	
Number of riser tubes			**315.00**	210.00	126.00	90.00	46.00	25.00	
Total RAS flow from sides [L/min]			**699.30**	641.84	503.50	412.72	256.35	159.60	
Total RAS option I [L/min]			**3711.59**						
Total RAS option II [L/min]			**3831.60**						

The optimum is presented in bold. Total RAS flows were calculated by adding the optimum water flow above the module and the optimum water flow in the side for option I and II, respectively.

Table D.36: Scenario C, 0.5 MGD ($1.83 * 10^6$ L/day), 75% of air above module, 25% on sides.

	L [m]	H [m]	Air above module, air per riser tube [L/min]				
	0.46	0.3	**4.00**	10.00	13.66	17.00	24.45
Water flow per riser tube [L/min]			**2.21**	3.96	4.45	4.74	5.16
Number of riser tubes			**1182.00**	473.00	346.00	278.00	193.00
Total RAS flow above module [L/min]			**2609.15**	1874.50	1538.38	1317.72	995.59
			Air on sides, option I, air per riser tube [L/min]				
	0.66	0.5	**2.00**	3.00	4.00	5.00	7.00
Water flow per riser tube [L/min]			**1.84**	2.72	3.29	3.71	4.31
Number of riser tubes			**788.00**	525.00	394.00	315.00	225.00
Total RAS flow from sides [L/min]			**1449.13**	1428.53	1297.13	1169.34	969.98
			Air on sides, option II, air per riser tube [L/min]				
	0.76	0.6	**2.00**	3.00	5.00		
Water flow per riser tube [L/min]			**2.22**	3.06	4.00		
Number of riser tubes			**788.00**	525.00	315.00		
Total RAS flow from sides [L/min]			**1749.36**	1604.61	1258.74		
Total RAS option I [L/min]			**4058.28**				
Total RAS option II [L/min]			**4358.51**				

The optimum is presented in bold. Total RAS flows were calculated by adding the optimum water flow above the module and the optimum water flow in the side for option I and II, respectively.

Table D.37: Scenario C, 0.75 MGD ($2.84 * 10^6$ L/day), 100% of air above module.

	L [m]	H [m]	Air above module, air per riser tube [L/min]							
	0.53	0.3	2.68	3.90	5.13	**6.35**	7.57	8.79	10.01	11.24
Water flow per riser tube [L/min]			0.40	1.28	1.91	**2.38**	2.74	3.03	3.27	3.47
Number of riser tubes			3584.00	2462.00	1875.00	**1514.00**	1269.00	1093.00	959.00	855.00
Total RAS flow above module [L/min]			1415.74	3153.17	3581.11	**3597.96**	3474.33	3309.07	3131.93	2963.36

The optimum is presented in bold.

Table D.38: Scenario C, 0.75 MGD ($2.84 * 10^6$ L/day), 90% of air above module, 10% on sides.

	L [m]	H [m]	Air above module, air per riser tube [L/min]						
	0.53	0.3	2.68	3.90	5.13	**6.35**	7.57	8.79	10.01
Water flow per riser tube [L/min]			0.40	1.28	1.91	**2.38**	2.74	3.03	3.27
Number of riser tubes			3225.00	1944.00	1481.00	**1195.00**	1002.00	865.00	758.00
Total RAS flow above module [L/min]			1273.93	2489.75	2828.60	**2839.87**	2743.32	2618.80	2475.50
			Air on sides, option I, air per riser tube [L/min]						
	0.73	0.5	2.68	**3.90**	5.13	6.35	7.57	8.79	10.01
Water flow per riser tube [L/min]			1.75	**2.58**	3.14	3.56	3.88	4.14	4.35
Number of riser tubes			358.00	**246.00**	187.00	151.00	126.00	109.00	95.00
Total RAS flow from sides [L/min]			626.41	**635.38**	587.99	537.21	488.75	451.04	413.47
			Air on sides, option II, air per riser tube [L/min]						
	0.83	0.6	**2.68**	3.90	5.13	6.35	7.57	8.79	
Water flow per riser tube [L/min]			**2.18**	2.97	3.51	3.90	4.21	4.46	
Number of riser tubes			**358.00**	246.00	187.00	151.00	126.00	109.00	
Total RAS flow from sides [L/min]			**779.64**	730.96	655.95	589.57	530.96	486.61	
Total RAS option I [L/min]			**3475.25**						
Total RAS option II [L/min]			**3619.50**						

The optimum is presented in bold. Total RAS flows were calculated by adding the optimum water flow above the module and the optimum water flow in the side for option I and II, respectively.

Table D.39: Scenario C, 0.75 MGD ($2.84 * 10^6$ L/day), 75% of air above module, 25% on sides.

	L [m]	H [m]	Air above module, air per riser tube [L/min]					
	0.53	0.3	2.68	**5.43**	8.18	10.93	13.68	24.45
Water flow per riser tube [L/min]			0.40	**2.04**	2.89	3.42	3.78	5.16
Number of riser tubes			2688.00	**1327.00**	881.00	659.00	527.00	294.00
Total RAS flow above module [L/min]			1061.81	**2705.76**	2546.22	2253.08	1994.31	1516.59
			Air on sides, option I, air per riser tube [L/min]					
	0.73	0.5	2.68	**3.90**	5.13	6.35	7.57	
Water flow per riser tube [L/min]			1.75	**2.58**	3.14	3.56	3.88	
Number of riser tubes			896.00	**615.00**	468.00	378.00	317.00	
Total RAS flow from sides [L/min]			1567.78	**1588.46**	1471.56	1344.81	1229.63	
			Air on sides, option II, air per riser tube [L/min]					
	0.83	0.6	**2.68**	3.90	5.13			
Water flow per riser tube [L/min]			**2.18**	2.97	3.51			
Number of riser tubes			**896.00**	615.00	468.00			
Total RAS flow from sides [L/min]			**1951.27**	1827.40	1641.62			
Total RAS option I [L/min]			**4294.22**					
Total RAS option II [L/min]			**4657.03**					

The optimum is presented in bold. Total RAS flows were calculated by adding the optimum water flow above the module and the optimum water flow in the side for option I and II, respectively.

Table D.40: Scenario C, 1 MGD ($3.79 * 10^6$ L/day), 100% of air above module.

	L [m]	H [m]	Air above module, air per riser tube [L/min]						
	0.62	0.3	10.01	11.24	12.46	13.68	**24.36**	35.11	45.86
Water flow per riser tube [L/min]			0.19	0.44	0.65	0.85	**3.78**	4.17	4.39
Number of riser tubes			1259.00	1122.00	1012.00	922.00	**517.00**	359.00	275.00
Total RAS flow above module [L/min]			236.20	488.32	661.71	780.89	**1955.27**	1496.75	1207.48

The optimum is presented in bold.

Table D.41: Scenario C, 1 MGD ($3.79 * 10^6$ L/day), 90% of air above module, 10% on sides.

	L [m]	H [m]	Air above module, air per riser tube [L/min]						
	0.62	0.3	11.24	12.46	13.68	**24.36**			
Water flow per riser tube [L/min]			0.44	0.65	0.85	**3.78**			
Number of riser tubes			1010.00	911.00	830.00	**466.00**			
Total RAS flow above module [L/min]			439.57	595.67	702.97	**1762.39**			
			Air on sides, option I, air per riser tube [L/min]						
	0.82	0.5	2.68	3.90	**5.13**	6.35	7.57	8.79	10.01
Water flow per riser tube [L/min]			0.84	1.73	**2.34**	2.80	3.15	3.43	3.67
Number of riser tubes			470.00	323.00	**246.00**	198.00	166.00	143.00	125.00
Total RAS flow from sides [L/min]			392.51	558.17	**576.76**	554.16	523.01	490.94	458.25
			Air on sides, option II, air per riser tube [L/min]						
	0.92	0.6	2.68	**3.90**	5.13	6.35	7.57	8.79	
Water flow per riser tube [L/min]			1.33	**2.20**	2.79	3.22	3.56	3.83	
Number of riser tubes			470.00	**323.00**	246.00	198.00	166.00	143.00	
Total RAS flow from sides [L/min]			623.51	**709.89**	685.98	638.14	590.93	547.83	
Total RAS option I [L/min]			**2339.16**						
Total RAS option II [L/min]			**2472.29**						

The optimum is presented in bold. Total RAS flows were calculated by adding the optimum water flow above the module and the optimum water flow in the side for option I and II, respectively.

Table D.42: Scenario C, 1 MGD ($3.79 * 10^6$ L/day), 75% of air above module, 25% on sides.

	L [m]	H [m]	Air above module, air per riser tube [L/min]				
	0.62	0.3	11.24	12.46	13.68	**24.36**	
Water flow per riser tube [L/min]			0.44	0.65	0.85	**3.78**	
Number of riser tubes			842.00	759.00	691.00	**388.00**	
Total RAS flow above module [L/min]			366.46	496.28	585.25	**1467.40**	
			Air on sides, option I, air per riser tube [L/min]				
	0.82	0.5	2.68	3.90	**5.13**	6.35	7.57
Water flow per riser tube [L/min]			0.84	1.73	**2.34**	2.80	3.15
Number of riser tubes			1176.00	807.00	**615.00**	496.00	416.00
Total RAS flow from sides [L/min]			982.12	1394.57	**1441.91**	1388.21	1310.67
			Air on sides, option II, air per riser tube [L/min]				
	0.92	0.6	2.68	**3.90**	5.13		
Water flow per riser tube [L/min]			1.33	**2.20**	2.79		
Number of riser tubes			1176.00	**807.00**	615.00		
Total RAS flow from sides [L/min]			1560.09	**1773.64**	1714.95		
Total RAS option I [L/min]			**2909.31**				
Total RAS option II [L/min]			**3241.03**				

The optimum is presented in bold. Total RAS flows were calculated by adding the optimum water flow above the module and the optimum water flow in the side for option I and II, respectively.

Table D.43: Scenario C, 2 MGD ($7.57 * 10^6$ L/day), 100% of air above module.

	L [m]	H [m]	Air above module, air per riser tube [L/min]					
	0.99	0.3	11.24	12.46	13.61	**24.36**	35.11	45.86
Water flow per riser tube [L/min]			0.18	0.40	0.59	**1.65**	2.15	2.44
Number of riser tubes			2245.00	2025.00	1853.00	**1035.00**	718.00	550.00
Total RAS flow above module [L/min]			404.25	811.23	1087.09	**1712.25**	1545.85	1341.05

The optimum is presented in bold.

Table D.44: Scenario C, 2 MGD ($7.59 * 10^6$ L/day), 90% of air above module, 10% on sides.

	L [m]	H [m]	Air above module, air per riser tube [L/min]						
	0.99	0.3	11.24	12.46	13.68	**24.36**			
Water flow per riser tube [L/min]			0.18	0.40	0.60	**1.65**			
Number of riser tubes			2021.00	1822.00	1660.00	**932.00**			
Total RAS flow above module [L/min]			363.91	729.91	991.39	**1541.85**			
			Air on sides, option I, air per riser tube [L/min]						
	1.19	0.5	6.35	7.57	8.79	10.01	**11.24**	12.46	13.68
Water flow per riser tube [L/min]			0.68	1.08	1.41	1.69	**1.93**	2.13	2.31
Number of riser tubes			397.00	333.00	287.00	251.00	**224.00**	202.00	184.00
Total RAS flow from sides [L/min]			268.27	359.21	405.57	424.98	**432.39**	430.99	424.99
			Air on sides, option II, air per riser tube [L/min]						
	1.29	0.6	7.57	**8.79**	10.01	11.24	12.46	13.68	
Water flow per riser tube [L/min]			1.65	**1.97**	2.24	2.47	2.66	2.83	
Number of riser tubes			333.00	**287.00**	251.00	224.00	202.00	184.00	
Total RAS flow from sides [L/min]			548.14	**566.03**	562.88	553.34	538.29	521.29	
Total RAS option I [L/min]			**1974.24**						
Total RAS option II [L/min]			**2107.89**						

The optimum is presented in bold. Total RAS flows were calculated by adding the optimum water flow above the module and the optimum water flow in the side for option I and II, respectively.

Table D.45: Scenario C, 2 MGD ($7.59 * 10^6$ L/day), 75% of air above module, 25% on sides.

	L [m]	H [m]	Air above module, air per riser tube [L/min]				
	0.99	0.3	11.24	12.46	13.68	**24.36**	
Water flow per riser tube [L/min]			0.18	0.40	0.60	**1.65**	
Number of riser tubes			1684.00	1519.00	1383.00	**776.00**	
Total RAS flow above module [L/min]			303.23	608.53	825.96	**1283.78**	
			Air on sides, option I, air per riser tube [L/min]				
	1.19	0.5	6.35	7.57	8.79	10.01	**11.24**
Water flow per riser tube [L/min]			0.68	1.08	1.41	1.69	**1.93**
Number of riser tubes			993.00	833.00	717.00	629.00	**561.00**
Total RAS flow from sides [L/min]			671.01	898.58	1013.22	1064.98	**1082.90**
			Air on sides, option II, air per riser tube [L/min]				
	1.29	0.6	7.57	**8.79**	10.01		
Water flow per riser tube [L/min]			1.65	**1.97**	2.24		
Number of riser tubes			833.00	**717.00**	629.00		
Total RAS flow from sides [L/min]			1371.17	**1414.10**	1410.57		
Total RAS option I [L/min]			**2366.68**				
Total RAS option II [L/min]			**2697.88**				

The optimum is presented in bold. Total RAS flows were calculated by adding the optimum water flow above the module and the optimum water flow in the side for option I and II, respectively.

Table D.46: Scenario C, 5 MGD ($18.93 * 10^6$ L/day), 100% of air above module.

	L [m]	H [m]	Air above module, air per riser tube [L/min]	
	1.63	0.3	88.85	**99.60**
Water flow per riser tube [L/min]			0.18	**0.32**
Number of riser tubes			709.00	**633.00**
Total RAS flow above module [L/min]			125.77	**204.30**

The optimum is presented in bold.

Table D.47: Scenario C, 5 MGD ($18.93 * 10^6$ L/day), 90% of air above module, 10% on sides.

	L [m]	H [m]	Air above module, air per riser tube [L/min]						
	1.63	0.3	88.85	**99.60**					
Water flow per riser tube [L/min]			0.18	**0.32**					
Number of riser tubes			638.00	**500.00**					
Total RAS flow above module [L/min]			113.17	**161.37**					
			Air on sides, option I, air per riser tube [L/min]						
	1.83	0.5	13.61	**24.36**	35.11	45.86	56.61	67.35	78.10
Water flow per riser tube [L/min]			0.66	**1.73**	2.23	2.51	2.70	2.83	2.92
Number of riser tubes			463.00	**258.00**	179.00	137.00	111	93	80
Total RAS flow from sides [L/min]			304.48	**445.49**	398.62	344.36	299.52	262.90	233.68
			Air on sides, option II, air per riser tube [L/min]						
	1.93	0.6	13.61	**24.36**	35.11	45.86	56.61	67.35	
Water flow per riser tube [L/min]			0.71	**1.78**	2.28	2.56	2.75	2.87	
Number of riser tubes			463.00	**258.00**	179.00	137.00	111	93	
Total RAS flow from sides [L/min]			329.00	**458.43**	407.33	350.91	304.7809	267.282	
Total RAS option I [L/min]			**606.86**						
Total RAS option II [L/min]			**619.80**						

The optimum is presented in bold. Total RAS flows were calculated by adding the optimum water flow above the module and the optimum water flow in the side for option I and II, respectively.

Table D.48: Scenario C, 5 MGD ($18.93 * 10^6$ L/day), 75% of air above module, 25% on sides.

	L [m]	H [m]	Air above module, air per riser tube [L/min]				
	1.63	0.3	88.85	**99.60**			
Water flow per riser tube [L/min]			0.18	**0.32**			
Number of riser tubes			532.00	**475.00**			
Total RAS flow above module [L/min]			94.37	**153.30**			
			Air on sides, option I, air per riser tube [L/min]				
	1.83	0.5	13.61	**24.36**	35.11	45.86	56.61
Water flow per riser tube [L/min]			0.66	**1.73**	2.23	2.51	2.70
Number of riser tubes			1158.00	**647.00**	449.00	343.00	278
Total RAS flow from sides [L/min]			761.52	**1117.18**	999.90	862.15	750.14
			Air on sides, option II, air per riser tube [L/min]				
	1.93	0.6	13.61	**24.36**	35.11	45.86	56.61
Water flow per riser tube [L/min]			0.71	**1.78**	2.28	2.56	2.75
Number of riser tubes			1158.00	**647.00**	449.00	343.00	278
Total RAS flow from sides [L/min]			822.86	**1149.62**	1021.74	878.57	763.33
Total RAS option I [L/min]			**1270.48**				
Total RAS option II [L/min]			**1302.93**				

The optimum is presented in bold. Total RAS flows were calculated by adding the optimum water flow above the module and the optimum water flow in the side for option I and II, respectively.

Table D.49: Scenario C, 10 MGD ($37.85 * 10^6$ L/day), 100% of air above module.

	L [m]	H [m]	Air above module, air per riser tube [L/min]
	2.67	0.2	
Water flow per riser tube [L/min]			Submergence ratio is too high to pump water
Number of riser tubes			
Total RAS flow above module [L/min]			

Table D.50: Scenario C, 10 MGD ($37.85 * 10^6$ L/day), 90% of air above module, 10% on sides.

	L [m]	H [m]	Air above module, air per riser tube [L/min]				
	2.67	0.3					
Water flow per riser tube [L/min]			Submergence ratio is too high to pump water				
Number of riser tubes							
Total RAS flow above module [L/min]							
			Air on sides, option I, air per riser tube [L/min]				
	2.87	0.5	67.35	78.10	88.85	**99.60**	
Water flow per riser tube [L/min]			0.09	0.31	0.47	**0.58**	
Number of riser tubes			187.00	161.00	141.00	**126.00**	
Total RAS flow from sides [L/min]			16.72	50.48	66.01	**73.51**	
			Air on sides, option II, air per riser tube [L/min]				
	2.97	0.6	**56.61**	67.35	78.10	88.85	99.60
Water flow per riser tube [L/min]			**1.03**	1.20	1.33	1.43	1.51
Number of riser tubes			**222.00**	187.00	161.00	141.00	126.00
Total RAS flow from sides [L/min]			**227.71**	225.24	214.84	202.04	190.25
Total RAS option I [L/min]			**73.51**				
Total RAS option II [L/min]			**227.71**				

The optimum is presented in bold. Total RAS flows were calculated by adding the optimum water flow above the module and the optimum water flow in the side for option I and II, respectively.

Table D.51: Scenario C, 10 MGD ($37.85 * 10^6$ L/day), 75% of air above module, 25% on sides.

	L [m]	H [m]	Air above module, air per riser tube [L/min]				
	2.67	0.3					
Water flow per riser tube [L/min]			Submergence ratio is too high to pump water				
Number of riser tubes							
Total RAS flow above module [L/min]		[L/min]					
			Air on sides, option I, air per riser tube [L/min]				
	2.87	0.5	67.35	78.10	88.85	**99.60**	
Water flow per riser tube [L/min]			0.09	0.31	0.47	**0.58**	
Number of riser tubes			468.00	403.00	354.00	**316.00**	
Total RAS flow from sides [L/min]			41.85	126.35	165.74	**184.35**	
			Air on sides, option II, air per riser tube [L/min]				
	2.97	0.6	**56.61**	67.35	78.10	88.85	99.60
Water flow per riser tube [L/min]			**1.03**	1.20	1.33	1.43	1.51
Number of riser tubes			**557.00**	468.00	403.00	354.00	316.00
Total RAS flow from sides [L/min]			**571.33**	563.71	537.78	507.24	477.13
Total RAS option I [L/min]			**184.35**				
Total RAS option II [L/min]			**571.33**				

The optimum is presented in bold. Total RAS flows were calculated by adding the optimum water flow above the module and the optimum water flow in the side for option I and II, respectively.